Oxime Based Manganese Molecular Magnets

Ross Inglis

A Thesis Submitted for the degree of Doctor of Philosophy

School of Chemistry

Faculty of Science and Engineering

University of Edinburgh

Edinburgh – September 2010

Abstract

The synthesis and characterisation of a large family of hexametallic [Mn^{III}_6] Single-Molecule Magnets with general formula [$Mn^{III}_6O_2$(R-sao)$_6$(X)$_2$(L)$_{4-6}$] (where sao^{2-} = dianion of salicylaldoxime; R = H, Me, Et, Ph; X = $^-O_2CR'$ (R' = H, Me, Ph *etc*), Hal^-, $^-O_2PHPh$ or $^-O_2P(Ph)_2$; L = solvent) are presented. Deliberate structural distortions of the [Mn_3O] trinuclear moieties within the complexes are used to tune the observed magnetic properties. These findings highlight a qualitative magneto-structural correlation whereby the type (anti- or ferromagentic) of each Mn_2 pairwise magnetic exchange is dominated by the magnitude of each individual Mn-N-O-Mn torsion angle.

To shed further light on this intriguing family of nanomagnets, a large family of the analogous "half" molecules has been synthesised and fully characterised. These trimetallic [Mn^{III}_3] complexes can be divided into three categories with general formulae (*type 1*) [Mn^{III}_3O(R-sao)$_3$(X)(sol)$_{3-4}$] (where R = H, Me, ^{t}Bu; X = ^-O_2CR (R = H, Me, Ph etc); sol = py and / or H_2O), (*type 2*) [Mn^{III}_3O(R-sao)$_3$(X)(sol)$_{3-5}$] (where R = Me, Et, Ph, ^{t}Bu; X = ^-O_2CR (R = H, Me, Ph etc); sol = MeOH, EtOH and / or H_2O), and (*type 3*) [Mn^{III}_3O(R-sao)$_3$(sol)$_3$](XO_4) (where R = H, Et, Ph, Naphth; sol = py, MeOH, *β*-pic, Et-py, ^{t}Bu-py; X = Cl, Re). In the crystals the ferromagnetic triangles are involved in extensive inter-molecular H-bonding which is clearly manifested in the magnetic behaviour, producing exchange-biased SMMs. These interactions can be removed by ligand replacement to give "simpler" SMMs.

The [Mn^{III}_6] and [Mn^{III}_3] molecular nanomagnets are then exploited as building blocks to construct supramolecular architectures by means of host-guest interactions and coordination driven self-assembly. A number of discrete and infinite architectures based on the molecular triangle [Mn_3] and various pyridyl-type ligands were obtained and structurally and magnetically characterised.

Acknowledgements

First and foremost I would like to thank “the boss” – Dr. Euan Brechin – for giving me the chance to do a PhD and for allowing me do some “top science” over the past three years. It’s been a pleasure to work for such a friendly and enthusiastic boss and all his encouragement and guidance throughout has been great. Thanks for the trips to the Tennent’s pubs in Edinburgh and for liking a game of pool and/or snooker (even better when in a Tennent’s pub).

Next I must thank the postdocs who were in the group when I started. First, Dr. Costas Milios for encouraging me to do a PhD and for allowing me to continue on with the great work that he started. A great scientist and fan of 80s rock, both of which were on show in and out of the lab. Second, Dr. Leigh Jones for getting me started in the lab and for all his help during my first year.

I would also like to thank my fellow “Brechin group” members. It’s been fantastic to meet and work with so many great people over the last three years: Ian Gass (for supporting Queen of the South and for some great chat in the lab, usually involving music , films and football); Maria Manoli (for showing me how to fit magnetism data and for making us keep the lab tidy); Giorgos Karotsis (for being such an entertaining character and for allowing me to visit the great nation of Greece); Alex Prescimone (for trying to teach me crystallography and for keeping me company in the office the past few months); Richard Scott (for two summers in the lab with great banter); Kevin Mason (for being “awesome” despite being a Rangers fan and for always being up for going big); Stephanie Taylor (for putting up with our constant football talk and for having another Biffy fan in the group) and Tom Hooper (for putting up with our enjoyment of the England team’s performance at the World Cup).

I would also like to thank Prof. Simon Parsons and his group for solving the majority of my crystal structures: Dr. Anna Collins, Dr. Fraser White, Dr. Stephen Moggach, Russell Johnstone, Laura Budd, Nick Funnell and Pete Byrne.

I must also thank the people outside of the Joseph Black Building who helped with various measurements of my samples: Prof. Wolfgang Wernsdorfer for the single-crystal hysteresis measurements; Prof. Stephen Hill and Saiti Datta from his group

for the high field electron paramagnetic resonance studies; Dr. Scott Dalgarno from Heroit-Watt for solving a number of my crystal structures and Sylvia Williamson for elemental analysis.

Last but not least, I would like to thank my family, Mum and Dad, Lee and Morag and my grandparents. Their support throughout has been fantastic.

Declaration

I hereby declare that except where specific reference is made to other sources, the work contained in this thesis is the original work of the author. It has been composed by the candidate and has not been submitted, in whole or in part, for any other degree, diploma, or other qualification.

Ross Inglis

28th September 2010

Format of the Thesis

Each chapter of this thesis, with the exception of Chapter 1, is made up of published papers. To fulfil the requirements of the University of Edinburgh regarding the preparation and submission of a thesis for the degree of PhD, they have been reformatted accordingly.

Chapter 2:

1. R. Inglis, L. F. Jones, C. J. Milios, S. Datta, A. Collins, S. Parsons, W. Wernsdorfer, S. Hill, S. P. Perlepes, S. Piligkos and E. K. Brechin, *Dalton Trans.*, 2009, **18**, 3403.
2. R. Inglis, S. J. Dalgarno and E. K. Brechin, *Dalton Trans.*, 2010, **39**, 4826.

Chapter 3:

1. R. Inglis, S. M. Taylor, L. F. Jones, G. S. Papaefstathiou, S. P. Perlepes, S. Datta, S. Hill, W. Wernsdorfer and E. K. Brechin, *Dalton Trans.*, 2009, 9157.

Chapter 4:

1. R. Inglis, A. D. Katsenis, A. Collins, F. White, C. J. Milios, G. S. Papaefstathiou and E. K. Brechin, *CrystEngComm*, 2010, **12**, 2064.

Measurements carried out by other people:

Single-crystal hysteresis measurements – Prof. Wolfgang Wernsdorfer.
High frequency electron paramagnetic resonance studies – Prof. Stephen Hill.

Publications

1. R. Inglis, J. Bendix, T. Brock-Nannestad, H. Weihe, E. K. Brechin and S. Piligkos, *Chem. Sci.*, 2010, accepted for publication.
2. R. Inglis, A. D. Katsenis, A. Collins, F. White, C. J. Milios, G. S. Papaefstathiou and E. K. Brechin, *CrystEngComm*, 2010, **12**, 2064.
3. R. Inglis, S. J. Dalgarno and E. K. Brechin, *Dalton Trans.*, 2010, **39**, 4826.
4. R. Inglis, C. C. Stoumpos, A. Prescimone, M. Siczek, T. Lis, W. Wernsdorfer, E. K. Brechin and C. J. Milios, *Dalton Trans.*, 2010, **39**, 4777.
5. S. Hill, S. Datta, J. Liu, R. Inglis, C. J. Milios, P. L. Feng, J. J. Henderson, E. d. Barco, E. K. Brechin and D. N. Hendrickson, *Dalton Trans.*, 2010, **39**, 4693.
6. C. C. Stoumpos, R. Inglis, O. Roubeau, H. Sartzi, A. Kitos, C. J. Milios, G. Aromí, A. J. Tasiopoulos, V. Nastopoulos, E. K. Brechin and S. P. Perlepes, *Inorg. Chem.*, 2010, **49**, 4388.
7. J. L. Atwood, E. K. Brechin, S. J. Dalgarno, R. Inglis, L. F. Jones, A. Mossine, M. J. Paterson, N. P. Power and S. J. Teat, *Chem. Commun.*, 2010, **46**, 3484.
8. S. Zhang, L. Zhen, B. Xu, R. Inglis, K. Li, Y. Zhang, K. F. Konidaris, S. P. Perlepes, E. K. Brechin and Y. Li, *Dalton Trans.*, 2010, **39**, 3563.
9. R. Inglis, S. M. Taylor, L. F. Jones, G. S. Papaefstathiou, S. P. Perlepes, S. Datta, S. Hill, W. Wernsdorfer and E. K. Brechin, *Dalton Trans.*, 2009, 9157.
10. A. D. Katsenis, R. Inglis, A. M. Z. Slawin, V. G. Kessler, E. K. Brechin and G. S. Papaefstathiou, *CrystEngComm*, 2009, **11**, 2117.
11. R. Inglis, G. S. Papaefstathiou, W. Wernsdorfer and E. K. Brechin, *Aust. J. Chem.*, 2009, **62**, 1108.
12. R. Inglis, L. F. Jones, C. J. Milios, S. Datta, A. Collins, S. Parsons, W. Wernsdorfer, S. Hill, S. P. Perlepes, S. Piligkos and E. K. Brechin, *Dalton Trans.*, 2009, **18**, 3403.
13. C. J. Milios, R. Inglis, L. F. Jones, A. Prescimone, S. Parsons, W. Wernsdorfer and E. K. Brechin, *Dalton Trans.*, 2009, **15**, 2812.
14. S. Datta, E. Bolin, R. Inglis, C. J. Milios, E. K. Brechin and S. Hill, *Polyhedron*, 2009, **28**, 1788.
15. C. C. Stoumpos, R. Inglis, G. Karotsis, L. F. Jones, A. Collins, S. Parsons, C. J. Milios, G. S. Papaefstathiou and E. K. Brechin, *Cryst. Growth Des.*, 2009, **9**, 24.
16. R. Inglis, L. F. Jones, G. Karotsis, A. Collins, S. Parsons, S. P. Perlepes, W. Wernsdorfer and E. K. Brechin, *Chem. Commun.*, 2008, 5924.
17. L. F. Jones, R. Inglis, M. E. Cochrane, K. Mason, A. Collins, S. Parsons, S. P. Perlepes and E. K. Brechin, *Dalton Trans.*, 2008, **44**, 6205.
18. R. Inglis, L. F. Jones, K. Mason, A. Collins, S. A. Moggach, S. Parsons, S. P. Perlepes, W. Wernsdorfer and E. K. Brechin, *Chem. Eur. J*, 2008, **14**, 9117.
19. C. J. Milios, R. Inglis, A. Vinslava, R. Baghi, W. Wernsdorfer, S. Parsons, S. P. Perlepes, G. Christou and E. K. Brechin, *J. Am. Chem. Soc.*, 2007, **129**, 12505.

20. C. J. Milios, R. Inglis, R. Bagai, W. Wernsdorfer, A. Collins, S. A. Moggach, S. Parsons, S. P. Perlepes, G. Christou and E. K. Brechin, *Chem. Commun.*, 2007, **33**, 3476.
21. C. J. Milios, R. Inglis, A. Vinslava, A. Prescimone, S. Parsons, S. P. Perlepes, G. Christou and E. K. Brechin, *Chem. Commun.*, 2007, **26**, 2738.

Conferences attended

2009 Scottish Dalton Inorganic Meeting (Glasgow, UK).

42nd IUPAC Congress: Chemistry Solutions (Glasgow, UK) – 20 minute presentation given.

2008 11th International Conference on Molecule-based Magnets (Florence, Italy) – poster presented.

Royal Society Of Chemistry Discussion Group Meeting: Inorganic Reaction Mechanisms/Coordination Chemistry (Edinburgh, UK) – poster presented.

Contents

ABSTRACT ..... **I**

ACKNOWLEDGEMENTS ..... **II**

DECLARATION ..... **IV**

FORMAT OF THE THESIS ..... **V**

PUBLICATIONS ..... **VI**

CONFERENCES ATTENDED ..... **VII**

CONTENTS ..... **VIII**

ABBREVIATIONS ..... **XI**

LIST OF COMPLEXES ..... **XII**

CHAPTER 1: INTRODUCTION **1**

1.1 MAGNETO-STRUCTURAL CORRELATIONS **2**

1.2 PHENOLIC OXIMES **4**

1.3 SINGLE-MOLECULE MAGNETS. **5**

1.4 MANGANESE SMMS. **10**

1.5 SMMS USING OTHER 3*d* METALS. **17**

1.6 SUPPORTING INFORMATION. **20**

1.7 REFERENCES **20**

CHAPTER 2: RELATING STRUCTURE AND MAGNETISM IN A LARGE FAMILY OF Mn_6 SMMS **25**

2.1 INTRODUCTION **26**

2.2 TOWARDS A MAGNETO-STRUCTURAL CORRELATION FOR A LARGE FAMILY OF Mn_6 SMMS **28**

2.2.1 EXPERIMENTAL SECTION 28

Synthesis *28*

X-ray crystallography *29*

Magnetic measurements. *29*

2.2.2 RESULTS AND DISCUSSION 29
Description of structures *29*
2.2.3 MAGNETOCHEMISTRY 32
Dc magnetic susceptibility and magnetisation measurements *32*
Ac magnetic susceptibility and hysteresis loop measurements *37*
High Frequency Electron Paramagnetic Resonance Studies *41*
Discussion *42*
Conclusions *45*
2.3 A NEW FAMILY OF Mn_6 SMMS USING HALIDES AND PHOSPHINATES 48
2.3.1 EXPERIMENTAL SECTION 48
Synthesis *48*
X-ray crystallography *48*
2.3.2 RESULTS AND DISCUSSION 49
Description of structures *49*
2.3.3 MAGNETOCHEMISTRY 51
Dc magnetic susceptibility and magnetisation measurements *51*
Ac magnetic susceptibility measurements *54*
Discussion *57*
Conclusions *57*
2.4 REFERENCES 60
CHAPTER 3: STRATEGIES FOR MAKING FERROMAGNETIC Mn_3 TRIANGLES 63
3.1 INTRODUCTION 64
3.2 STRATEGIES FOR MAKING FERROMAGNETIC Mn_3 TRIANGLES 67
3.2.1 EXPERIMENTAL SECTION 67
Synthesis *67*
X-ray crystallography *68*
Magnetic measurements. *68*
3.2.2 RESULTS AND DISCUSSION 68
Description of structures *68*
3.2.3 MAGNETOCHEMISTRY 75
Dc magnetic susceptibility and magnetisation measurements *75*
Ac magnetic susceptibility and hysteresis loop measurements *80*
High Frequency Electron Paramagnetic Resonance Studies *85*

Discussion and Conclusions *91*

3.3 REFERENCES **96**

CHAPTER 4: ASSEMBLING MOLECULAR TRIANGLES INTO DISCRETE AND INFINITE ARCHITECTURES **99**

4.1 INTRODUCTION **100**

4.2 ASSEMBLING MOLECULAR TRIANGLES INTO DISCRETE AND INFINITE ARCHITECTURES **102**

4.2.1 EXPERIMENTAL SECTION 102

Synthesis *102*

X-ray crystallography *102*

Magnetic measurements. *102*

4.2.2 RESULTS AND DISCUSSION 103

Description of structures *103*

4.2.3 MAGNETOCHEMISTRY 115

Dc magnetic susceptibility and magnetisation measurements *115*

Conclusions *117*

4.3 REFERENCES **119**

Abbreviations

ac	Alternating current
AF	Antiferromagnetic Exchange
β-pic	*β*-picoline
bpe	bis(4-pyridyl)ethylene
bpy	Bipyridine
BVS	Bond Valence Sum
D	Zero-Field Splitting Parameter
dc	Direct current
DFT	Density Functional Theory
EPR	Electron Paramagnetic Resonance
Et-py	Ethyl-pyridine
F	Ferromagnetic Exchange
HF EPR	High Field Electron Paramagnetic Resonance
JT	Jahn-Teller
[Mn_{12}OAc]	[$Mn_{12}O_{12}(O_2CMe)_{16}(H_2O)_4$]
py	Pyridine
QPI	Quantum Phase Interference
QTM	Quantum Tunnelling of the Magnetisation
s.e.	Symmetry equivalent
saoH_2	Salicylaldoxime
sbz	Stilbazole
SMMs	Single Molecule Magnets
ZFS	Zero-field splitting

List of Complexes

Complex	Chapter	Complex No.
$[Mn_6O_2(sao)_6(O_2CH)_2(MeOH)_4]$	2	2.1
$[Mn_6O_2(Me\text{-}sao)_6(O_2CCPh_3)_2(EtOH)_4]$	2	2.2
$[Mn_6O_2(sao)_6(ketoacetate)_2(EtOH)_2(H_2O)_2]$	2	2.3
$[Mn_6O_2(sao)_6(O_2CPh)_2(MeCN)_2(H_2O)_2]$	2	2.4
$[Mn_6O_2(sao)_6(1\text{-}Me\text{-}cyclohex)_2(MeOH)_4]$	2	2.5
$[Mn_6O_2(Me\text{-}sao)_6(O_2C\text{-}th)_2(EtOH)_4(H_2O)_2]$	2	2.6
$[Mn_6O_2(Et\text{-}sao)_6(O_2CC_{12}H_{17})_2(EtOH)_4(H_2O)_2]$	2	2.7
$[Mn_6O_2(Et\text{-}sao)_6(O_2CC(CH_3)_3)_2(MeOH)_6]$	2	2.8
$[Mn_6O_2(Et\text{-}sao)_6(O_2CC(CH_3)_3)_2(EtOH)_5]$	2	2.9
$[Mn_6O_2(Et\text{-}sao)_6(O_2CPh^2OPh)_2(EtOH)_4]$	2	2.10
$[Mn_6O_2(Et\text{-}sao)_6(O_2CPh^4OPh)_2(EtOH)_4(H_2O)_2]$	2	2.11
$[Mn_6O_2(Me\text{-}sao)_6(O_2CPhBr)_2(EtOH)_6]$	2	2.12
$[Mn_6O_2(Me\text{-}sao)_6(O_2CC(CH_3)_3)_2(MeOH)_6]$	2	2.13
$[Mn_6O_2(Et\text{-}sao)_6(O_2CPh)_2(EtOH)_4(H_2O)_2]$	2	2.14
$[Mn_6O_2(Et\text{-}sao)_6(O_2CPh(Me)_2)_2(EtOH)_6]$	2	2.15
$[Mn_6O_2(Et\text{-}sao)_6(O_2C_{11}H_{15})_2(EtOH)_6]$	2	2.16
$[Mn_6O_2(Et\text{-}sao)_6(O_2CPh(Me))_2(EtOH)_4(H_2O)_2]$	2	2.17
$[Mn_6O_2(Et\text{-}sao)_6(O_2C\text{-}Naphth)_2(EtOH)_4(H_2O)_2]$	2	2.18
$[Mn_6O_2(Et\text{-}sao)_6(O_2C\text{-}Anthra)_2(EtOH)_4(H_2O)_2]$	2	2.19
$[Mn_6O_2(Et\text{-}sao)_6(O_2CPh(C{\equiv}CH)_2(EtOH)_4(H_2O)_2]$	2	2.20
$[Mn_6O_2(Me\text{-}sao)_6(O_2CPh(C{\equiv}CH))_2(EtOH)_6]$	2	2.21
$[Mn_6O_2(Me\text{-}sao)_6(O_2CPh(Cl)_2)_2(MeOH)_6]$	2	2.22
$[Mn_6O_2(Et\text{-}sao)_6(Br)_2(EtOH)_6]$	2	2.23
$[Mn_6O_2(Me\text{-}sao)_6(I)_2(EtOH)_6]$	2	2.24
$[Mn_6O_2(sao)_6(O_2P(Ph)_2)_2(MeOH)_6]$	2	2.25
$[Mn_6O_2(Me\text{-}sao)_6(O_2P(Ph)_2)_2(MeOH)_6].3MeOH$	2	2.26
$[Mn_6O_2(Et\text{-}sao)_6(O_2P(Ph)_2)_2(MeOH)_6]$	2	2.27
$[Mn_6O_2(Ph\text{-}sao)_6(O_2P(Ph)_2)_2(MeOH)_4]$	2	2.28
$[Mn_6O_2(Me\text{-}sao)_6(O_2PHPh)_2(MeOH)_6].MeOH$	2	2.29

Complex	Chapter	Complex No.
$[Mn_6O_2(Et\text{-}sao)_6(O_2PHPh)_2(MeOH)_6].MeOH$	2	2.30
$[Mn_3O(Naphth\text{-}sao)_3(py)_3](ClO_4)$	3	3.1
$[Mn_3O(sao)_3(Et\text{-}py)_3](ClO_4)$	3	3.2
$[Mn_3O(sao)_3(O_2CPh)(H_2O)(py)_3]$	3	3.3
$[Mn_3O(sao)_3(O_2C\text{-}Naphth)(py)_3].(py)$	3	3.4
$[Mn_3O(sao)_3(O_2CC_{10}H_{13})(py)_3].EtOH$	3	3.5
$[Mn_3O(sao)_3(O_2CCH_3)(H_2O)(py)_3].(py)$	3	3.6
$[Mn_3O(Me\text{-}sao)_3(O_2CCH_3)(MeOH)_5].(Me\text{-}saoH_2)$	3	3.7
$(Na)(PyH)[Mn_3O(Me\text{-}sao)_3(O_2C\text{-}Anthra)(py)_3]_2[ClO_4]_2.py$	3	3.8
$[Mn_3O(Me\text{-}sao)_3(O_2CCH_3)(py)_4].2(py)$	3	3.9
$[Mn_3O(^tBu\text{-}sao)_3(O_2CC_9O_3H_{11})(py)_3]$	3	3.10
$[Mn_3O(^tBu\text{-}sao)_3(O_2CPh(CH_3)_2)(MeOH)_4]$	3	3.11
$[Mn_3O(Et\text{-}sao)_3(O_2CPh(Cl)_2)(H_2O)(MeOH)_3]$	3	3.12
$[Mn_3O(Et\text{-}sao)_3(MeOH)_3](ClO_4)$	3	3.13
$[Mn_3O(Et\text{-}sao)_3(O_2CPh)(C_6H_{16}NO_3)(O_2CPh)(H_2O)_2]$	3	3.14
$[Mn_3O(Et\text{-}sao)_3(O_2CPh(CF_3)_2)(EtOH)(H_2O)_3].EtOH$	3	3.15
$[Mn_3O(Et\text{-}sao)_3(\beta\text{-}pic)_3](ClO_4)$	3	3.16
$[Mn_3O(Et\text{-}sao)_3(Et\text{-}py)_3](ClO_4)$	3	3.17
$[Mn_3O(Et\text{-}sao)_3(^tBu\text{-}py)_3](ClO_4)$	3	3.18
$[Mn_3O(Et\text{-}sao)_3(EtOH)(H_2O)_2](ReO_4).3EtOH$	3	3.19
$[Mn_3O(Ph\text{-}sao)_3(O_2C\text{-}Anthra)(MeOH)_4].(Ph\text{-}saoH_2)$	3	3.20
$[Mn_3O(Ph\text{-}sao)_3(\beta\text{-}pic)_3](ClO_4)$	3	3.21
$[Mn_3O(Ph\text{-}sao)_3(4Cl\text{-}sbz)_3(MeOH)_3]_2(OH)(ClO_4).2MeOH$	4	4.1
$[Mn_3O(Ph\text{-}sao)_3(4Me\text{-}sbz)_3(EtOH)_3]_2(OH)(NO_3)$	4	4.2
$\{[Mn_3O(Et\text{-}sao)_3(4,4'\text{-}bpy)_2(MeOH)](ClO_4).1.5MeOH.Et_2O\}_n$	4	4.3
$\{[Mn_3O(sao)_3(4,4'\text{-}bpe)_{1.5}](ClO_4).3MeOH\}_n$	4	4.4
$[\{Mn_3O(Et\text{-}sao)_3(O_2CPh)(EtOH)\}_2\{4,4'\text{-}bpe\}_2]$	4	4.5

Chapter 1
Introduction

This thesis describes the synthesis of a large number of polynuclear manganese complexes and the study of their magnetic properties, in an attempt to understand the relationship between structure and magnetism. These complexes are then used as building blocks to create supramolecular architectures using various polycarboxylate and polypyridyl-type ligands. Many of the complexes reported are Single-Molecule Magnets (SMMs). An introduction to previous magneto-structural correlations is given along with a discussion of the main ligands used in this thesis. The phenomenon of single-molecule magnetism is then explained with respect to previously synthesised manganese complexes, along with a brief description of SMMs made using other 3*d* transition metal ions.

1.1 Magneto-structural Correlations

It has long been recognised that for polymetallic compounds, some correlation must exist between the type and magnitude of magnetic interaction and the relative positions of the metal ions. Magnetic studies on copper(II) acetate hydrate[1] and basic metal carboxylates[2] revealed antiferromagnetic interactions, from which their respective dinuclear and trinuclear structures, solved later,[3, 4] were correctly predicted. Magnetic studies on polynuclear metal complexes started in 1952 when Bleaney and Bowers[1] established a theoretical expression for the magnetic susceptibility of copper(II) acetate hydrate (Scheme 1.1) as a function of the temperature and the energy parameter J characterising the interaction between the Cu^{II} centres within the molecule.

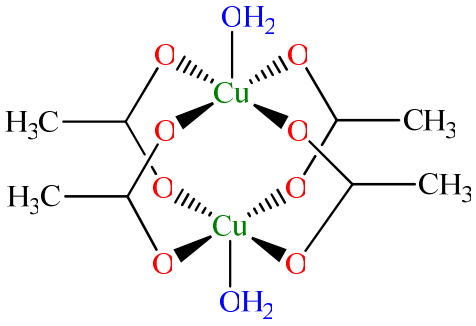

Scheme 1.1 Schematic structure of copper(II) acetate hydrate.

By the mid-seventies numerous complexes had been synthesised, whose *J*-parameters were determined by comparing experimental magnetic susceptibility data with the appropriate theoretical laws.[5-7] Many researchers then attempted to rationalise the sign and size of *J* in light of structural data. This allowed qualitative or quantitative correlations between structural and magnetic properties to be made (hence "magneto-structural correlations") and constituted an important step toward the understanding of the mechanism of interaction between metal centres.[8, 9] The earliest of these correlations was established by Hatfield and Hodgson who showed a linear relationship between the magnetic parameter *J* and the Cu-O-Cu bridging angle φ in planar bis(μ-hydroxo)copper(II) dimers (Scheme 1.2),[10, 11] with the Cu-O distance being less important. The crossover from ferromagnetic to antiferromagnetic exchange occurs at approximately 97.5°.

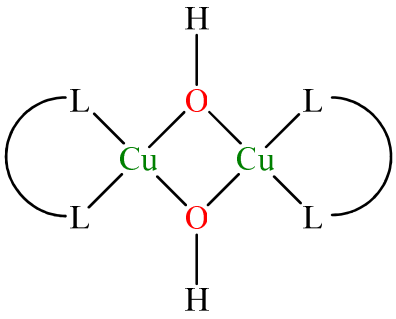

Scheme 1.2 Schematic structure of a planar bis(μ-hydroxo)copper(II) dimer containing two chelating ligands, L-L.

In the case of bis(μ-hydroxo)dichromium(III) complexes, both the Cr-O distance and the Cr-O-Cr angle are important; the major factor, however, seems to be the hybridisation of the bridging oxygen atom, as reflected in the variation of the angle between the O-H vector and the Cr_2O_2 plane.[12-14] Other elegant correlations concerning bis(μ-halogeno)dicopper(II) compounds,[11, 15, 16] dinuclear copper(II) complexes with equatorial diazine/μ-1,1-azide bridge combinations,[17] (μ-oxo)diiron(III) species,[18, 19] Fe^{III}_4 butterfly-type clusters,[20-23] and other dinuclear[24, 25] and oligonuclear[26-28] systems were also established. These correlations have shown that the type and magnitude of the magnetic exchange interaction depends on the bridge identity, the metal-metal separation, the bond angles subtended at the bridging

atoms, the dihedral angles between coordination planes containing the metal ions, the metal ligand bond lengths, and the metal ion stereochemistries.[17]

In recent years there has been a clear evolution from the initial studies in molecular magnetism[29] that addressed mostly dinuclear complexes, for which a detailed experimental and theoretical analysis of the correlation between structure and magnetic properties has been established, to polynuclear metal complexes or "clusters". Due to the increased structural complexity of clusters (especially so as the nuclearity increases) and the presence of many different exchange pathways in one molecule, a detailed study of the exchange interactions is often impossible. It should be recalled[20-23] that for large polynuclear metal complexes it may not be possible to extract a set of exchange coupling constants (*J*) from magnetic susceptibility data since (a) the size of the system and currently available computational resources may forbid fitting or simulation, and (b) the existence of many solutions that perfectly fit the experimental data makes uncertain which is the physically acceptable set of *J* values. Thus, with a limited number of exceptions,[20, 26-28] magneto-structural correlations are unknown for clusters. Even less developed is theoretical analysis: despite the important role (and much recent success) that theoretical methods based on density functional theory can play in this field,[20-23] such studies have generally been employed to calculate *J* values (and to compare them with experimental data) or to help select a "*correct*" set of fitted values, rather than to obtain magneto-structural correlations - presumably due to the complexity of the systems.[30]

1.2 Phenolic oximes

Phenolic oximes (examples of the oximes discussed in this thesis are given in Scheme 1.3) are used extensively in industry for metal extraction from waste streams, mainly for the extraction of copper,[31] and as corrosion inhibitors in protective coatings.[32] They show a remarkable selectivity for copper(II) over other metals in pregnant leach solutions, notably over iron which is present in similar or even higher concentrations. Complex formation is favourable at low pH values of <2.0 to ensure that the iron remains in solution. The recovery of copper by solvent extraction produces around one fifth of the total world production of copper.[33] The favourable selectivity of complex formation with copper is due to the copper fitting

perfectly within the cavity formed by two hydrogen bonded ligands, forming a stable pseudo-macrocyclic monomer (Scheme 1.4). Co^{2+}, Ni^{2+}, Cu^{2+} and Zn^{2+} all form these mononuclear complexes with phenolic oximes.[34] Another important feature of phenolic oximes is their ability to form polynuclear complexes as both the oximate and phenolate groups can bridge metals. Polynuclear complexes with Cr,[35] Mn,[36] Fe,[37] and Co[38] have been reported, with the iron chemistry of these ligands leading to commercial application in corrosion inhibition.[32]

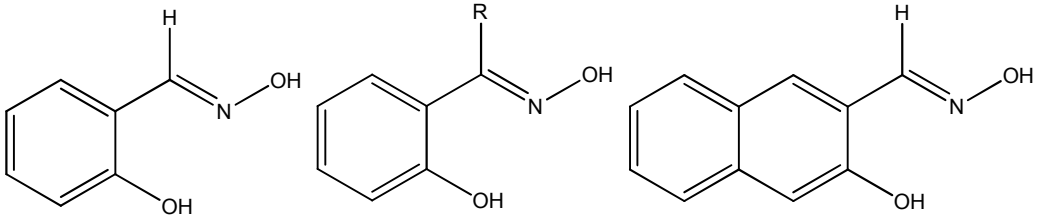

$saoH_2$ | R-$saoH_2$ (R=Me, Et, Ph) | Naphth-$saoH_2$

Scheme 1.3 The structural formulae of the phenolic oxime ligands discussed in the text: $saoH_2$ = salicylaldoxime (2-hydroxybenzaldehyde oxime), Me-$saoH_2$ = 2-hydroxyacetophenone oxime, Et-$saoH_2$ = 2-hydroxypropiophenone oxime, Ph-$saoH_2$ = 2-hydroxybenzophenone oxime, Naphth-$saoH_2$ = 2-hydroxy-1-naphthaldehyde oxime.

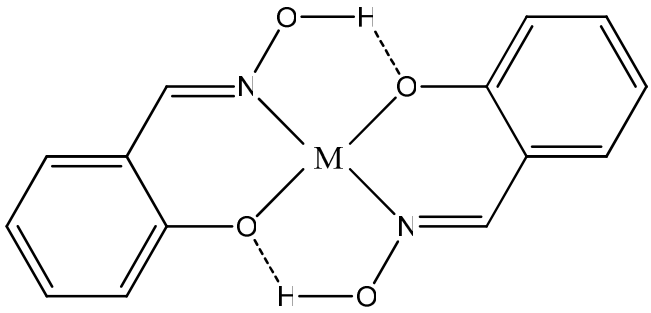

Scheme 1.4 The pseudo-macrocyclic cavity created via Hydrogen-bonding between phenolic oximes a in 2:1 metal complex. M is in the 2+ oxidation state.

1.3 Single-Molecule Magnets

It has been nearly 20 years since the discovery of single molecules that can act as nanomagnets at very low temperatures.[39-41] Such molecules, called Single-Molecule Magnets (SMMs), can retain their magnetisation in the absence of an external field below a certain blocking temperature, T_B, and represent the smallest magnetic device

that may potentially be used in applications such as information storage and quantum computation.[42-45] Their behaviour is due to a large spin ground state, S, and a large, easy-axis (Ising) type anisotropy, characterised by the negative zero-field splitting (ZFS) parameter, D. The ZFS of the ground state creates an energy barrier (Fig. 1.1) for the reorientation of the magnetisation, U, with the $M_S = \pm S$ lying lowest in energy and $M_S = 0$ highest in energy. The upper limit for this energy barrier is given by $S^2|D|$ (for integer spin) or $(S^2-1/4)|D|$ (for half-integer spin). Due to the presence of this energy barrier, the magnetisation induced by an external field is retained when the field is removed and gives rise to hysteresis loops in magnetisation versus field studies (Fig. 1.2) below T_B. At low temperatures the thermally activated reversal of the magnetisation follows the Arrhenius law (1):

$$\tau = \tau_o \exp(U_{eff}/(kT)) \qquad (1)$$

where τ_o is the pre-exponential factor, τ is the relaxation time, U_{eff} is the barrier to the relaxation of the magnetisation and k is the Boltzmann constant. The relaxation times can be of the order of months or even years at very low (< 2 K) temperatures.

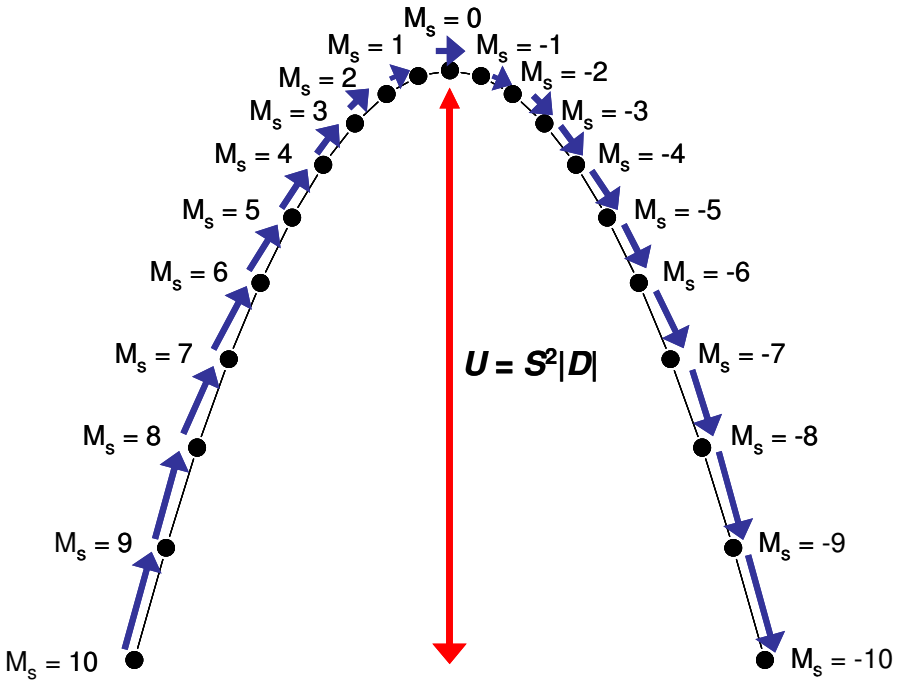

Figure 1.1 Energy diagram showing the zero-field splitting of the M_S levels for a hypothetical $S = 10$ ground state and the energy barrier (U) between the $+M_S$ and $-M_S$ levels. Re-orientation from "spin-up" to "spin-down" requires the magnetisation to go up and over the energy barrier.

Because of their size SMMs truly straddle the quantum/classical interface and were the objects with which theoretically predicted quantum phenomena, such as quantum tunnelling of the magnetisation (QTM)[46, 47] and quantum phase interference (QPI),[48] were first experimentally observed. QTM occurs between energetically matched M_S levels on opposite sides of the barrier and can be observed as steps (relating to a loss of magnetisation) in the hysteresis loops (Fig. 1.2). This behaviour can be described by the following spin-Hamiltonian (2):

$$\hat{\mathcal{H}} = D\hat{S}_z^2 + E(\hat{S}_x - \hat{S}_y) + \mu_B g H \hat{S} \qquad (2)$$

The first term refers to the axial (z) anisotropy of the system responsible for the energy barrier which separates the $+M_S$ and $-M_S$ levels (Fig. 1.1). The third term is the Zeeman splitting caused by the applied field, H, and the second term refers to the transverse anisotropy in the xy plane which does not commute with the axial term allowing the $+M_S$ and $-M_S$ levels to mix and gives rise to tunnelling (Fig. 1.3). That is, in any molecule that possesses symmetry lower than axial, the rhombic term in the

Hamiltonian can mix $+M_S$ and $-M_S$. In truly axial symmetry, QTM is [strictly] forbidden. In zero-field the $+M_S$ and $-M_S$ levels are equal in energy and this corresponds to the most favourable condition to observe tunnelling. When a magnetic field is applied along the z axis (Fig. 1.3) the pairs of $\pm M_S$ levels are no longer degenerate and the tunnelling is suppressed, except for values of $H_z = nD/g\mu_B$ (where n = 0, 1, 2...) when the levels are brought back into resonance again, corresponding to steps seen in hysteresis loops. When tunnelling occurs between any M_S levels, this provides a faster relaxation for the magnetisation resulting in the effective energy barrier (U_{eff}) being smaller than the theoretical upper limit calculated from $S^2|D|$.

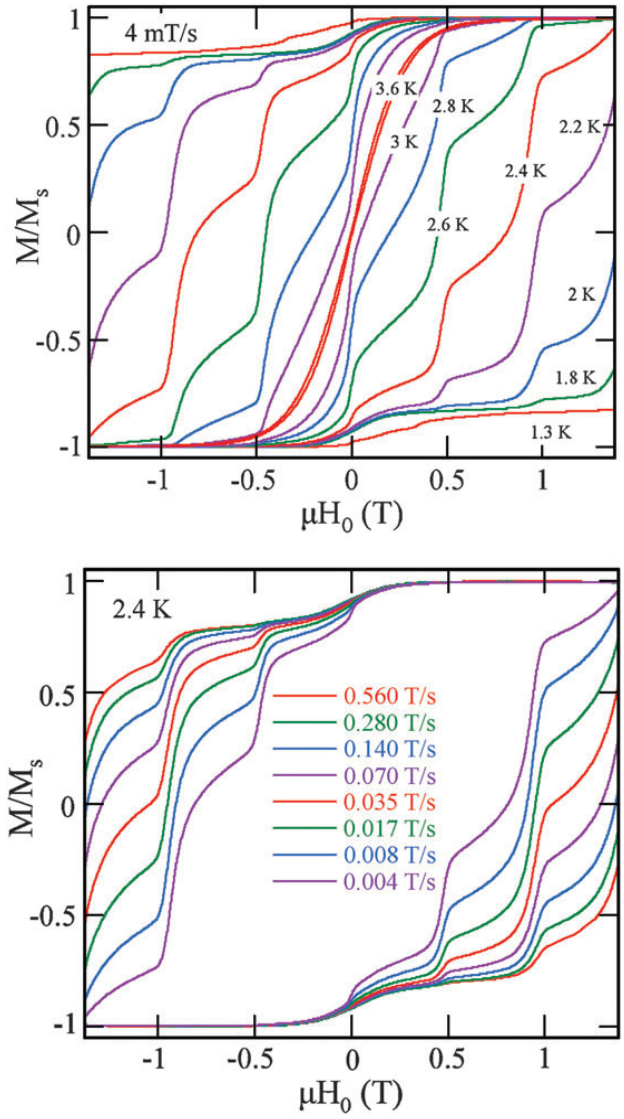

Figure 1.2 Magnetisation (*M, normalised to its saturation value Ms*) versus field hysteresis loops for a single crystal of [Mn_{12}] showing the temperature dependence at a fixed sweep rate (top) and sweep rate dependence at a fixed temperature (bottom). Loops taken from reference [60].

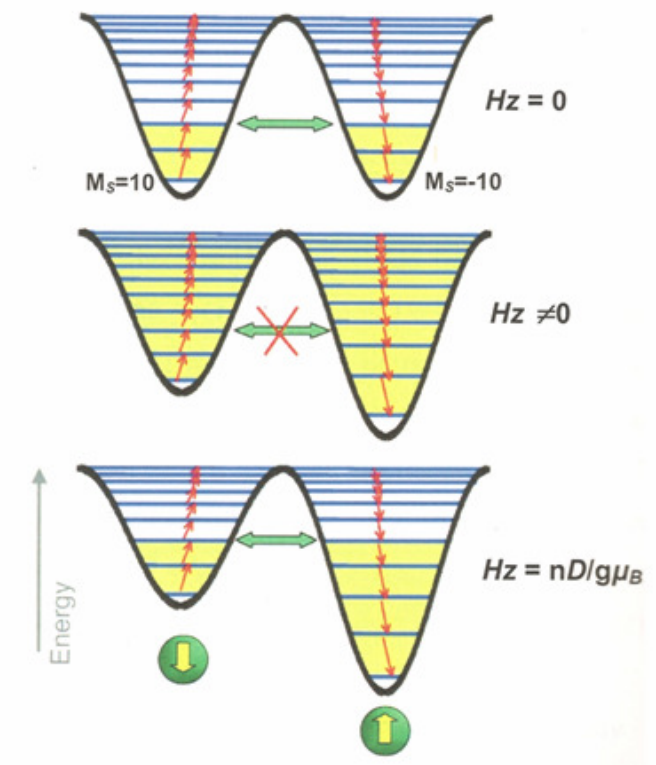

Figure 1.3 Schematic showing the zero-field splitting of the M_S levels for an $S = 10$ ground state. Overcoming the barrier can occur through thermal activation ("up and over the barrier"; red arrows) or through quantum tunnelling of the magnetisation ("through the barrier"; green arrows) (top). When an axial field is applied the levels are no longer degenerate and therefore the tunnelling is suppressed (middle). When the levels come back into resonance at certain values of H_z the tunnelling occurs again (bottom).

1.4 Manganese SMMs

The majority of SMMs reported are made using the 3*d* transition metals, and amongst these manganese is by far the most common.[49] Manganese is a popular choice for two fundamental reasons. 1) In polymetallic complexes, Mn commonly exists in three different oxidation states, Mn^{2+}, Mn^{3+} and Mn^{4+}. Indeed it is rather rare to find reports of homo-valent Mn cluster compounds. Since the overwhelming majority (> 90 %) of nearest-neighbour metal-metal interactions are antiferromagnetic (↑↓) the presence of metal ions in different oxidation states, and thus possessing different numbers of unpaired electrons, will likely lead to the stabilisation of a non-zero ground state. In other words, compared to other 3*d* transition metals, complexes containing Mn ions, are far more likely to have large spin ground state (*S*) values. 2) Mn^{3+} (d^4) ions exhibit a Jahn-Teller distortion (Fig.

1.4), This reduction in symmetry ($O_h \rightarrow D_{4h}$) is crucial because it increases the anisotropy of the ion (d_{ion}) and thus increases the anisotropy of the cluster ($D_{cluster}$), since to a crude approximation $D_{cluster}$ is a vectorial addition of d_{ion}. Thus, the combination of factors (1) and (2) are both conducive to a large value of $S^2|D|$.

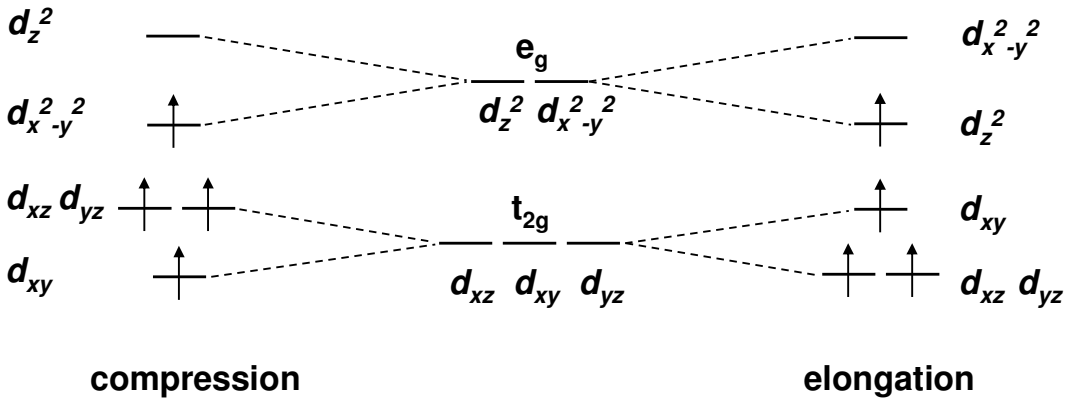

Figure 1.4 Jahn-Teller distortion in a Mn^{3+} ion, showing both compression and elongation along the z-axis.

There are two synthetic methodologies used by coordination chemists in an attempt to construct new complexes with SMM behaviour. The first, and most successful, method is serendipitous self-assembly, whereby ligands with various coordination modes are mixed with a metal salt in a suitable solvent and the outcome is rarely known.[50] This approach has led to the majority of [and best performing] SMMs created so far, with the most famous being the formation of the first SMM, Mn_{12} (*vide infra*). The second method involves using reactants [metals and ligands] possessing less (or no) flexibility in coordination so that the geometry and properties of the product can be [at least in part] predicted. This method is known as "rational molecular design" and typically involves the use of molecular Prussian Blue analogues (*i.e.* they are based on the $[M(CN)_6]^{n-}$ hexacyanometalate ions,) in which transition metal ions have a number of coordination sites filled via polydentate chelating ligands and are bridged to their neighbouring metal ion(s) through the linear CN^- ion.[51] For example, reacting a Ni^{II} salt, tetraethylenepentamine (tetren) pentahydrochloride and $K_3[Co^{III}(CN)_6]$ leads to the formation of a series of $CoNi_n$ species ranging from CoNi to $CoNi_6$.[51] The $CoNi_2$ complex is shown in Fig. 1.5. A

similar approach is to employ more complicated polytopic ligands which contain regularly spaced coordination pockets; for example the use of dihydrazide-type ligands for the formation of grid-like M^{II}_9 complexes (Fig. 1.6).[52] Although aesthetically very pleasing to the eye (and chemically very beautiful), they have proved to be less interesting magnetically.

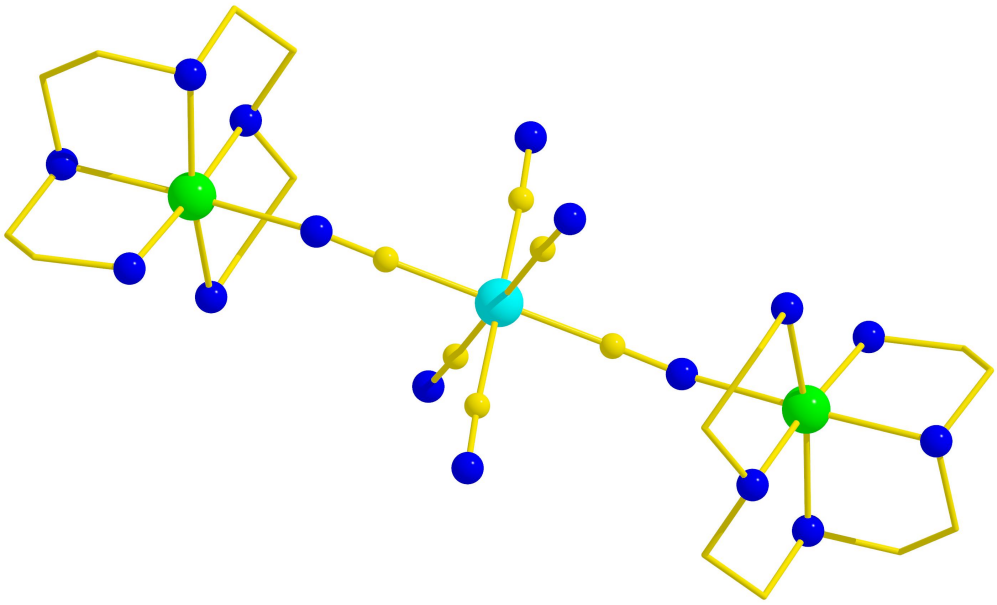

Figure 1.5 The molecular structure of the $[Co^{III}(CN)_4\{(CNNi^{II}(tetren))_2\}]^+$ cation where tetren = tetraethylenepentamine. H-atoms omitted for clarity. Colour code: Co = cyan, Ni = green, N = blue, C = gold.

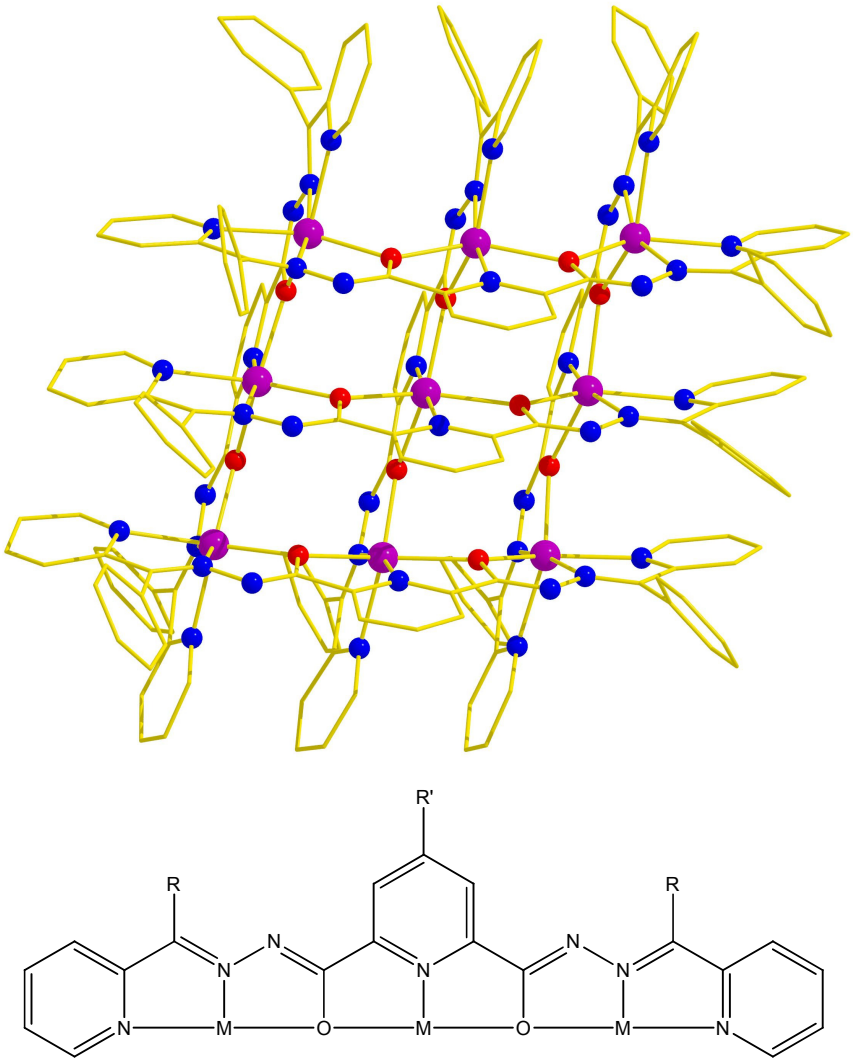

Figure 1.6 The grid-like structure of $[Mn^{II}_{9}(2popp)_{6}]^{6+}$ (top). Tritopic ligand schematic structure (bottom), where R' = H, R = Ph (2popp). H-atoms omitted for clarity. Colour code: Mn = purple, O = red, N = blue, C = gold.

SMM chemistry began with the formation of the dodecanuclear complex $[Mn_{12}O_{12}(O_2CMe)_{16}(H_2O)_4]$, hereafter abbreviated $[Mn_{12}OAc]$ (Fig. 1.7). It was first synthesised and structurally characterised by Lis in 1980, however the initial magnetic measurements reported were not interpreted.[53] It took the serendipitous discovery of a similar complex by the Christou group almost a decade later, $[Mn_{12}O_{12}(O_2CPh)_{16}(H_2O)_4]$,[54] before $[Mn_{12}OAc]$ was fully studied by several techniques including high-field magnetisation, high-frequency EPR and ac susceptibility measurements. The complex was found to have a spin ground state of S = 10 resulting from the eight outer Mn^{III} centres being antiferromagnetically coupled

to the four inner Mn^{IV} centres.[39] The out-of-phase component of the ac susceptibility (χ'') displayed frequency-dependent peaks indicating slow relaxation of the magnetisation and this was confirmed by magnetisation versus field measurements exhibiting hysteresis when cooled to around 2 K. Along with S = 10, the ZFS parameter was found to be $D = -0.50$ cm^{-1}, with $T_B \sim 3$ K giving an effective energy barrier to the reorientation of the magnetisation, U_{eff} = 60-64 K.[40, 41] Despite being the first SMM, the effective energy barrier for [Mn_{12}OAc] remained the highest barrier recorded for over a decade.

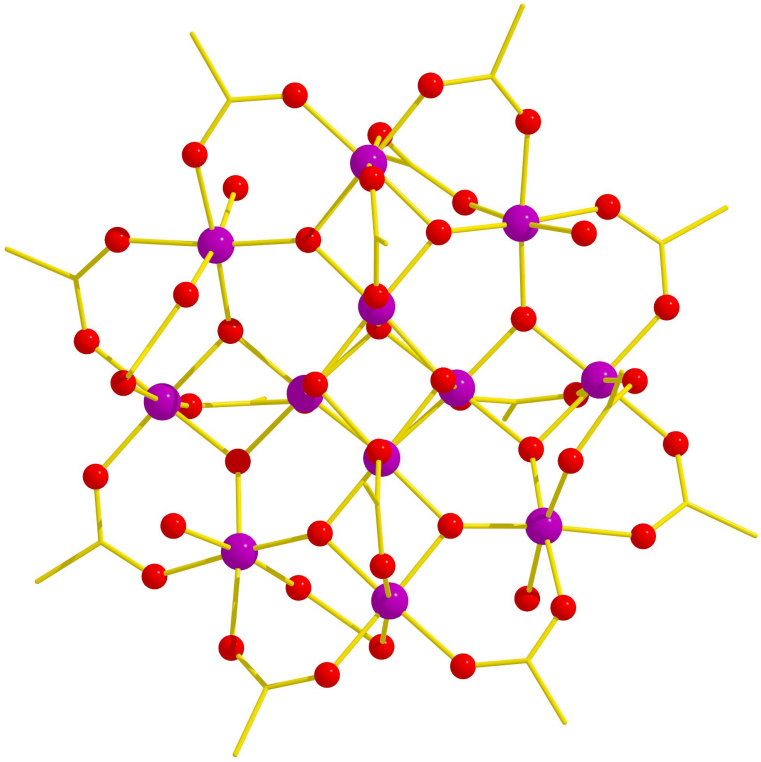

Figure 1.7 The molecular structure of [Mn_{12}OAc]. H-atoms omitted for clarity. Colour code: Mn = purple, O = red, C = gold.

[Mn_{12}OAc] is formed quickly and in high yield, from the oxidation of $Mn(OAc)_2{\cdot}4H_2O$ with MnO_4^- in an acetic acid/water mixture. Since it is extremely easy to make, a large number of [Mn_{12}] derivatives have been formed using different carboxylates,[55] nitrates,[56] phosphinates,[57] sulfonates[58] and dicarboxylates.[59, 60] In 2006, the Christou group synthesised the bromoacetate analogue $[Mn_{12}O_{12}(O_2CCH_2Br)_{16}(H_2O)_4]$ with T_B = 3.5 K and U_{eff} = 74.4 K.[61] The large [Mn_{12}] family is the most studied family of SMMs with detailed analysis of both

their chemistry and physics, and were the first compounds to exhibit quantum tunnelling of the magnetisation[46, 47] and quantum phase interference.[48] Although there are now many Mn SMMs – the reader's attention is drawn to reference [49] for a recent comprehensive review – perhaps the most spectacular (and by far the largest) SMM synthesised is the giant wheel-like complex $[Mn_{84}O_{72}(O_2CMe)_{78}(OMe)_{24}(OH)_6(MeOH)_{12}(H_2O)_{42}]$ (Fig. 1.8).[62] This results from the reaction of $[Mn_{12}OAc]$ with MnO_4^- in a mixture of acetic acid and methanol, producing a molecule with a diameter of ~4.2 nm. Despite its massive size, its magnetic properties are somewhat dull. Dominant antiferromagnetic exchange results in a small spin ground state ($S \approx 6$) and a small effective energy barrier to magnetisation reversal of only U_{eff} = 18 K, approximately 50 K smaller than $Mn_{12}OAc$ and its analogues.

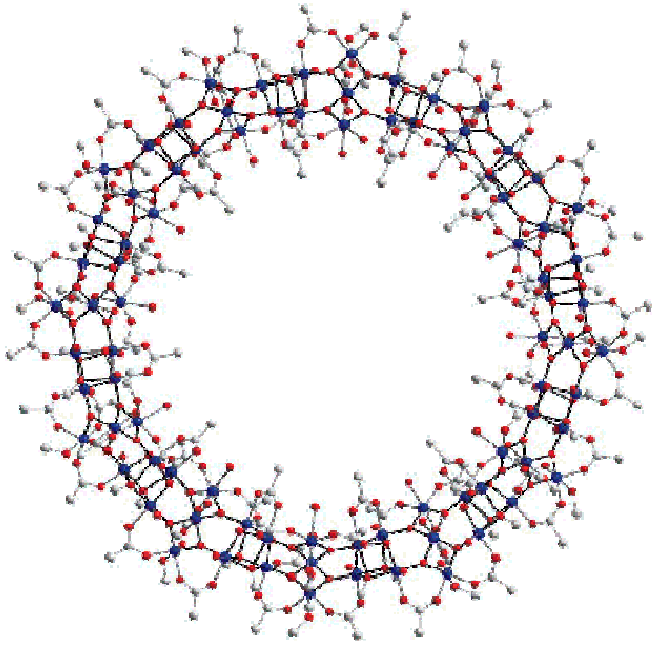

Figure 1.8 The molecular structure of the $[Mn_{84}]$ wheel-like SMM of reference [62]. H-atoms omitted for clarity. Colour code: Mn = blue, O = red, C = grey.

For SMMs to function in real applications – however specialised they may be – the blocking temperature (T_B) to magnetisation reversal needs to be raised. Despite massive interest in this area of chemistry over the last 20 years, until recently the original $[Mn_{12}]$ family of SMMs displayed the highest blocking temperatures. In 2007, the Brechin group synthesised a number of hexanuclear complexes based on the $[Mn^{III}_6O_2(sao)_6(O_2CR)_2L_4]$ (S = 4, U_{eff} = 28 K) family of SMMs (where R = H,

Me, Ph etc, sao^{2-} is the dianion of salicylaldoxime, L = MeOH or EtOH).[36] They found that by using derivatised versions of the salicylaldoxime ligand (Scheme 1.3), it was possible to change the spin ground state from $S = 4$ to $S = 12$, leading to a new family of SMMs with general formula $[Mn^{III}_6O_2(R\text{-}sao)_6(O_2CR')_2L_{4\text{-}6}]$ (where R, R' = H, Me, Et, Ph etc; L = ROH, MeCN, H_2O) with enhanced blocking temperatures.[63, 64] Substituting the ligand from $saoH_2$ to R-$saoH_2$ (Scheme 1.3) causes a subtle structural distortion to the core of the molecule, shown by an increase in the "twisting" of the oxime moiety (Mn-N-O-Mn). It was found that when the Mn-N-O-Mn torsion angle increased above approximately 31.3°, the exchange between the metal centres would switch from weakly antiferromagnetic to weakly ferromagnetic. One of the complexes synthesised was $[Mn^{III}_6O_2(Et\text{-}sao)_6(O_2CPh(Me)_2)_2(EtOH)_6]$ (Fig. 1.9) and was found to have the largest energy barrier for the reversal of the magnetisation with $U_{eff} = 86.4$ K and $T_B = 5$ K.[65]

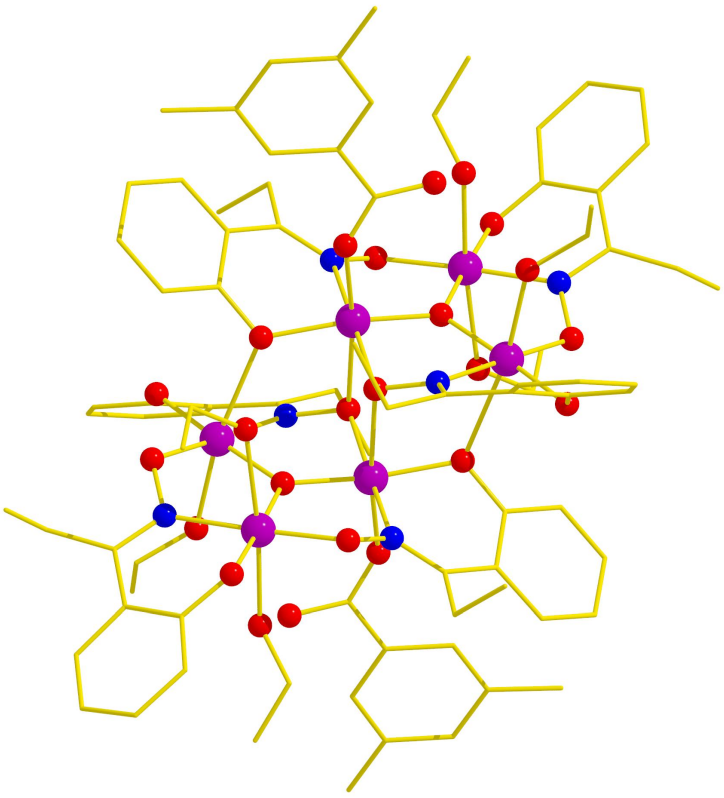

Figure 1.9 The molecular structure of the SMM $[Mn_6O_2(Et\text{-}sao)_6(O_2CPh(Me)_2)_2(EtOH)_6]$. H-atoms omitted for clarity. Colour code: Mn = purple, O = red, N = blue, C = gold.

1.5 SMMs using other 3*d* Metals

Iron (in the 2+ and 3+ oxidation states) complexes make up the second largest [albeit much smaller] family of SMMs, behind manganese, the most famous complex being $[Fe^{III}_8O_2(OH)_{12}(tacn)_6]Br_8$ (where tacn = 1,4,7-triazacyclononane) (Fig. 1.10).[66] Indeed this was the second molecule, after $[Mn_{12}OAc]$, found to exhibit SMM behaviour.[67] Similarly to $[Mn_{12}OAc]$, the complex was discovered almost a decade before it's magnetic properties were identified (S = 10 ground state, D = –0.34 cm^{-1}).[68] Subsequent experimental studies [for the first time] unveiled a plethora of beautiful quantum effects (QTM);[69-71] the detailed physics discovered in this work laying the foundations for our understanding of the physical properties of molecular magnets.

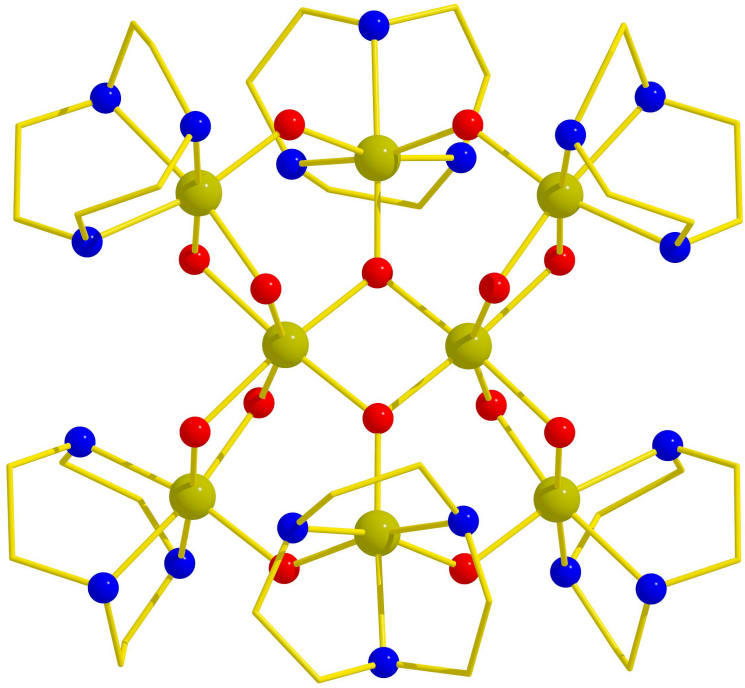

Figure 1.10 The molecular structure of the SMM $[Fe^{III}_8O_2(OH)_{12}(tacn)_6]Br_8$ (where tacn = 1,4,7-triazacyclononane). H-atoms and Br-atoms omitted for clarity. Colour code: Fe = olive green, O = red, N = blue, C = gold.

There are numerous nickel complexes that behave as SMMs, though almost all of them possess very low anisotropy barriers (despite the fact that d_{Ni} can be extremely large).[72] The first synthesised was the wheel-like complex $[Ni^{II}_{12}(chp)_{12}(O_2CMe)_{12}(thf)_6(H_2O)_6]$ (where chp = anion of

chlorohydroxypyridine)[73] which was found to have an $S = 12$ ground state and $D = -0.05$ cm^{-1}.[74] There then followed numerous reports of ferromagnetically coupled Ni_4 cubanes with $S = 4$ ground states[75] that behave as SMMs, but the largest energy barrier to magnetisation reversal belongs to the complex $[Ni_{10}(tmp)_2(N_3)_8(acac)_6(MeOH)_6]$ (H_3tmp = 1,1,1-tris(hydroxymethyl)propane); a ferromagnet with $S = 10$, $D = -0.14$ cm^{-1} and $U_{eff} = 14$ K.[76, 77] Incorporating highly anisotropic single ions into SMM synthesis is of course a very sensible idea since the magnitude of the barrier, at least to a crude first approximation, is dependent upon both S and D. Thus a natural extension to Ni^{2+} coordination chemistry is the examination of Co^{2+}. One might expect the chemistries of these two ions to be somewhat similar and indeed there are also numerous reports of Co^{2+} cubanes purported to be SMMs; the first example being $[Co^{II}_4(hmp)_4(MeOH)_4Cl_4]$ (where hmp = hydroxymethylpyridine)[78] (Fig. 1.11) with an $S = 6$ ground state and $D = -2.78$ cm^{-1}. Other examples include the citrate-based $(C(NH_2)_3)_8[Co_4(cit)_4]$ with $U_{eff} = 21$ K,[79] and the hexanuclear complex $(NMe_4)_3Na[Co^{II}_6(cit)_4(H_2O)_{10}]$ with $S = 3$ whose central core is a cubane.[80] However, in none of these examples – and indeed for any published Co "SMM" – is there clear evidence for sweep rate and temperature dependent hysteresis loops in M vs H studies. Strictly speaking, molecules with zero coercivity at $H = 0$ cannot be labelled as magnets. The explanation for this strange behaviour is still a matter of some debate, but likely results from the huge single ion anisotropy of Co^{2+} (d^7) inducing ultra-fast tunnelling of the magnetisation; *i.e.* the tunnelling between $+M_S$ and $-M_S$ levels is extremely efficient and therefore very fast, and is manifested by the appearance of a very large step at $H = 0$ in the M vs H loops.

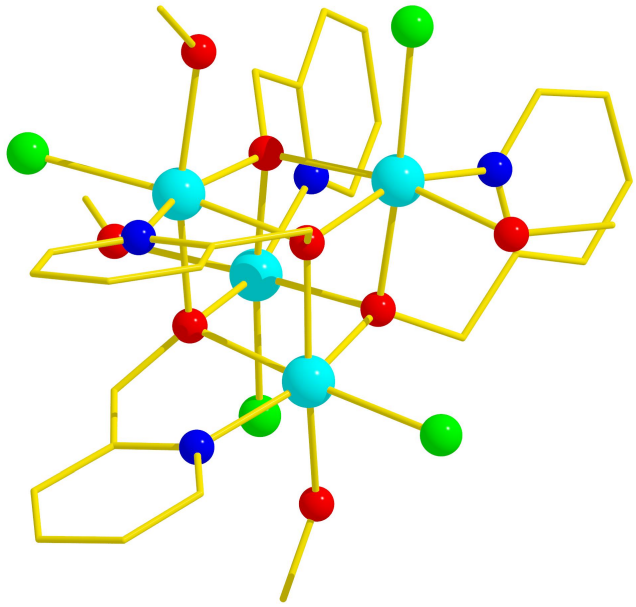

Figure 1.11 The molecular structure of $[Co^{II}_4(hmp)_4(MeOH)_4Cl_4]$ (where hmp = hydroxymethylpyridine). H-atoms omitted for clarity. Colour code: Co = cyan , O = red, N = blue, C = gold, Cl = green.

The *f*-block elements are the most anisotropic in the Periodic Table (as well as providing up to 7 unpaired electrons) and the recent observation that a *mononuclear* Ln^{III} complex could display SMM behaviour – a scenario unheard of in transition metal chemistry – was a remarkable modern development that has re-invigorated research effort in homometallic (*f*) and heterometallic (*d/f*) cluster chemistry.[81-83] The complexes $[LnPc_2]^-$ (Ln = Tb, Dy; Pc = phthalocyanine) show beautiful hysteresis loops in single crystal micro-SQUID studies (Fig 1.12).[82] The origin of this relaxation behaviour is complicated [and different to that seen in the transition metals] but is thought to arise from the zero-field splitting of the ground state angular momentum (*J*) when placed in certain ligand field symmetries, with the anisotropy derived from the sub levels having a large J_z value, thus achieving an easy axis of magnetisation.

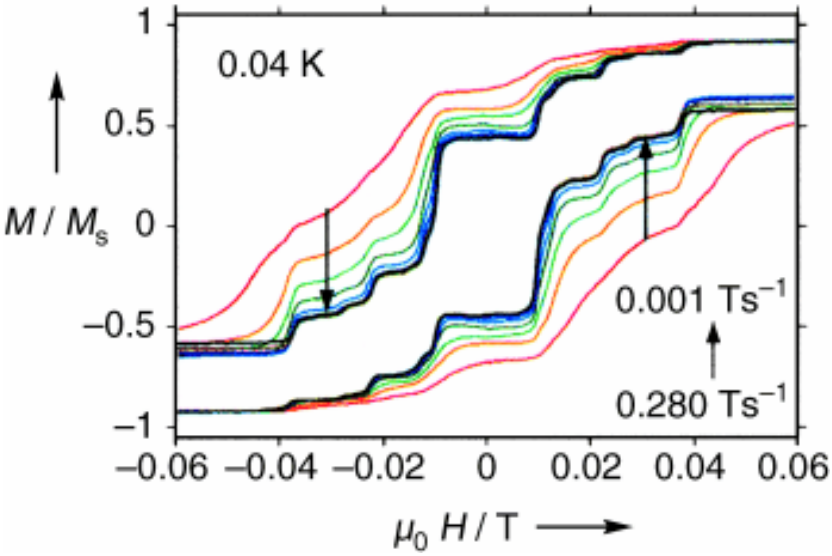

Figure 1.12 Hysteresis loop for $[TbPc_2]^-$ measured at 0.04 K with varying sweep rate. Loops taken from reference [82].

Since this publication several 3*d*-4*f* SMMs, particularly containing Mn(III) or Fe(III), have been synthesised including $[Mn_6Dy_6(H_2shi)_4(Hshi)_{10}(MeOH)_{10}(H_2O)_2]$ (where H_3shi = salicylhydroxamic acid),[84] a $[Mn_{11}Ln_4]^{45+}$ family where Ln = Nd, Gd, Dy, Ho, Eu,[85] $Mn_{11}Gd_2$,[86] a Mn_5Ln_4 family where Ln = Tb, Dy, Ho, Y,[87] Mn_2Dy_2,[88] Fe_2Dy_2[89] and Fe_2Ho_2.[89] Unfortunately detailed interpretation of their magnetic properties can be extremely difficult due to the strong, non-negligible spin-orbit coupling effects of the anisotropic lanthanide ions, and none, as yet, have a T_B higher than $[Mn_6]$.

1.6 Supporting Information

CIF files for the complexes described in the following chapters can be found on the attached CD.

1.7 References

1. B. Bleaney and K. D. Bowers, *Proc. R. Soc. London*, 1952, **A214**, 451.
2. K. Kambe, *J. Phys. Soc. Jpn.*, 1950, **5**, 48.
3. J. N. Van Niekerk and F. R. L. Schoening, *Acta Crystallogr.*, 1953, **6**, 227.
4. B. N. Figgis and G. B. Robertson, *Nature*, 1965, **205**, 694.
5. M. Kato, J. H. B. and J. C. Fanning, *Chem. Rev.*, 1963, **64**, 99.
6. R. J. Doedens, *Prog. Inorg. Chem.*, 1976, **21**, 209.

7. R. L. Martin, *New Pathways in Inorganic Chemistry*, Cambridge University Press, Cambridge, 1968.
8. O. Kahn, *Angew. Chem., Int. Ed.*, 1985, **24**, 834.
9. D. Gatteschi, O. Kahn and R. D. Willett, *Magneto Structural Correlation in Exchange Coupled Systems*, D. Reidel, Dordrecht, 1985.
10. V. H. Crawford, H. W. Richardson, J. R. Wasson, D. J. Hodgson and W. E. Hatfield, *Inorg. Chem.*, 1976, **15**, 2107.
11. W. E. Hatfield, *Comments on Inorganic Chemistry*, 1981, **1**, 105.
12. J. Glerup, D. J. Hodgson and E. Petersen, *Acta Chem. Scand. A*, 1983, **A37**, 161.
13. M. F. Charlot, O. Kahn and M. Drillon, *Chem. Phys.*, 1982, **70**, 177.
14. D. J. Hodgson, in *Magneto Structural Correlations in Exchange Coupled Systems*, eds. D. Gatteschi, O. Kahn and R. D. Willett, Reidel, D, Dordrecht, 1985, pp. 497-522.
15. W. E. Marsh, K. C. Patel, W. E. Hatfield and D. J. Hodgson, *Inorg. Chem.*, 1983, **22**, 511.
16. C. P. Landee and R. E. Greeney, *Inorg. Chem.*, 1986, **25**, 3371.
17. S. S. Tandon, L. K. Thompson, M. E. Manuel and J. N. Brisdon, *Inorg. Chem.*, 1994, **33**, 5555.
18. S. M. Gorun and S. J. Lippard, *Inorg. Chem.*, 1991, **30**, 1625-1630.
19. H. Weihe and H. U. Güdel, *J. Am. Chem. Soc.*, 1997, **119**, 6539.
20. T. Cauchy, E. Ruiz and S. Alvarez, *J. Am. Chem. Soc.*, 2006, **128**, 15722.
21. F. Neese, *J. Am. Chem. Soc.*, 2006, **128**, 10213.
22. M. R. Pederson and S. N. Khanna, *Phys. Rev. B*, 1999, **59**, R693.
23. A. V. Postnikov, J. Kortus and M. R. Pederson, *Physica Status Solidi B*, 2006, **243**, 2533.
24. M. Melnik, *Coord. Chem. Rev.*, 1982, **42**, 259.
25. M. Kato and Y. Muto, *Coord. Chem. Rev.*, 1988, **92**, 45.
26. K. Isele, F. Gigon, A. F. Williams, G. Bernardinelli, P. Franz and S. Decurtins, *Dalton Trans.*, 2007, 332.
27. M. A. Halcrow, J.-S. Sun, J. C. Huffman and G. Christou, *Inorg. Chem.*, 1995, **34**, 4167.
28. J. M. Clemente-Juan, B. Chansou, B. Donnadieu and J.-P. Tuchagues, *Inorg. Chem.*, 2000, **39**, 5515.
29. O. Kahn, *Molecular Magnetism*, VCH Publishers, New York, 1993.
30. E. Ruiz, in *Structure and Bonding*, Springer, 2004, vol. 113.
31. P. A. Tasker, P. G. Plieger and L. C. West, *Compr. Coord. Chem. II*, 2004, **9**, 759.
32. J. M. Thorpe, R. L. Beddoes, D. Collison, C. D. Garner, M. Helliwell, J. M. Holmes and P. A. Tasker, *Angew. Chem., Int. Ed.*, 1999, **38**, 1119.
33. J. Szymanowski, *J. Radioan. Nucl. Ch. Ar.*, 1996, **208**, 183.
34. A. G. Smith, P. A. Tasker and D. J. White, *Coord. Chem. Rev.*, 2003, **241**, 61.
35. P. Chaudhuri, M. Hess, E. Rentschler, T. Weyhermüller and U. Flörke, *New. J. Chem.*, 1998, 553.
36. C. J. Milios, C. P. Raptopoulou, A. Terzis, F. Lloret, R. Vicente, S. P. Perlepes and A. Escuer, *Angew. Chem., Int. Ed.*, 2004, **43**, 210.
37. K. Mason, I. A. Gass, S. Parsons, A. Collins, F. J. White, A. M. Z. Slawin, E. K. Brechin and P. A. Tasker, *Dalton Trans.*, 2010, **39**, 2727.

38. W.-K. Dong, J.-L. Duan, Y.-H. Guan, J.-Y. Shi and C.-Y. Zhao, *Inorg. Chim. Acta*, 2009, **362**, 1129.
39. A. Caneschi, D. Gatteschi, R. Sessoli, A.-L. Barra, L. C. Brunel and M. Guillot, *J. Am. Chem. Soc.*, 1991, **113**, 5873.
40. R. Sessoli, H.-L. Tsai, A. R. Schake, S. Wang, J. B. Vincent, K. Folting, D. Gatteschi, G. Christou and D. N. Hendrickson, *J. Am. Chem. Soc.*, 1993, **115**, 1804.
41. R. Sessoli, D. Gatteschi, A. Caneschi and M. A. Novak, *Nature*, 1993, **365**, 141.
42. G. Christou, D. Gatteschi, D. N. Hendrickson and R. Sessoli, *MRS Bull.*, 2000, **25**, 266.
43. D. Gatteschi and R. Sessoli, *Angew. Chem., Int. Ed.*, 2003, **42**, 268.
44. R. Bircher, G. Chaboussant, C. Dobe, H. U. Güdel, S. T. Ochsenbein, A. Sieber and O. Waldmann, *Adv. Funct. Mater.*, 2006, **16**, 209.
45. J. Tejada, E. M. Chudnovsky, E. del Barco, J. M. Hernandez and T. P. Spiller, *Nanotechnology*, 2001, **12**, 181.
46. J. R. Friedman, M. P. Sarachik, J. Tejada and R. Ziolo, *Phys. Rev. Lett.*, 1996, **76**, 3830.
47. L. Thomas, F. Lionti, R. Ballou, D. Gatteschi, R. Sessoli and B. Barbara, *Nature*, 1996, **383**, 145.
48. W. Wernsdorfer and R. Sessoli, *Science*, 1999, **284**, 133.
49. G. Aromí and E. K. Brechin, in *Structure and Bonding*, Springer, 2006, vol. 122, ch. 1.
50. R. E. P. Winpenny, *J. Chem. Soc., Dalton Trans.*, 2002, 1.
51. V. Marvaud, C. Decroix, A. Scuiller, F. Tuyeras, C. Guyardduhayon, J. Vaissermann, M. Marrot, F. Gonnet and M. Verdaguer, *Chem. Eur. J*, 2003, **9**, 1692.
52. L. Zhao, Z. Xu, H. Grove, V. A. Milway, L. N. Dawe, T. S. M. Abedin, L. K. Thompson, T. L. Kelly, R. G. Harvey, D. O. Miller, L. Weeks, J. G. Shapter and K. J. Pope, *Inorg. Chem.*, 2004, **43**, 3812.
53. T. Lis, *Acta Crystallogr.*, 1980, **B36**, 2042.
54. P. D. W. Boyd, Q. Li, J. B. Vincent, K. Folting, H.-R. Chang, W. E. Streib, J. C. Huffman, G. Christou and D. N. Hendrickson, *J. Am. Chem. Soc.*, 1988, **110**, 8537.
55. H. J. Eppley, H.-L. Tsai, N. de Vries, K. Folting, G. Christou and D. N. Hendrickson, *J. Am. Chem. Soc.*, 1995, **117**, 301.
56. P. Artus, C. Boscovic, J. Yoo, W. E. Streib, L. C. Brunel, D. N. Hendrickson and G. Christou, *Inorg. Chem.*, 2001, **40**, 4199.
57. C. Boskovic, M. Pink, J. C. Huffman, D. N. Hendrickson and G. Christou, *J. Am. Chem. Soc.*, 2001, **123**, 9914.
58. N. E. Chakov, W. Wernsdorfer, K. A. Abboud, D. N. Hendrickson and G. Christou, *Dalton Trans.*, 2003, 2243.
59. M. Pacchioni, A. Cornia, A. C. Fabretti, L. Zobbi, D. Bonacchi, A. Caneschi, G. Chastanet, D. Gatteschi and R. Sessoli, *Chem. Commun.*, 2004, 2604.
60. R. Bagai and G. Christou, *Chem. Soc. Rev.*, 2009, **38**, 1011.
61. N. E. Chakov, S.-C. Lee, A. G. Harter, P. L. Kuhns, A. P. Reyes, S. O. Hill, N. S. Dalal, W. Wernsdorfer, K. A. Abboud and G. Christou, *J. Am. Chem. Soc.*, 2006, **128**, 6975.

62. A. J. Tasiopoulos, A. Vinslava, W. Wernsdorfer, K. A. Abboud and G. Christou, *Angew. Chem., Int. Ed.*, 2004, **43**, 2117.
63. C. J. Milios, A. Vinslava, W. Wernsdorfer, A. Prescimone, P. A. Wood, S. Parsons, S. P. Perlepes, G. Christou and E. K. Brechin, *J. Am. Chem. Soc.*, 2007, **129**, 6547.
64. C. J. Milios, R. Inglis, A. Vinslava, R. Baghi, W. Wernsdorfer, S. Parsons, S. P. Perlepes, G. Christou and E. K. Brechin, *J. Am. Chem. Soc.*, 2007, **129**, 12505.
65. C. J. Milios, A. Vinslava, W. Wernsdorfer, S. A. Moggach, S. Parsons, S. P. Perlepes, G. Christou and E. K. Brechin, *J. Am. Chem. Soc.*, 2007, **129**, 2754.
66. K. Wieghardt, K. Pohl, I. Jibril and G. Huttner, *Angew. Chem., Int. Ed.*, 1984, **23**, 77.
67. C. Sangregorio, T. Ohm, C. Paulsen, R. Sessoli and D. Gatteschi, *Phys. Rev. Lett.*, 1997, **78**, 4645.
68. C. Delfs, D. Gatteschi, L. Pardi, R. Sessoli, K. Wieghardt and D. Hanke, *Inorg. Chem.*, 1993, **32**, 3099.
69. T. Ohm, C. Sangregorio and C. Paulsen, *Eur. Phys. J. B*, 1998, **6**, 195.
70. T. Ohm, C. Sangregorio and C. Paulsen, *J. Low Temp. Phys.*, 1998, **113**, 1141.
71. W. Wernsdorfer, T. Ohm, C. Sangregorio, R. Sessoli, D. Mailly and C. Paulsen, *Phys. Rev. Lett.*, 1999, **82**, 3903.
72. R. Boča, *Coord. Chem. Rev.*, 2004, **248**, 757.
73. A. J. Blake, C. M. Grant, S. Parsons, J. M. Rawson and R. E. P. Winpenny, *J. Chem. Soc., Chem. Commun.*, 1994, 2363.
74. C. Cadiou, M. Murrie, C. Paulsen, V. Villar, W. Wernsdorfer and R. E. P. Winpenny, *Chem. Commun.*, 2001, 2666.
75. M. Moragues-Cánovas, M. Helliwell, L. Ricard, E. Rivière, W. Wernsdorfer, E. K. Brechin and T. Mallah, *Eur. J. Inorg. Chem*, 2004, 2219.
76. G. Aromí, S. Parsons, W. Wernsdorfer, E. K. Brechin and E. J. L. McInnes, *Chem. Commun.*, 2005, 5038.
77. R. T. W. Scott, L. F. Jones, I. S. Tidmarsh, B. Breeze, R. H. Laye, J. Wolowska, D. J. Stone, A. Collins, S. Parsons, W. Wernsdorfer, G. Aromí, E. J. L. McInnes and E. K. Brechin, *Chem. Eur. J*, 2009, **15**, 12389.
78. E.-C. Yang, D. N. Hendrickson, W. Wernsdorfer, M. Nakano, L. N. Zakharov, R. D. Sommer, A. L. Rheingold, M. Ledezma-Gairaud and G. Christou, *J. Appl. Phys.*, 2002, **91**, 7382.
79. K. W. Galloway, A. M. Whyte, W. Wernsdorfer, J. Sanchez-Benitez, K. V. Kamenev, A. Parkin, R. D. Peacock and M. Murrie, *Inorg. Chem.*, 2008, **47**, 7438.
80. M. Murrie, S. J. Teat, H. Stoeckli-Evans and H. Güdel, *Angew. Chem., Int. Ed.*, 2003, **42**, 4653.
81. N. Ishikawa, M. Sugita, T. Ishikawa, S.-Y. Koshihara and Y. Kaizu, *J. Phys. Chem. B*, 2004, **108**, 11265.
82. N. Ishikawa, M. Sugita and W. Wernsdorfer, *Angew. Chem., Int. Ed.*, 2005, **44**, 2931.
83. M. A. AlDamen, J. M. Clemente-Juan, E. Coronado, C. Martí-Gastaldo and A. Gaita-Arino, *J. Am. Chem. Soc.*, 2008, **130**, 8874.

84. C. Zaleski, E. Depperman, J. Kampf, M. Kirk and V. Pecoraro, *Angew. Chem., Int. Ed.*, 2004, **43**, 3912.
85. A. Mishra, W. Wernsdorfer, K. A. Abboud and G. Christou, *J. Am. Chem. Soc.*, 2004, **126**, 15648.
86. V. Mereacre, A. M. Ako, R. Clérac, W. Wernsdorfer, G. Filoti, J. Bartolomé, C. E. Anson and A. Powell, *J. Am. Chem. Soc.*, 2007, **129**, 9248.
87. V. Mereacre, A. M. Ako, R. Clérac, W. Wernsdorfer, I. Hewitt, C. E. Anson and A. Powell, *Chem. Eur. J*, 2008, **14**, 3577.
88. A. Mishra, W. Wernsdorfer, S. Parsons, G. Christou and E. K. Brechin, *Chem. Commun.*, 2005, 2086.
89. M. Murugesu, A. Mishra, W. Wernsdorfer, K. A. Abboud and G. Christou, *Polyhedron*, 2006, **25**, 613.

Chapter 2

Relating Structure and Magnetism in a Large Family of Mn_6 SMMs

2.1 Introduction

It is important not just to make new examples of SMMs, but also to build up families of related compounds so that structure-property relations can be investigated.[1, 2] For example, such studies on $[Mn_{12}O_{12}(O_2CR)_4(H_2O)_4]$ complexes have included variation of the carboxylate ligand,[3] variation of the oxidation level by cluster reduction[4-6] and replacement of the carboxylate ligands with non-carboxylate groups.[7, 8]

As part of our interest in the modification and reactivity properties of known SMMs, we have recently been turning our attention to the $[Mn^{III}_6O_2(sao)_6(O_2CR)_2L_4]$ family of SMMs,[9] where R = H, Me, Ph etc, sao^{2-} is the dianion of salicylaldoxime or 2-hydroxybenzaldeyhyde oxime (Scheme 2.1) and L a coordinated solvent, normally an alcohol. The core of these complexes (Figure 2.1) contains a non-planar $[Mn^{III}_6(\mu_3\text{-}O^{2-})_2(\mu_2\text{-}OR)_2]^{12+}$ unit of two off-set, stacked $[Mn^{III}_3(\mu_3\text{-}O^{2-})]^{7+}$ triangular subunits linked by two central oximate oxygen atoms, with the remaining four sao^{2-} ligands bridging in a $\eta^1{:}\eta^1{:}\eta^1{:}\mu$ fashion along the edges of the $[Mn^{III}_3(\mu_3\text{-}O^{2-})]^{7+}$ triangles. The four 'central' metal ions are six-coordinate and in distorted octahedral geometries, while the outermost Mn ions have square pyramidal geometries with an axial contact of 3.5 Å to a phenoxide oxygen. These complexes display an $S = 4$ spin ground state as a result of ferromagnetic exchange between the two antiferromagnetically coupled Mn^{III}_3 triangles.

The initial stimulus came from the study of the origin of the ferromagnetic exchange in a reported oxo-centered triangular Mn(III) SMM based on the derivatised oximate ligand methyl 2-pyridyl ketone oxime (mpkoH, Scheme 2.1);[10] this ferromagnetic behaviour is intriguing since the exchange in all other complexes containing the $[Mn^{III}_3(\mu_3\text{-}O^{2-})]^{7+}$ core, including the well known 'basic carboxylates' of general formula $[Mn^{III}_3O(O_2CR)_6L_3]^+$ (R=Me, Et, Ph; L= py, MeCN, H_2O, *etc*),[11] is antiferromagnetic. We speculate that a structural distortion in the molecule caused primarily by the '*twisting*' of the oximato groups with regard to the Mn_3 plane, is responsible. In order to evaluate the relative importance of this *'twisting'*, we decided to use a family of ligands based on $saoH_2$ in which the oximate carbon atom has been

derivatised to possess the 'bulky' Me (Me-saoH$_2$), Et (Et-saoH$_2$) and Ph (Ph-saoH$_2$) groups (Scheme 2.1) in combination with 'bulky' carboxylates, and synthesise analogues of the Mn_6/sao^{2-} family with general formula [$Mn^{III}_6O_2$(R-sao)$_6$(O_2CR')$_2$L$_{4-6}$], where R, R' = H, Me, Et, Ph etc; L = ROH, MeCN, H_2O. The central idea was to investigate whether the additional steric bulk would enforce similar minor structural distortions to that seen in the ferromagnetic Mn_3/O^{2-}/mpko$^-$ triangle,[10] and thus switch the magnetic behaviour from antiferromagnetic to ferromagnetic and improve the SMM properties.

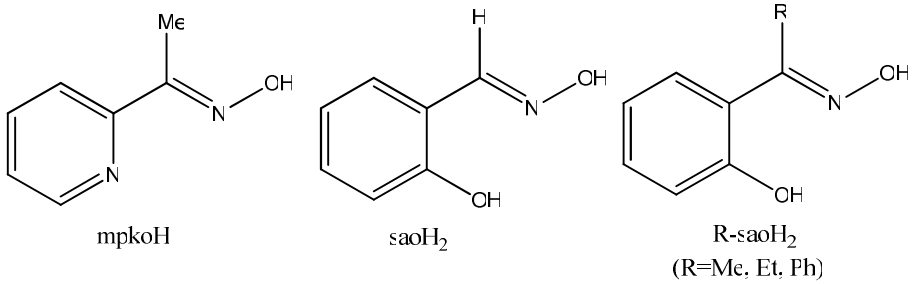

Scheme 2.1 The structural formulae of the main ligands discussed in the text.

This idea proved to be successful with the synthesis of several new Mn_6 complexes where we showed that it is indeed possible to *significantly* increase the spin ground state by controlled increase of the steric bulk within the oximate and carboxylate ligation. Specifically, the ligand-induced structural distortion (giving much larger Mn-N-O-Mn torsion angles) causes the ground state to increase from S = 4 to S = 12 and leads to enhanced SMM properties.[12, 13] The complex [$Mn^{III}_6O_2$(Et-sao)$_6$(O_2CPh(Me)$_2$)$_2$(EtOH)$_6$] has a record value for the energy barrier to magnetisation reversal, U_{eff} = 86.4 K, with sweep rate and temperature dependent hysteresis loops observed in *M vs*. *H* studies at temperatures up to 5 K.[14]

Initial studies on the first few members of this Mn_6 family suggested a correlation between the Mn-N-O-Mn torsion angles, J values and U_{eff}. That is, the bigger the torsion angle, the larger (more positive) the exchange, and the larger the U_{eff}. To try and establish a relationship between the structure and magnetic properties for this family of Mn_6 SMMs, a large number of examples need to be synthesised.

This chapter begins with the synthesis and characterisation of 22 members of the Mn_6 SMM family and highlights a magneto-structural correlation whereby the type

of each Mn_2 pairwise magnetic exchange is dominated by the magnitude of each individual Mn-N-O-Mn torsion angle.

With over 20 Mn^{III}_6/R-sao^{2-}/carboxylate complexes fully studied, one question that arose from these studies was whether the use of the bulky carboxylates was actually necessary and/or whether their presence at some point becomes a hindrance in the efforts to further distort the molecules. As a result we attempted to replace the carboxylate ligands with other negatively charged ligands, such as halides and phosphinates,[15-17] to examine the effect upon the structural geometry and the observed magnetic behaviour.

This chapter concludes with the synthesis and characterisation of a new sub-family of Mn_6 complexes with the general formula $[Mn^{III}_6O_2(R\text{-sao})_6(X)_2(ROH)_{4-6}]$, where R = H, Me, Et or Ph; X = Br, I, O_2PHPh or $O_2P(Ph)_2$.

2.2 Towards a Magneto-structural Correlation for a Large Family of Mn_6 SMMs

2.2.1 Experimental Section

Synthesis

All manipulations were performed under aerobic conditions, using materials as received. CAUTION! Although no problems were encountered in this work, care should be taken when using the potentially explosive perchlorate anion.

Two methods (A and B) were used in synthesising the twenty two complexes. Method A was attempted first, producing complexes **2.1**, **2.3**-**2.7**. When Method A was unsuccessful, Method B was attempted and yielded the rest of the complexes. General synthetic strategies:

Method A. To pale pink solutions of $Mn(ClO_4)_2{\cdot}6H_2O$ (1 mmol) in MeOH (EtOH or MeCN) were added the derivatised oximes (1 mmol), the corresponding carboxylic acid (1 mmol) and CH_3ONa (or NEt_4OH) (1 mmol). The solutions were left stirring for ~30 min, filtered and then left to slowly evaporate. In each case suitable crystals grew after a period of 3-5 days.

Method B. The sodium salt of the corresponding carboxylic acid was treated with equivalent amounts of $Mn(ClO_4)_2 \cdot 6H_2O$, the derivatised oximes and CH_3ONa (or NEt_4OH) in MeOH (or EtOH), again with a 1:1:1:1 molar ratio. After ~30 min of stirring, the solutions were filtered and left to slowly evaporate. X-ray quality single crystals grew after 3-5 days.

X-ray crystallography

Diffraction data were collected at 150 K on a Bruker Smart Apex CCDC diffractometer, equipped with an Oxford Cryosystems LT device, using Mo radiation.[18] See CIF files for full details.

Magnetic measurements

Variable temperature, solid-state direct current (dc) and alternating current (ac) magnetic susceptibility data down to 1.8 K were collected on a Quantum Design MPMS-XL SQUID magnetometer equipped with a 7 T dc magnet. Diamagnetic corrections were applied to the observed paramagnetic susceptibilities using Pascal's constants. Magnetic studies below 1.8 K were carried out on single crystals using a micro-SQUID apparatus operating down to 40 mK.[19]

2.2.2 Results and Discussion

Description of structures

All twenty two complexes display very similar molecular structures; interatomic distances and angles relevant to the discussion herein are shown in Table 2.1 (page 46). All molecules possess an inversion centre, besides complex **2.9** which lacks any molecular symmetry. They can be described (Figs. 2.1 and 2.2) as consisting of two parallel off-set, stacked $[Mn^{III}_3(\mu_3\text{-}O)]^{7+}$ triangular subunits linked *via* two 'central' oximate O-atoms (O_{oxim}) and two 'peripheral' phenolate O-atoms (O_{ph}), leading to a $[Mn^{III}_6(\mu_3\text{-}O)_2(\mu_3\text{-}ONR)_2(\mu\text{-}ONR)_4]^{8+}$ core. The bridging between neighbouring Mn ions within each triangle occurs through an NO oximate group, such that each Mn_2 pair forms a -Mn-N-O-Mn- moiety, and thus the Mn_3 triangle a $(\text{-Mn-O-N-})_3$ ring. In all complexes the coordination spheres of the Mn ions are completed by two terminal carboxylates (one on each triangle; except for complexes **2.1, 2.3-2.5** where the

carboxylates are bridging in a $\eta^1:\eta^1:\mu$ fashion), a phenoxide O-atom, and by terminal alcohol solvate molecules and/or H_2O molecules. All Mn ions are in the 3+ oxidation state, as confirmed by a combination of bond-length considerations, BVS calculations[20-23] and charge-balance with their Jahn-Teller axes all lying perpendicular to the $[Mn_3O]^{7+}$ planes.

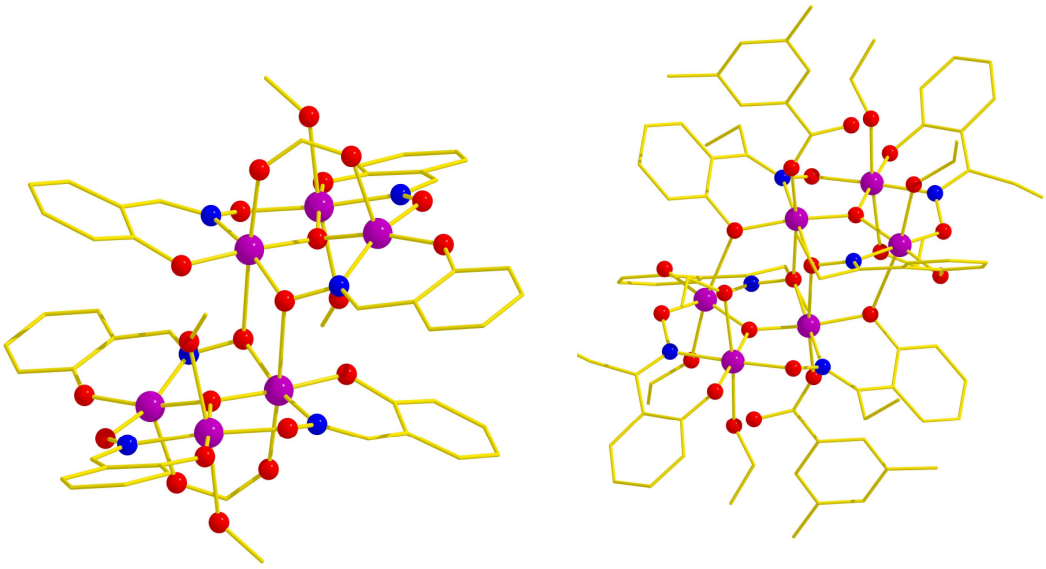

Figure 2.1 The molecular structures of **2.1** (left) and **2.15** (right) representing the two different structural types in the $[Mn_6]$ family. Colour code: Purple = Manganese, Red = Oxygen and Blue = Nitrogen.

More detailed structural comparisons show that we can subdivide the 22-member family into two general types, $[Mn^{III}_6O_2(R\text{-}sao)_6(X)_2(sol)_4]$ and $[Mn^{III}_6O_2(R\text{-}sao)_6(X)_2(sol)_{5,6}]$, as a consequence of the distortion imparted on the core via the inclusion of increasingly bulky oxime ligands. This is illustrated in Figs. 2.1 and 2.2. Approximately half the family appear to possess two symmetry equivalent (s.e.) square-based pyramidal five-coordinate Mn^{III} ions (Fig 2.2). On closer inspection it becomes clear that the Mn-O_{phen} distances vary greatly and range from a relatively short 2.374 Å in **2.17** to a rather long 3.524 Å in **2.1**. These Mn-O_{phen} interactions form two symmetry equivalent bridges (when sufficiently close) between the two $[Mn_3O(R\text{-}sao)_3]^+$ units which add to the two ever-present symmetry equivalent Mn-O_{oxim} bridges located at the "centre" of the $[Mn_6]$ cores (Fig. 2.2). $[Mn_6O_2(Et\text{-}sao)_6(O_2CPh^2OPh)_2(EtOH)_4]$ (**2.10**) differs to all others in this respect by possessing a genuine five coordinate Mn^{III} situated at the periphery of the $[Mn_6]$ core and

isolated from any O_{phen} or O_{oxim} donor atoms. Table 2.1 shows that the Mn-O_{phen} distances decrease as the [Mn_6] cores become more structurally distorted (the oximes employed are bulkier). The second major structural difference lies in the individual Mn-N-O-Mn torsion angles (α) within each [Mn_3O(R-sao)$_3$] unit which range from a minimum of 8.36º (in **2.4**) to a maximum of 47.56º (in **2.10**). As previously suggested,[24] it is clear that the individual Mn-N-O-Mn torsion angles are relatively small when the underivatised (or "planar") sao^{2-} ligands are employed in their construction (ranging from 8.36 to 29.83º), and become much larger (ranging from 16.76 to 47.56º) when the functionalised ("non-planar") Me-sao^{2-} and Et-sao^{2-} ligands are used. Finally, we can see that as the bulk of the oxime is increased and the triangles become more puckered it becomes impossible for the carboxylate ligand to bridge and it becomes terminally ligated instead of μ-bridging, with the vacated site occupied by an additional solvent molecule.

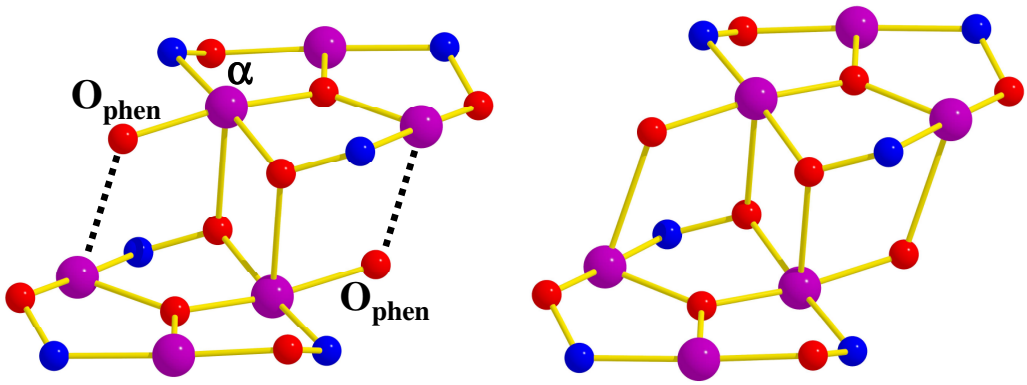

Figure 2.2 (left) The [Mn_6] core common to **2.1** and its analogues in which the carboxylate is bridging, showing the Mn-O_{phen} interaction involving a 5-coordinate Mn^{III} ion. (right) The [Mn_6] core common to **2.15** and its analogues in which the carboxylate is terminally bonded. The Mn-N-O-Mn torsion angle is denoted α. Colour code as Fig. 1.

In short, as we replace sao^{2-} with its bulkier analogues R-sao^{2-} we force the carboxylate to bridge terminally, the Mn-O-N-Mn angle to be increasingly twisted (non-planar) and the Mn-O_{phen} distance to become shorter.

In general there are no significant intermolecular interactions observed between the individual [Mn_6] clusters containing bridging / terminal carboxylates (**2.1**-**2.22**). In some cases non-bonding solvent molecules of crystallisation (MeOH / EtOH) act as H-bonding connectors, linking the [Mn_6] moieties together via ROH…O_{phen} (R = Me, Et) interactions (e.g. as observed in **2.2**, **2.3**, **2.6** and **2.17**).

2.2.3 Magnetochemistry

Dc magnetic susceptibility and magnetisation measurements

Dc magnetic susceptibility studies were carried out on crystalline samples of **2.1**-**2.22** in the 5 - 300 K temperature range in a field of 0.1 T. The magnetic susceptibility data obtained from each member were simulated using the MAGPACK[25] program employing the Hamiltonians in (1)-(3) (Scheme 2.2) to provide the isotropic parameters *S*, *J* and *g* summarised in Table 2.2. Figs. 2.3 and 2.4 show the $\chi_M T$ vs. *T* data and, where possible, their associated simulations (solid lines). It is clear from Table 2.2 that the experimental data do not really allow for an unequivocal determination of the ground spin state since there are many *S* states that are essentially degenerate; for example, see complexes **2.7**, **2.10**, **2.11**, **2.12** and **2.13**. However, we enter the values from the simulations for completeness. The magnetic susceptibility curves obtained illustrate how, despite their structural similarities, complexes **2.1**-**2.22** show dramatically different magnetic behaviour.

$$\hat{H} = -2J(\hat{S}_1\cdot\hat{S}_2 + \hat{S}_2\cdot\hat{S}_3 + \hat{S}_1\cdot\hat{S}_3 + \hat{S}_1\cdot\hat{S}_{2'} + \hat{S}_{2'}\cdot\hat{S}_{3'} + \hat{S}_1\cdot\hat{S}_{3'} + \hat{S}_2\cdot\hat{S}_{3'} + \hat{S}_{2'}\cdot\hat{S}_3 + \hat{S}_2\cdot\hat{S}_{2'}) \quad (1)$$

$$\hat{H} = -2J_1(\hat{S}_1\cdot\hat{S}_2 + \hat{S}_2\cdot\hat{S}_3 + \hat{S}_2\cdot\hat{S}_{3'} + \hat{S}_{2'}\cdot\hat{S}_3 + \hat{S}_1\cdot\hat{S}_{2'} + \hat{S}_2\cdot\hat{S}_{2'} + \hat{S}_{2'}\cdot\hat{S}_{3'}) - 2J_2(\hat{S}_1\cdot\hat{S}_3 + \hat{S}_1\cdot\hat{S}_{3'}) \quad (2)$$

$$\hat{H} = -2J_1(\hat{S}_1\cdot\hat{S}_2 + \hat{S}_2\cdot\hat{S}_3 + \hat{S}_1\cdot\hat{S}_{2'} + \hat{S}_{2'}\cdot\hat{S}_{3'}) - 2J_2(\hat{S}_1\cdot\hat{S}_3 + \hat{S}_1\cdot\hat{S}_{3'}) - 2J_3(\hat{S}_2\cdot\hat{S}_{3'} + \hat{S}_2\cdot\hat{S}_{2'} + \hat{S}_{2'}\cdot\hat{S}_3) \quad (3)$$

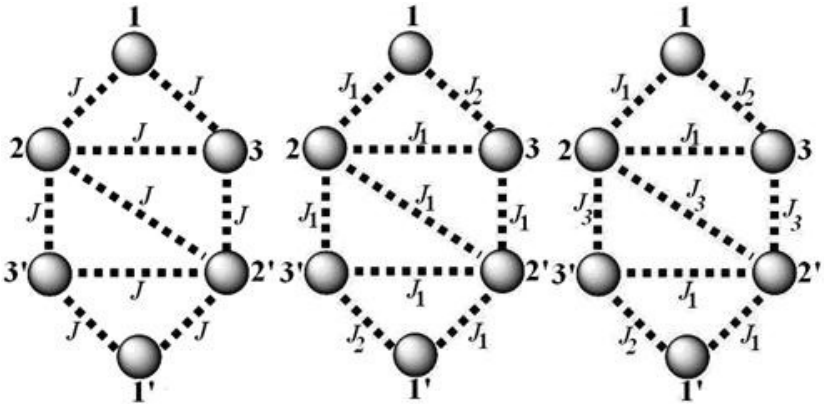

Scheme 2.2 Schematic detailing the 1, 2- and 3-*J* models employed to simulate the experimental data.

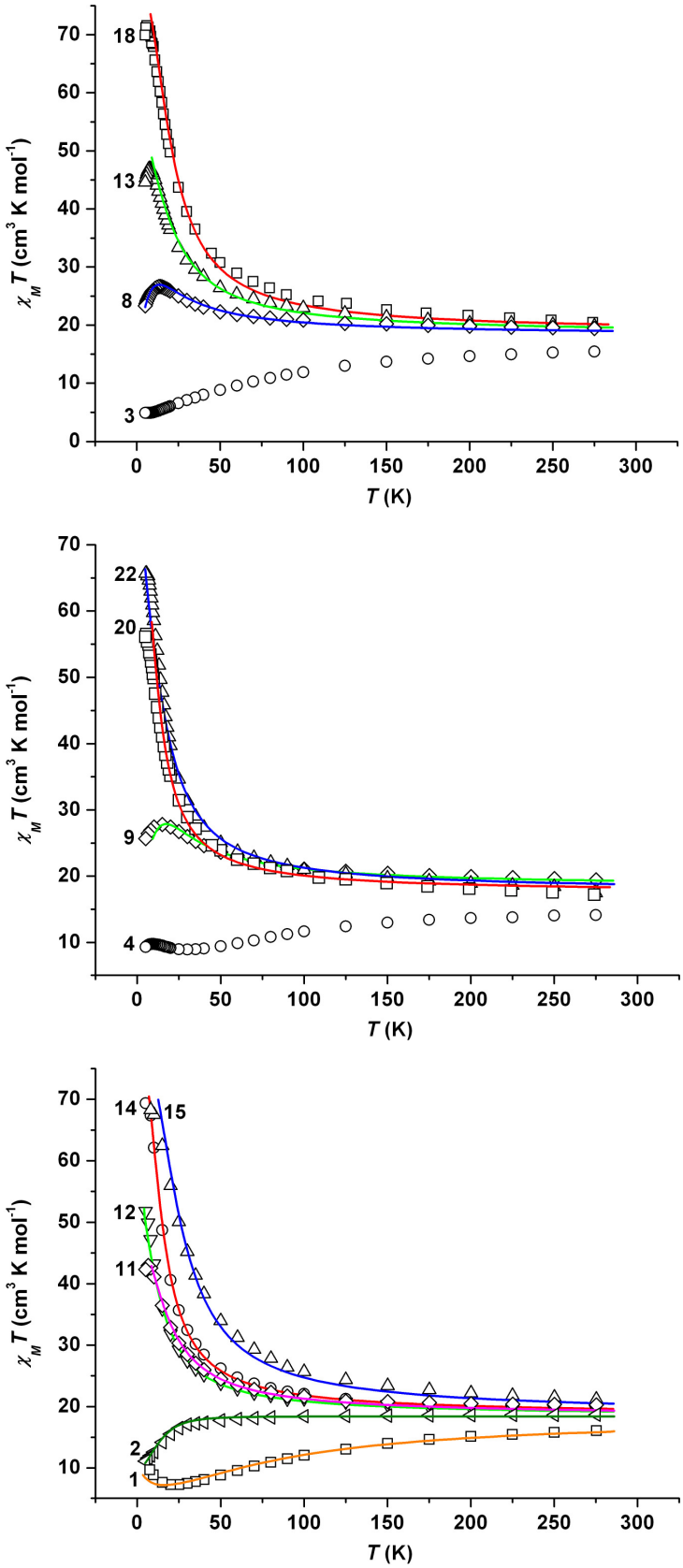

Figure 2.3 Plots of $\chi_M T$ vs. T for complexes **2.1-2.22**. The solid lines represent simulations of the experimental data in the temperature range 300 – 5 K. For parameters see Table 2.2.

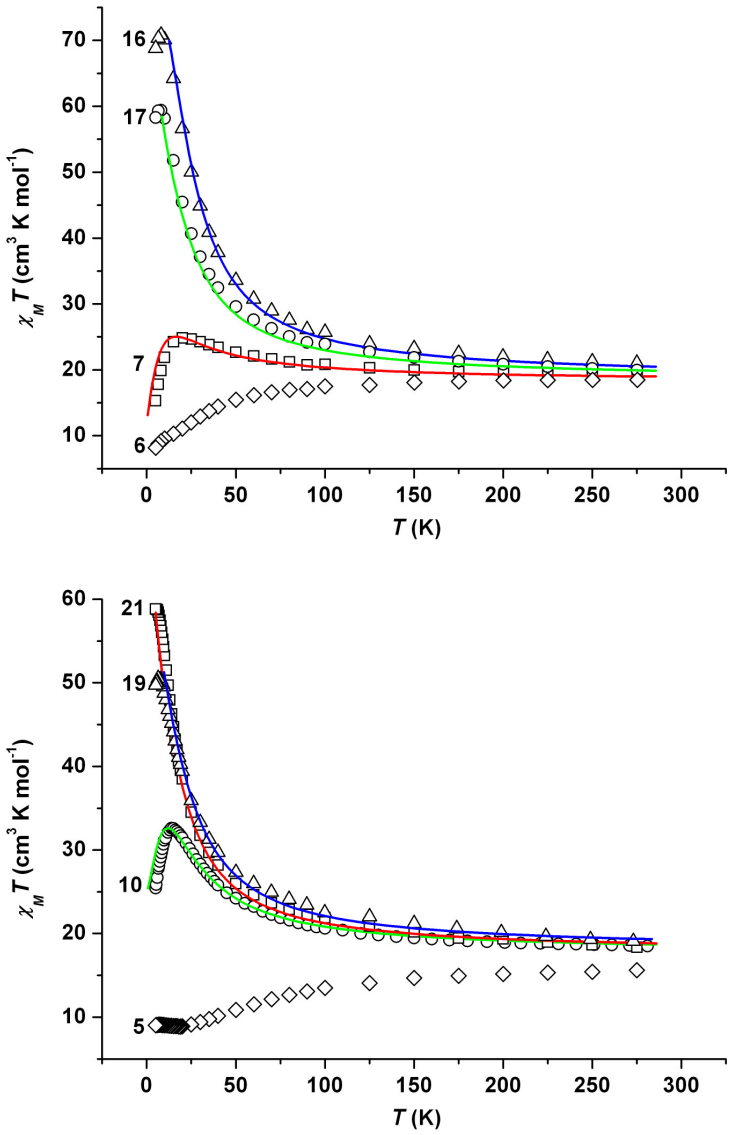

Figure 2.4 Plots of $\chi_M T$ vs. T for complexes **2.1**-**2.22**. The solid lines represent simulations of the experimental data in the temperature range 300 – 5 K. For parameters see Table 2.2.

The $\chi_M T$ vs. T curves obtained for complexes **2.1**-**2.6** show dominant antiferromagnetic exchange with room temperature values ranging from 13.88 to 18.38 cm^3 K mol^{-1}. In each case $\chi_M T$ remains approximately constant before dropping more rapidly at temperatures below 100 K and reaching values of between 4.91 and 11.12 cm^3 K mol^{-1}. In the case of **2.1** a slight upturn in $\chi_M T$ was observed at 25 K reaching a maximum value of 9.71 cm^3 K mol^{-1} at 5 K.

Despite attempts to use the 1-J and 2-J models of Scheme 2.2, the data obtained for complex **2.1** could only be simulated with the 3-J model described by Eqn. (3), giving $S = 4$, $J_1 = 1.25$, $J_2 = -4.6$, $J_3 = -1.8$ cm^{-1} and $g = 1.99$. A 2-J model (Eqn.

(2)) was employed to simulate the experimental data obtained from complex **2.2** to yield the parameters $S = 4$, $J_1 = +1.2$, $J_2 = -1.95$ cm^{-1}, $g = 2.01$. Despite much effort we were unable to successfully simulate the data for complexes **2.3**-**2.6**. The $\chi_M T$ vs. T curves obtained from complexes $[Mn_6O_2(Et\text{-}sao)_6(O_2CC_{12}H_{17})_2(EtOH)_4(H_2O)_2]$ (**7**) and $[Mn_6O_2(Et\text{-}sao)_6(O_2CC(CH_3)_3)_2(MeOH)_6]$ (**2.8**) appear very similar in line shape to those obtained from **2.1**-**2.6** with similar room temperature values of 18.54 and 19.41 cm^3 K mol^{-1}, respectively. In both cases $\chi_M T$ remains constant until a temperature of approximately 50 K where a gradual increase occurs before reaching maxima at 20 and 10 K and $\chi_M T$ values of 28.80 and 26.02 cm^3 K mol^{-1}, respectively. The value then drops sharply in both cases to 15.29 and 23.32 cm^3 K mol^{-1} at 5 K. Simulation of these data using the 2-J model (2) suggests ground spin states of $S = 5\pm1$ (**2.7**) and $S = 5$ (**2.8**) (Table 2.2) but with many (excited) states that are essentially degenerate.

Magnetic susceptibility studies on complexes **2.9**-**2.13** show room temperature $\chi_M T$ values in the 18.48 - 19.88 cm^3 mol^{-1} K range which gradually increase with decreasing temperature, reaching low temperature values of between 25.43 and 42.32 cm^3 K mol^{-1}. Such values lie between the two $S = 4$ (10 cm^3 K mol^{-1}) and $S = 12$ (78 cm^3 K mol^{-1}) extremes and suggest 'intermediate' ($4 < S < 12$) ground spin states, diagnostic of competing anti- and ferromagnetic exchange between the Mn^{III} ions. This is corroborated by the spin Hamiltonian parameters obtained from the simulation of the experimental data (see Table 2.2): a 2-J model was employed for complexes **2.9**-**2.13** affording $S = 6$, $g = 2.01$, $J_1 = 1.39$ and $J_2 = -1.92$ cm^{-1} (**2.9**); $S = 7\pm1$, $g = 1.97$, $J_1 = 1.76$ and $J_2 = -1.92$ cm^{-1} (**2.10**); and $S = 9\pm1$, $g = 1.98$, $J_1 = 1.39$ and $J_2 = -0.99$ cm^{-1} (**2.11**). The simulations for **2.12** and **2.13** give $S = 11\pm1$ ground states. Again it is clear that in each case the presence of weak exchange leads to a situation in which many S states are essentially degenerate making assignment of a ground state difficult and in some cases perhaps inappropriate.

The third type of susceptibility curve (complexes **2.14**-**2.22**) shows a constant increase in $\chi_M T$ with decreasing temperature indicative of ferromagnetic exchange between the Mn centres. The room temperature $\chi_M T$ values are all above 18.0 cm^3 K mol^{-1} and in each case increase gradually before rising more abruptly in the 75-100 K temperature region. The maximum $\chi_M T$ values range between 49.71 and 69.95 cm^3

K mol^{-1}. All exhibit S = 12 ground states with S = 11 excited states at energies of up to 9 cm^{-1} (Table 2.2) above the ground state. The S = 12 ground states may be simply explained as a product of six ferromagnetically coupled Mn^{III} ions, while the S = 4 ground spin states may be rationalised as two antiferromagnetically coupled (S = 2) [Mn^{III}_3] triangles which are ferromagnetically coupled to one another.[10, 13, 24, 26-29] Each Mn···Mn pair is relatively weakly coupled with J values of < 2 cm^{-1} - in line with previously reported values for oxime-bridged Mn^{III}···Mn^{III} complexes.[30] Many, indeed probably all, members of this large family exhibit non-isolated spin ground states,[24, 31, 32] the "nesting" of excited states on the ground state being a direct result of the weak magnetic coupling - resulting in the breakdown of the so-called "*giant spin*" model.[31, 32] With this in mind and within the confines of our simplistic model, variable field and temperature dc magnetisation data were collected in the 0.5–7 T and 2-7 K field and temperature ranges. In each case we attempted to fit the data with an axial ZFS plus Zeeman Hamiltonian (4) by a method described recently by Piligkos in the whole field and temperature range,[33]

$$\hat{\mathcal{H}} = D(\hat{S}_z^2 - S(S+1)/3) + \mu_B g H \hat{S} \qquad (4)$$

where D is the axial anisotropy, μ_B is the Bohr magneton, $\hat{S}_z$ is the easy-axis spin operator, and H is the applied field. The results are summarised in Table 2.2 with representative plots given in Fig. 2.5. Complexes **2.1**-**2.9** possess relatively low spin ground states (S = 4, 5 and 6) with D values ranging from –0.75 to –1.59 cm^{-1}, while the ferromagnetic complexes (**2.14**-**2.22**) in the lower half of Table 2.2 possess much smaller ZFS parameters ranging from D = –0.34 cm^{-1} to –0.44 cm^{-1}.[10, 13, 24, 26-29] A previously reported ligand field study on a sub-group of this [Mn_6] family revealed the differences in their ground state anisotropies stem from the difference in projection coefficients of the single ion anisotropy to spin states of different total spin quantum number (S) and not the geometrical distortions of the individual metal ions.[34, 35]

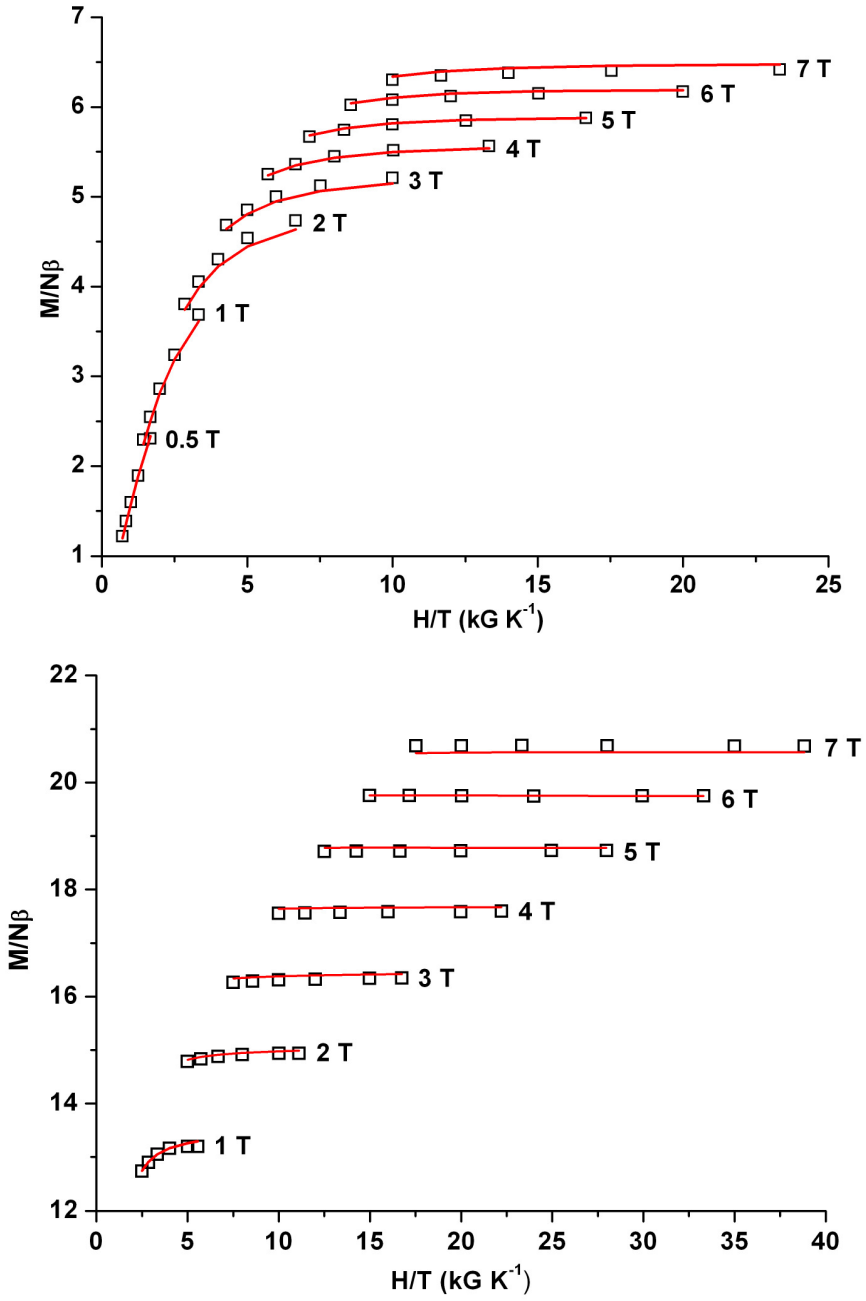

Figure 2.5 Plots of reduced magnetisation ($M/N\mu_B$) versus H/T for **2.4** (top), and **2.16** (bottom) in the noted field ranges and the 2 – 7 K temperature range. The solid lines correspond to the fit of the data as documented in Table 2.2.

Ac magnetic susceptibility and hysteresis loop measurements

Ac magnetic susceptibility measurements were carried out on crystalline samples of **2.1**-**2.22** in the 2 – 10 K temperature range in a 3.5 G ac field oscillating at frequencies ranging from 50 to 1000 Hz. Fully visible out-of-phase (χ_M'') signals

indicative of SMM behaviour (Fig. 2.6 shows those obtained for complex **2.14**) were observed for *all* family members except for $[Mn_6O_2(sao)_6(keto\text{-}acetate)_2(EtOH)_2(H_2O)_2]$ (**2.3**) and $[Mn_6O_2(Me\text{-}sao)_6(O_2C\text{-}th)_2(EtOH)_4(H_2O)_2]$ (**2.6**), in which only the tails and not the peaks of the signals were observed. The ac data obtained were combined with single-crystal dc relaxation measurements performed on a micro-SQUID[19] and fitted to the Arrhenius equation (5),

$$\tau = \tau_o \exp(U_{eff}/(kT)) \qquad (5)$$

where τ_o is the pre-exponential factor, τ is the relaxation time, U_{eff} is the barrier to the relaxation of the magnetisation and k is the Boltzmann constant, to give the effective barrier to magnetisation reorientation (U_{eff}) for each $[Mn_6]$ complex. These data are summarised in Fig. 2.7 and Table 2.2 and span barrier heights between ~24-86 K.

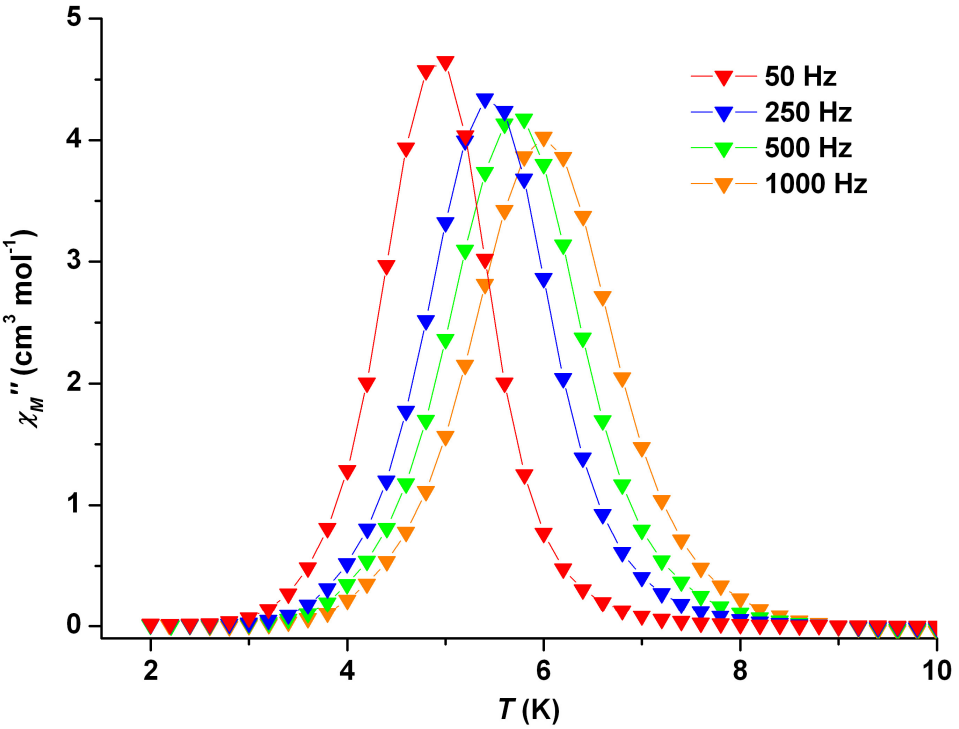

Figure 2.6 AC out-of-phase χ''_M vs. T plot obtained for complex **2.16** in an oscillating field of 3.5 Oe and frequencies of 50-1000 Hz.

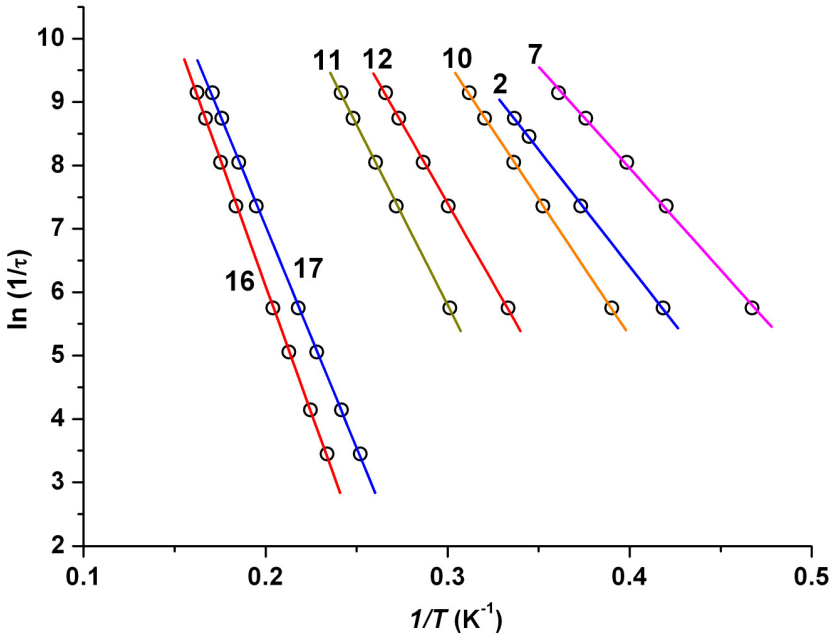

Figure 2.7 Plots of ln(1/ τ) vs. 1/T obtained from ac magnetic susceptibility data for a cross section of family members.

Temperature and sweep rate dependent hysteresis loops were observed for all complexes. Loops for complex **2.17** are shown in Fig. 2.8 and display hysteresis up to approximately 3.5 K at a 0.14 mT s^{-1} sweep rate. Each of the loops exhibit well defined steps due to the rapid relaxation of the magnetisation at a given magnetic field. However in each case the loops are rather complicated: step positions arising from the ground state transitions are difficult to assign, and it is clear that many additional features are present. These additional steps probably originate from resonant tunnelling between M_S-levels of the ground state, which are shifted to other fields due to fourth order anisotropy terms,[36] or from tunnelling between levels of the ground state and low lying excited spin states.

This is perhaps not surprising given that in each case the susceptibility studies suggested the presence of low lying excited states in close proximity to the ground state, presumably as a consequence of the weak exchange between the metal centres. The result is therefore the unavoidable population of excited states even at very low temperatures. The presence of intermolecular interactions (H-bonded solvate molecules) in the crystal and the low molecular and crystallographic symmetry will also affect the loops but their relative significance to the tunnelling is difficult to quantify.

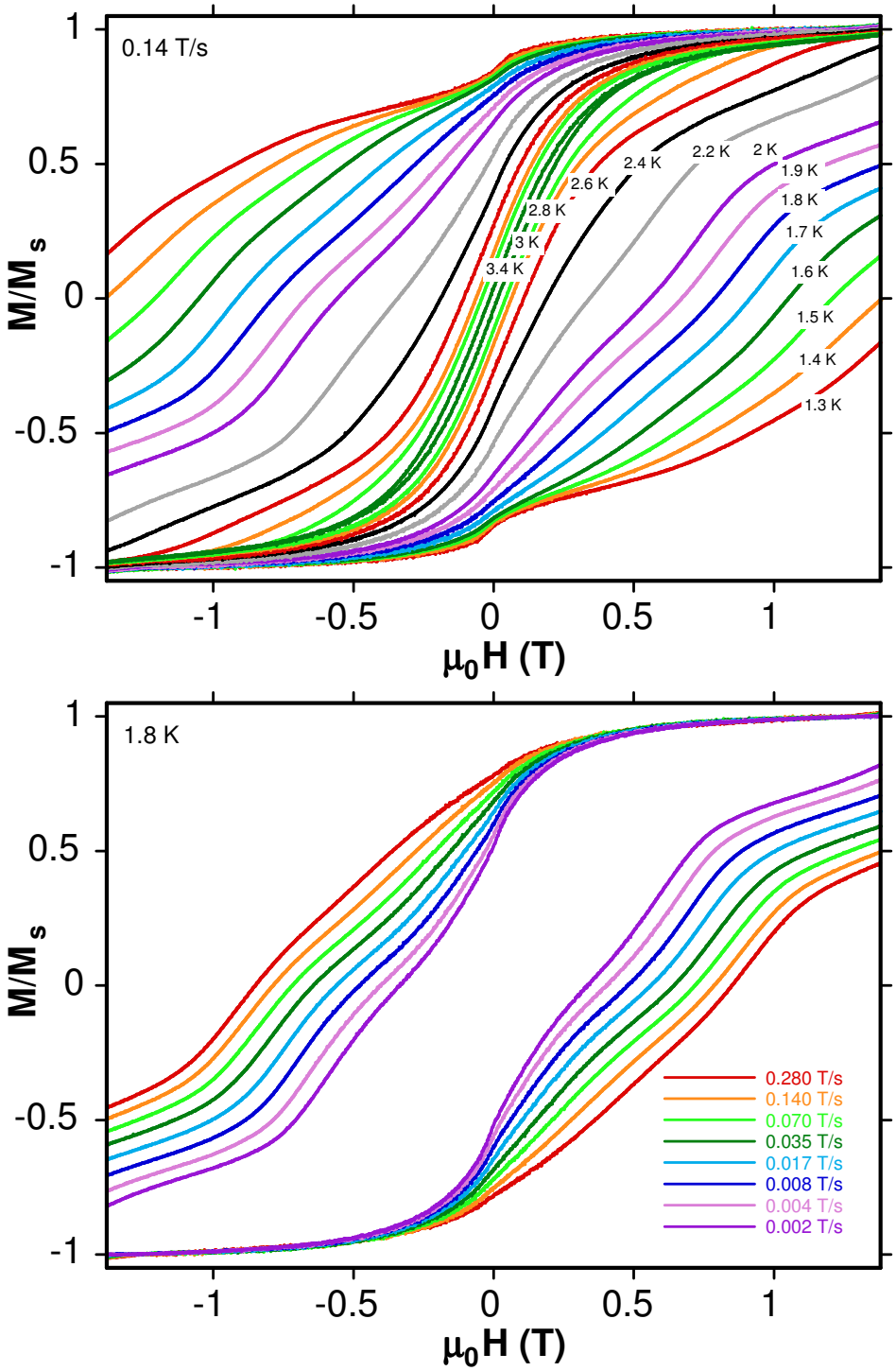

Figure 2.8 Magnetisation versus field hysteresis loops for a single crystal of **2.17** at the indicated temperatures and field sweep rates (bottom). *M* is normalised to its saturation value.

High Frequency Electron Paramagnetic Resonance Studies

High frequency EPR measurements were performed on single crystals of complex **2.2** (S = 4) and **2.15** (S = 12) to verify the ground state spin value and the zero field splitting (ZFS) parameters. Details of the experimental technique can be found elsewhere.[37, 38] Fig. 2.9 displays easy-axis ($B//c$) temperature dependent spectra obtained for complex **2.15** at 331 GHz. With increasing temperature, several strong peaks labelled ***a***, ***b***, ***c***, ***d*** and ***e*** are observed within the field range of the magnet, corresponding to the following fine-structure transitions: $m_S = -12 \rightarrow -11$, $-11 \rightarrow -10$, $-10 \rightarrow -9$, $-9 \rightarrow -8$ and $-8 \rightarrow -7$, respectively, where m_S represents the spin projection onto the easy axis of the crystal. Weaker satellite peaks seen as shoulders on the main peaks appear to be caused by a slight *D*-strain in the sample, i.e. a small fraction of molecules experiencing different microenvironments and, hence, different (lower) *D*-values.[39] Multi-frequency measurements enabled accurate determination of the following ZFS parameters for the majority species (strongest resonance peaks) associated with complex **2.15**: $D = -0.360(5)$ cm^{-1}, $B_4^0 = -5.7(5) \times 10^{-6}$ cm^{-1} and $g = 1.98(1)$ for this $S = 12$ complex.

The inset to Fig. 2.9 shows the easy-axis spectrum for complex **2.2** obtained at 285 GHz and 15 K. Several resonances are again observed, most of which can be assigned to fine-structure transitions within an $S = 4$ ground state, i.e. $m_S = -4 \rightarrow -3$, $-3 \rightarrow -2$, etc. However, attempts to fit the entire spectrum using a single-spin description were not entirely satisfactory. Nevertheless, through combined multi-frequency and temperature dependent measurements, we were able to ascertain that some of the peaks correspond to transitions within low-lying excited spin multiplets (labeled *ES* in the inset to Fig. 2.9).[40, 41] The remaining peaks could then be fit to a $S = 4$ model, allowing us to determine approximate ZFS parameters associated with this multiplet: $D = -1.27(2)$ cm^{-1} and $B_4^0 = +1.3(3) \times 10^{-4}$ cm^{-1}. The observation of excited state intensity in the spectrum of complex **2.2** is not surprising given the frustrated interactions within the triangular Mn_3 units.

The use of a giant spin description to fit the EPR spectra allows for direct comparisons with magnetic measurements. In particular, one can estimate the magnetisation reversal barriers for both complexes: 29.2 K for the low spin system

(**2.2**) and 75 K for the high spin system (**2.15**), *i.e.* an increase of 2.56, which is in good agreement with the AC susceptibility measurements (an increase of 2.70).[40, 41]

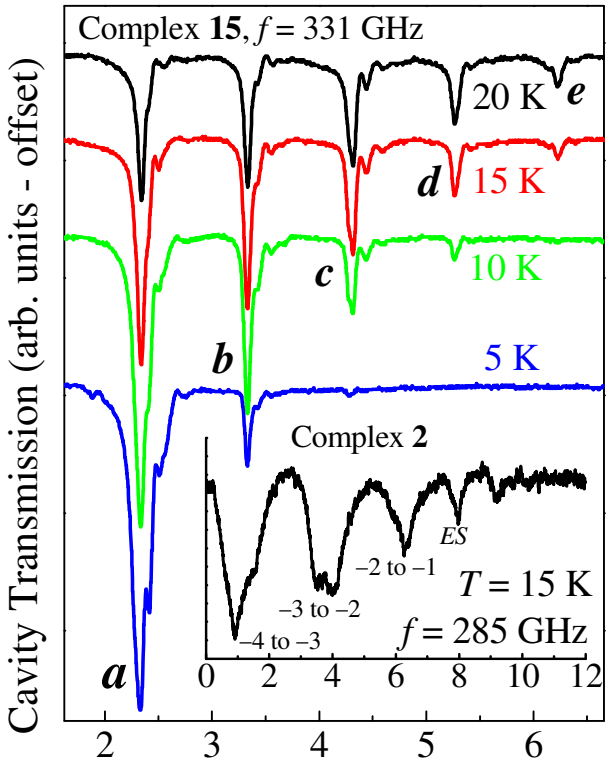

Figure 2.9 Easy axis temperature dependence spectra for complex **2.15** at 331 GHz. The inset shows the easy axis spectrum for complex **2.2** at 285 GHz, 15 K.

Discussion

Understanding the relationship between structure and magnetic behaviour in polymetallic cluster compounds is an extremely difficult task, and increasingly so as the nuclearity increases, since one must consider all contributions to the exchange, including, for example, the innocence or non-innocence of (terminal) co-ligands.[42-51] For the [Mn_6] family this means we must consider the combination of four different ligand types (oxime, phenoxide, oxide and carboxylate) and the bond lengths and angles associated with each; and at least four different exchange interactions. A comprehensive *quantitative* analysis is thus rather difficult to achieve and will require theoretical input.[52-58] In earlier work we suggested that while clearly *all* magnetic pathways must play some role in determining the size and magnitude of the Mn···Mn exchange, the dominant factor was the twisting of the Mn-O-N-Mn moiety as induced by the distortion imposed on the molecule by bulkier oximes (R-sao^{2-}).[24]

In order to shed further light on this we have examined all of the structural parameters in the magnetic cores of complexes **2.1**-**2.22**. In particular we have examined the relationship between the observed *J*-value for a particular Mn···Mn exchange and (a) the out-of-plane shift of the central oxide - previous studies on analogous trinuclear systems have suggested an increasingly ferromagnetic interaction as this distance increases;[59] (b) the Mn-(μ_3-O)-Mn angle - experimental studies of $[Mn^{III}_3O(O_2CR)_6L_3]^+$ species suggest a switch from antiferromagnetic to ferromagnetic at angles below ~ 120º;[11, 60] (c) the Mn^{III}-O^{2-} distances; (d) the Mn-N-O-Mn distances; (e) the Mn-N-O-Mn torsion angles, α. An examination of the data of Tables 2.1 and 2.2 allows us to make some general conclusions:

i) In all cases the exchange *between* the $[Mn_3]$ triangles appears to be ferromagnetic.

ii) The exchange between Mn_2 pairs is dominated by the Mn-O-N-Mn torsion angles; the larger the torsion angle, the more ferromagnetic the pairwise interaction; the smaller the Mn-N-O-Mn torsion angle the more antiferromagnetic the pairwise interaction.

iii) Above a torsion angle of approximately 31° the exchange switches from antiferromagnetic to ferromagnetic, i.e. if $\alpha > 31^o$, then J > 0 (F); if $\alpha < 31^o$ then J < 0 (AF). When a $[Mn_3]$ triangle contains torsion angles that are both above and below this value the data can only be simulated using both F and AF exchange.

iv) It is the individual torsion angles between neighbouring Mn ions that dictates the behaviour of the complex, and *not* the average torsion angle. For example, complex **2.2** has $\alpha_v = 32.5^o$ but an $S = 4$ ground state, complex **2.14** has $\alpha_v = 36.5^o$ and an $S = 12$ ground state, and complex **2.11** has $\alpha_v = 37.4^o$ and an $S \approx 9$ ground state.

v) The presence of the carboxylate in either coordinating mode (μ or terminally bonded) appears to have little effect on the sign of *J*. This is exemplified by complexes **2.1** and **2.6**, both of which display $S = 4$ ground states despite the fact that the former contains a bridging carboxylate and the latter a terminal carboxylate.

vi) If each Mn_2 exchange is ferromagnetic (i.e. an $S = 12$ complex), the larger the Mn-N-O-Mn torsion angle (α), the larger the barrier to magnetisation relaxation (U_{eff}). For example, comparing complexes **2.14** and **2.16** (Table 2.2) with $J = +0.93$ cm^{-1} and $J = +1.60$ cm^{-1}, respectively, the U_{eff} values are 53.1 K and 79.9 K. This presumably arises because an increase in torsion angle leads to an increase in $|J|$

which results in a more isolated ground state, and a reduction in tunnelling.[31, 32] This is reflected in the simulation of the susceptibility data. For example in complex **2.14** (S = 12) where J = +0.93 cm^{-1}, the first excited state of S = 11 is located only 5 cm^{-1} above the ground-state, whereas in complex **2.15** (S = 12) where J = +1.63 cm^{-1} the first excited state of S = 11 is located 9 cm^{-1} above the ground-state, *i.e*. twice as high. However, given the complicated nature of the magnetic relaxation in such species,[31, 32] one has to treat this statement as somewhat speculative.

In summary, an examination of Tables 2.1 and 2.2 suggests no *obvious* correlation between J and any of (a)-(d), but there does appear to be a correlation between the magnitude of the exchange and the Mn-N-O-Mn torsion angle - the larger the torsion angle the more ferromagnetic the pairwise exchange. This has also been suggested in recent DFT calculations on analogous oxime-bridged [Mn_3] triangles.[26] Fig. 2.10 shows a plot of torsion angle (α) versus J-value for the [Mn_6] family; a linear fit suggesting J = 0 at a torsion angle value of approximately 31° - in good agreement with previous predictions.[24] It is important to emphasise of course that this is purely *qualitative* in nature, since in each case we simulated the experimental susceptibility data using the simplest model available, for example, for complex **2.15** we employed a 1-J model even though four different exchange interactions are present. Indeed it is clear that these are very complicated molecules. It is likely that most, if not all, possess excited states nested upon the ground state rendering the analysis and interpretation of the data within the giant-spin model somewhat difficult and qualitative in nature, albeit with clearly defined trends.

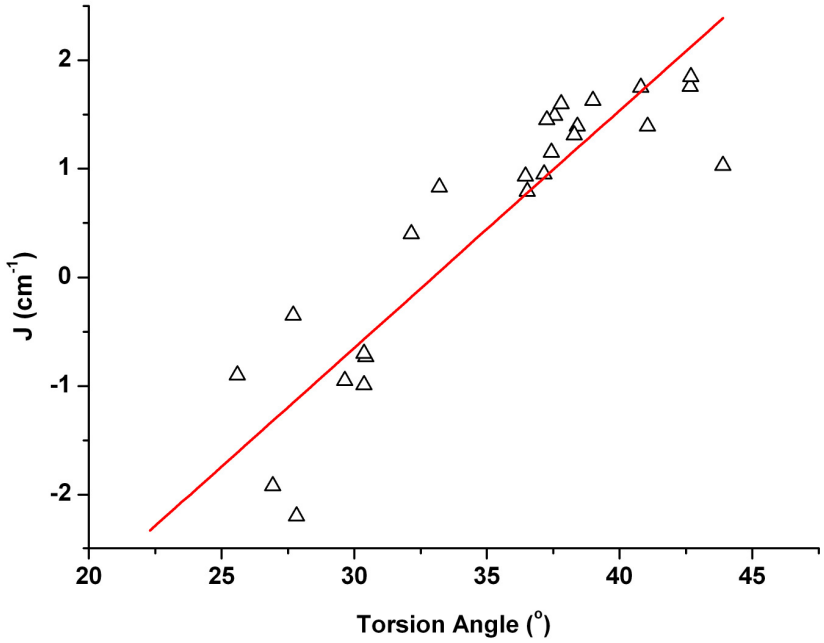

Figure 2.10 Plot of best fit parameter J vs. Mn-N-O-Mn torsion angle (°) taken from all members of the [Mn_6] family. Note: As necessary due the confines of this study, the mean average torsion angles were used to construct this *qualitative* plot.

Conclusions

We have synthesised and characterised twenty two members of a hexametallic [Mn_6] family of Single-Molecule Magnets. Each member possesses a common $[Mn_6O_2(R\text{-}sao)_6]^{2+}$ core comprising two linked $[Mn_3O(R\text{-}sao)_3]^{+}$ triangles. The type of magnetic exchange within the molecule can be controlled using targeted structural distortion of the core. By employing "planar" non-derivatised oximes ($saoH_2$) the molecules are "unpuckered", the dominant intra-triangle exchange is antiferromagnetic and the molecules have low spin (S = 4 ground states). By derivatising the oxime carbon atom to contain bulkier substituents, the [Mn_6] molecules become increasingly puckered as evidenced by large increases in the Mn-N-O-Mn torsion angles. The result is that pairwise exchange becomes increasingly ferromagnetic, resulting in ferromagnetic molecules with S = 12 spin ground states. Qualitatively, the "switch" from antiferromagnetic to ferromagnetic comes at an Mn-N-O-Mn angle above approximately 31°.

Table 2.1 Selected interatomic distances (Å) and angles (°) for complexes **2.1**-**2.22**.

Complex	Mn-(μ_3-O) distance (Å) Mn1-O, Mn2-O, Mn3-O	Mn-(μ_3-O)-Mn angles (°) Mn1-2, Mn2-3, Mn1-3	Mn_{3plane}-(μ_3-O) (Å)	Mn-O_{phen} (Å)	Mn-O_2CR distance (Å)
$[Mn_6O_2(sao)_6(O_2CH)_2(MeOH)_4]$ (**2.1**)	1.872(2), 1.879(2), 1.857(2)	119.36(8), 121.42(8), 114.90(8)	0.226	3.524	2.138(2), 2.112(2)
$[Mn_6O_2(Me\text{-}sao)_6(O_2CCPh_3)_2(EtOH)_4]$ (**2.2**)	1.874(2), 1.898(2), 1.864(2)	119.76(9), 119.55(9), 120.18(9)	0.078	2.384	2.062(2)
$[Mn_6O_2(sao)_6(ketoacetate)_2(EtOH)_2(H_2O)_2]$ (**2.3**)	1.863(2), 1.869(2), 1.877(2)	115.33(8), 120.75(8), 120.16(8)	0.211	3.582	2.096(2), 2.129(2)
$[Mn_6O_2(sao)_6(O_2CPh)_2(MeCN)_2(H_2O)_2]$ (**2.4**)	1.868(2), 1.873(2), 1.872(2)	115.28(9), 120.50(9), 121.27(9)	0.186	3.271	2.104(2), 2.148(2)
$[Mn_6O_2(sao)_6(1\text{-}Me\text{-}cyclohex)_2(MeOH)_4]$ (**2.5**)[a]	1.869(2), 1.867(2), 1.877(2)	122.04(11), 115.71(11), 119.37(11)	0.184	3.348	2.127(2), 2.116(2)
	1.878(2), 1.850(2), 1.875(2)	121.50(11), 115.82(10), 119.84(10)	0.182	3.606	2.099(2), 2.106(2)
$[Mn_6O_2(Me\text{-}sao)_6(O_2C\text{-}th)_2(EtOH)_4(H_2O)_2]$ (**2.6**)	1.882(2), 1.863(2), 1.880(2)	119.43(10), 121.73(11), 118.79(11)	0.025	2.619	2.135(2)
$[Mn_6O_2(Et\text{-}sao)_6(O_2CC_{12}H_{17})_2(EtOH)_4(H_2O)_2]$ (**2.7**)	1.875(2), 1.884(2), 1.887(2)	120.22(6), 117.50(5), 121.45(5)	0.100	2.519	2.114(2)
$[Mn_6O_2(Et\text{-}sao)_6(O_2CC(CH_3)_3)_2(MeOH)_6]$ (**2.8**)	1.872(4), 1.883(3), 1.892(4)	119.93(19), 118.17(18), 120.95(18)	0.107	2.478	2.115(4)
$[Mn_6O_2(Et\text{-}sao)_6(O_2CC(CH_3)_3)_2(EtOH)_5]$ (**2.9**)[b]	1.891(3), 1.885(3), 1.876(3)	119.09(13), 119.93(13), 120.55(13)	0.072	2.458	2.104(3)
	1.883(3), 1.864(3), 1.892(3)	120.15(14), 120.28(13), 118.63(13)	0.105	2.388	2.131(3)
$[Mn_6O_2(Et\text{-}sao)_6(O_2CPh^2OPh)_2(EtOH)_4]$ (**2.10**)	1.881(4), 1.887(4), 1.853(4)	119.10(2), 119.60(2), 121.00(2)	0.057	2.379	2.098(5)
$[Mn_6O_2(Et\text{-}sao)_6(O_2CPh^4OPh)_2(EtOH)_4(H_2O)_2]$ (**2.11**)	1.875(1), 1.879(1),1.888(1)	120.56(5), 118.64(5), 120.53(5)	0.057	2.417	2.118(2)
$[Mn_6O_2(Me\text{-}sao)_6(O_2CPhBr)_2(EtOH)_6]$ (**2.12**)	1.941(2), 1.900(2), 1.837(2)	125.47(12), 116.36(12), 117.63(12)	0.080	2.491	2.086(2)
$[Mn_6O_2(Me\text{-}sao)_6(O_2CC(CH_3)_3)_2(MeOH)_6]$ (**2.13**)	1.874(2), 1.878(2), 1.886(2)	120.22(10), 118.67(9), 120.96(9)	0.042	2.411	2.072(2)
$[Mn_6O_2(Et\text{-}sao)_6(O_2CPh)_2(EtOH)_4(H_2O)_2]$ (**2.14**)	1.878(2), 1.884(2), 1.888(2)	119.99(8), 118.21(8), 121.12(8)	0.090	2.488	2.118(2)
$[Mn_6O_2(Et\text{-}sao)_6(O_2CPh(Me)_2)_2(EtOH)_6]$ (**2.15**)	1.890(3), 1.889(3), 1.877(2)	118.48(13), 121.31(13), 120.11(13)	0.034	2.480	2.131(3)
$[Mn_6O_2(Et\text{-}sao)_6(O_2C_{11}H_{15})_2(EtOH)_6]$ (**2.16**)	1.881(2), 1.889(2), 1.886(2)	121.04(7), 118.72(7), 120.01(7)	0.053	2.438	2.106(2)
$[Mn_6O_2(Et\text{-}sao)_6(O_2CPh(Me))_2(EtOH)_4(H_2O)_2]$ (**2.17**)	1.879(2), 1.894(2), 1.878(2)	120.39(7), 118.94(7), 120.12(7)	0.081	2.374	2.126(2)
$[Mn_6O_2(Et\text{-}sao)_6(O_2C\text{-}Naphth)_2(EtOH)_4(H_2O)_2]$ (**2.18**)	1.888(2), 1.870(2), 1.886(2)	121.35(11), 119.09(11), 118.67(11)	0.103	2.509	2.103(2)
$[Mn_6O_2(Et\text{-}sao)_6(O_2C\text{-}Anthra)_2(EtOH)_4(H_2O)_2]$ (**2.19**)	1.875(4), 1.886(4), 1.886(4)	120.9(2), 118.4(2), 120.0(2)	0.096	2.522	2.149(4)
$[Mn_6O_2(Et\text{-}sao)_6(O_2CPh(C{\equiv}CH)_2(EtOH)_4(H_2O)_2]$ (**2.20**)	1.876(2), 1.878(2), 1.881(2)	121.23(9), 117.87(9), 120.44(9)	0.074	2.482	2.116(2)
$[Mn_6O_2(Me\text{-}sao)_6(O_2CPh(C{\equiv}CH))_2(EtOH)_6]$ (**2.21**)	1.871(2), 1.892(2), 1.885(1)	119.91(9), 117.89(9), 121.52(10)	0.090	2.441	2.129(5)
$[Mn_6O_2(Me\text{-}sao)_6(O_2CPh(Cl)_2)_2(MeOH)_6]$ (**2.22**)	1.874(2), 1.883(2), 1.884(2)	120.19(10),118.38(9), 120.92(10)	0.081	2.447	2.114(2)

[a] Two Mn_6 complexes in the asymmetric unit, therefore two sets of data documented. [b] Complex **2.9** has no centre of symmetry.

Table 2.2 Magnetostructural parameters for complexes **2.1**-**2.22**; Mn-N-O-Mn torsion angles *vs.* *J* and *S*.

Cmpl.	Crystal Sys.	Sp. Grp.	α / ° Mn1-2 / Mn2-3 / Mn1-3	*J* / cm^{-1} [a] J_1 / J_2 / J_3	*S* [b]	$1^{st}_{exc.\ st.}$ (cm^{-1}) [b]	*g* [c]	*D* /cm^{-1} [d]	τ_0 / s [e]	U_{eff} / K [e]
(**2.1**)	Triclinic	P-1	25.57, 10.42, 18.01	+1.25/-4.6/-1.8	4	3 (8)	1.99	-1.39	2.0×10^{-8}	28.0
(**2.2**)	Monoclinic	C2/c	25.50, 42.44, 29.74	+1.2/-1.95	4	5 (10.5)	2.01	n.a.	6.8×10^{-10}	31.7
(**2.3**)	Triclinic	P-1	19.06, 18.89, 11.92	n.a.	4	n.a.	n.a.	n.a.	n.a.	n.a.
(**2.4**)	Triclinic	P-1	28.18, 16.18, 8.36	n.a.	4	n.a.	2.02	-1.59	6.57×10^{-8}	23.8
(**2.5**)	Triclinic	P-1	9.66, 29.83, 15.60 13.53, 23.80, 37.33	n.a.	4	n.a.	n.a	-1.18	1.70×10^{-8}	28.8
(**2.6**)	Triclinic	P-1	27.40, 31.10, 36.35	n.a.	n.a.	n.a.	n.a.	n.a.	n.a	n.a.
(**2.7**)	Triclinic	P-1	27.83, 40.07, 41.46	+1.55/ -2.20	5±1	4(0.01)	1.98	n.a.	9.3×10^{-10}	31.2
(**2.8**)	Triclinic	P-1	26.93, 34.45, 40.70	+1.49, -1.92	5	4(0.5)	2.01	n.a.	4.52×10^{-11}	59.2
(**2.9**)	Triclinic	P-1	36.92, 23.27, 42.12 32.33, 16.76, 42.24	+1.39/ -1.92	6	7(0.5)	2.01	-0.75	3.0×10^{-8}	30.0
(**2.10**)	Monoclinic	I2/a	47.56, 31.76, 23.75	+1.76/ -1.92	7±1	6 (0.1)	1.97	-0.39	1.5×10^{-10}	43.2
(**2.11**)	Triclinic	P-1	30.36, 38.38, 43.71	+1.39/ -0.99	9±1	8 (0.03)	1.98	-0.37	1.2×10^{10}	56.9
(**2.12**)	Triclinic	P-1	30.43, 42.94, 31.91	+1.15/ -0.73	11±1	12 (0.2)	1.98	-0.50	1.7×10^{-10}	50.2
(**2.13**)	Triclinic	P-1	29.64, 38.51, 44.47	+1.65, -0.95	11±1	12(0.02)	2.02	n.a	3.58×10^{-10}	57.6
(**2.14**)	Triclinic	P-1	31.26, 38.20, 39.92	+0.93	12	11 (5)	1.99	-0.43	8.0×10^{-10}	53.1
(**2.15**)	Monoclinic	$P2_1/n$	39.10, 43.04, 34.86	+1.63	12	11 (9)	1.99	-0.43	2×10^{-10}	86.4
(**2.16**)	Triclinic	P-1	42.61, 36.73, 34.07	+1.60	12	11 (7.6)	1.99	-0.43	2.5×10^{-10}	79.9
(**2.17**)	Triclinic	P-1	47.16, 38.19, 30.37	+1.85/-0.70	12	11 (1.4)	1.97	-0.44	7.5×10^{-10}	69.9
(**2.18**)	Monoclinic	$P2_1/c$	41.09, 33.28, 40.50	+1.31	12	11 (6.23)	2.03	-0.34	4.33×10^{-10}	60.1
(**2.19**)	Triclinic	P-1	42.32, 39.28, 25.60	+1.75, -0.90	12	11 (0.79)	2.00	-0.44	3.99×10^{-10}	60.1
(**2.20**)	Triclinic	P-1	38.85, 38.67, 32.06	+0.79	12	11 (3.75)	1.97	n.a.	6.23×10^{-11}	66.8
(**2.21**)	Triclinic	P-1	43.61, 33.72, 29.53	+1.57, -0.70	12	11 (0.91)	1.98	n.a.	4.37×10^{-10}	60.3
(**2.22**)	Triclinic	P-1	43.24, 27.61, 30.94	+1.45, -0.35	12	11(2.78)	1.98	-0.39	1.55×10^{-10}	48.5

[a]Calculated from dc susceptibility studies. [b]Calculated from both dc susceptibility and magnetization measurements. [c]Calculated from dc susceptibility measurements. [d]Calculated from magnetization measurements. [e]Calculated from ac susceptibility data and / or single-crystal relaxation measurements performed on a micro-SQUID; n.a. = not available.

2.3 A New Family of Mn_6 SMMs Using Halides and Phosphinates

2.3.1 Experimental Section

Synthesis

Synthetic strategy for complexes **2.23** and **2.24**:

$MnX_2{\cdot}4H_2O$ (X = Br^- (**2.23**), I^- (**2.24**)) was reacted with one equivalent of R-saoH_2 (R = Et (**2.23**), Me (**2.24**)) and NEt_4OH in EtOH. After stirring for ~30 min, the solution was filtered and single crystals grew upon slow evaporation.

Synthetic strategy for complexes **2.25**-**2.30**:

$Mn^{II}(ClO_4)_2{\cdot}6H_2O$, the (derivatised) salicylaldoxime ligand and the desired phosphinate ligand were dissolved in MeOH in a 1:1:1 ratio before addition of one equivalent of NEt_3, followed by stirring for 1 hour. The resulting dark green solutions were filtered and diffused with Et_2O. Suitable crystals grew after ~4 days.

X-ray crystallography

For **2.23** and **2.24**: Diffraction data were collected at 150 K on a Bruker Smart Apex CCDC diffractometer, equipped with an Oxford Cryosystems LT device, using Mo radiation.[18]

For **2.25**-**2.30**: Diffraction data were collected at 100 K on a Bruker Nonius X8 Apex II diffractometer, equipped with an Oxford Cryosystems LT device, using Mo-Kα radiation. Extreme disorder was present in the solvent of crystallisation in **2.25** and **2.28**. As this was the case, the routine SQUEEZE was applied in order to remove the diffuse electron density associated with this disorder.[61] This had the effect of markedly improving the agreement indices upon refinement.

2.3.2 Results and Discussion

Description of structures

All eight complexes display very similar structures (Fig. 2.11) and relevant interatomic distances and angles are given in Table 2.3. All molecules possess an inversion centre and can be described as two off-set $[Mn_3(\mu_3\text{-}O)]^{7+}$ triangular subunits linked via two oximate oxygen atoms from two $\eta^2:\eta^1:\eta^1:\mu^3$ R-sao^{2-} ligands and two phenolate oxygen atoms from two $\eta^1:\eta^1:\eta^2:\mu^3$ R-sao^{2-} ligands. The two remaining R-sao^{2-} ligands bridge two neighbouring Mn centres through an NO oximate group and a phenolate O-atom in a $\eta 1:\eta^1:\eta^1:\mu$ fashion. The coordination sites of the Mn centres are completed by two terminally bound halide or phosphinate ligands and terminal solvent molecules. Due to the large Ph-sao^{2-} ligands in complex **2.28**, Mn3 and its symmetry equivalent are only 5-coordinate. All Mn centres are in the 3+ oxidation state, confirmed by a combination of bond-length considerations, BVS calculations and charge-balance.[20-23] Each Mn centre is in a distorted octahedral geometry with the Jahn-Teller axes approximately perpendicular to the $[Mn_3]$ planes. All complexes have extensive intermolecular interactions between neighbouring molecules propagated in the main through alcohol molecules and the phenyl rings from both the phosphinate and R-saoH_2 ligands. As a result the molecules pack in a head-to-tail fashion in the crystals and for **2.25** this affords the aesthetically pleasing topology shown in Fig. 2.12. The halogen containing complexes **2.23** and **2.24** exhibit intra-molecular interactions between the X^- ions (X = Br (**2.23**), I (**2.24**)) and nearby terminal EtOH molecules (Br1···H14(O8) = 2.459 Å, I1···H441(O44) = 2.687 Å). Inter-molecular interactions observed in **2.23** are limited to H-bonding interactions between the terminal Br^- ligands and the aromatic protons belonging to the Et-sao^{2-} ligands of an adjacent $[Mn_6]$ complex (Br1…H17(C17) = 2.859 Å). The crystal structure of **2.24** shows two types of close contact interactions. More specifically the I^- and oxygen atoms (of terminal EtOH ligands) of each $[Mn_6]$ unit H-bond with the $-CH_3$ protons and aromatic C-$H_{aromatic}$ protons of nearest neighbour Me-sao^{2-} ligands, respectively (I1···H152(C15) = 3.178 Å, O38…H181(C18) = 2.713 Å). The structures are largely comparable to their carboxylate predecessors. One interesting difference however is seen in **2.25** where the phosphinate is terminally

bonded and the two triangular subunits are linked through two oximate oxygens and two phenolate oxygens. All previously reported structures with sao^{2-} have the carboxylate coordinating in a $\eta^1:\eta^1:\mu$ fashion with the triangular subunits linked only through the two oximate oxygens. The structural change is presumably the result of the presence of the very bulky phosphinate.

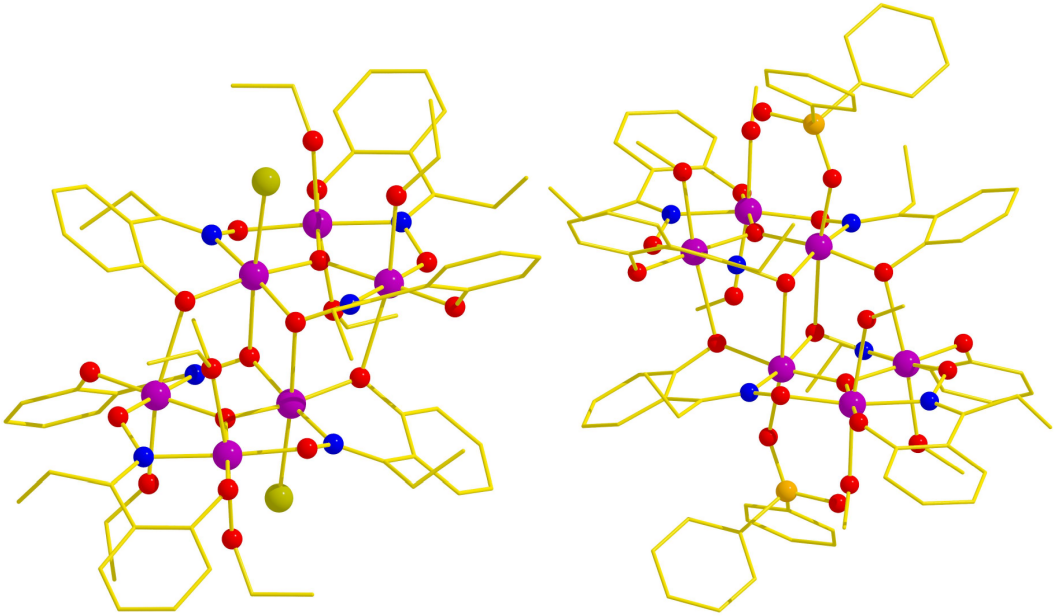

Figure 2.11 The molecular structures of **2.23** (left) and **2.27** (right). Colour code: Purple = Manganese, Red = Oxygen, Blue = Nitrogen, Yellow = Bromine and Orange = Phosphorus.

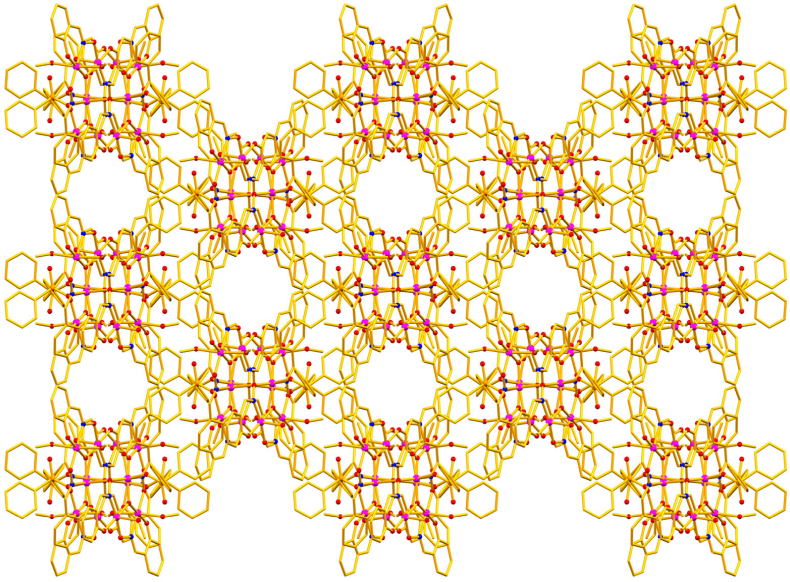

Figure 2.12 The packing of **2.25** viewed along the c-axis.

2.3.3 Magnetochemistry

Dc magnetic susceptibility and magnetisation measurements

Dc magnetic susceptibility measurements were carried out on crystalline samples of **2.23**-**2.30** from 5-300 K in a field of 0.1 T. The data obtained for each complex was simulated using the program MAGPACK[25] using the Hamiltonians in Eqn. (2)-(3) (Scheme 2.2) to give the isotropic parameters summarised in Table 2.4. The $\chi_M T$ vs. T data are plotted in Fig. 2.13 along with their associated simulations (solid lines).

The $\chi_M T$ vs. T curve for complex **2.25** shows weak antiferromagnetic exchange between the Mn^{III} centres with a room temperature value of 14.55 cm^3 K mol^{-1}, below the value of 18 cm^3 K mol^{-1} expected for six non-interacting $s = 2$ ions. $\chi_M T$ remains approximately constant until around 90 K before decreasing to 11.65 cm^3 K mol^{-1} at 5 K. Despite much effort we were unable to satisfactorily simulate the data for **2.25**. The data for complexes **2.26** and **2.28** are somewhat similar to **2.25**, with room temperature $\chi_M T$ values of 18.18 and 18.29 cm^3 K mol^{-1} respectively which gradually increase to maxima of 19.27 and 22.44 cm^3 K mol^{-1}, before decreasing to 14.41 and 11.10 cm^3 K mol^{-1} at 5 K. Unfortunately the data for **2.26** could not be simulated, but those for **2.28** could be by employing the *3-J* model of Eqn. (3) [based on the presence of three very different Mn-N-O-Mn torsion angles (see Table 2.4)], affording an $S = 4$ ground state with the parameters $g = 2.01$, $J_1 = -1.10$, $J_2 = 2.85$ and $J_3 = 1.55$ cm^{-1}. Complexes **2.23**-**2.24, 2.27**, **2.29** and **2.30** display a constant increase in $\chi_M T$ with decreasing temperature indicating the presence of ferromagnetic exchange between the metal centres. The room temperature $\chi_M T$ values range from 18.18 to 20.06 cm^3 K mol^{-1} and all increase gradually until around 75 K where they increase more rapidly to maximum values ranging from 57.46 to 69.54 cm^3 K mol^{-1}. Complex **2.27** reaches a maximum $\chi_M T$ value at 8.5 K before decreasing slightly to 56.05 cm^3 K mol^{-1} at 5 K. The data were successfully simulated using the *2-J* model of Eqn. (2) [based on the presence of two very different Mn-N-O-Mn torsion angles (see Table 2.4)]. It should be noted that the $\chi_M T$ vs. T curve obtained for **2.24** reaches a rather low maximum value 28.31 cm^3 mol^{-1} K suggestive of the presence of an "intermediate" spin ground state; however simulation of the data shows this not to be the case ($S = 12$, $g = 2.00$, $J_1 = +0.95$ and

J_2 = +0.40, Table 2.4) - the lineshape and the low temperature downturn in $\chi_M T$ being attributed to the significant inter-molecular interactions observed in its crystal structure.

As with all members of the large family of Mn_6 complexes,[62] these molecules have multiple low-lying excited states,[24, 31, 32] the result of the weak exchange between the Mn^{III} centres. For **2**.**24**, **2**.**27** and **2**.**30**, the first excited state S = 11 is only 2.05, 2.51 and 2.03 cm^{-1} above the ground state, respectively; for **2**.**23** and **2**.**29** the first excited state is slightly higher at 3.99 and 4.15 cm^{-1}.

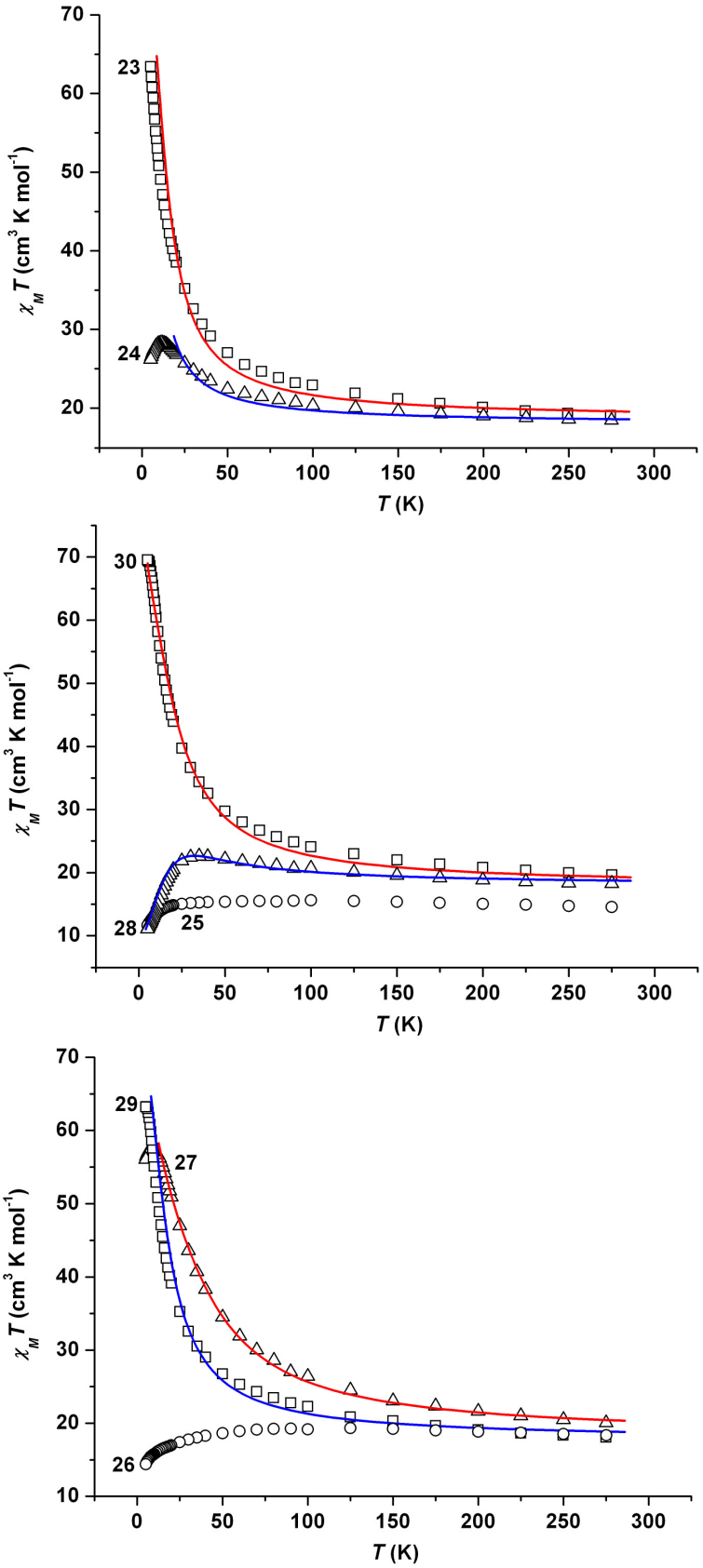

Figure 2.13 $\chi_M T$ vs. T plots for complexes **2.23**-**2.30**. The solid lines represent simulations of the experimental data in the temperature range 300 – 5 K. For parameters see Table 3.

Variable field and temperature dc magnetisation data were collected in the 0.5-7 T and 2-7 K field and temperature ranges for all compounds. In each case we attempted to fit the data with an axial ZFS plus Zeeman Hamiltonian (4) in the whole field and temperature range.[33] The results are summarised in Table 2.4 with a representative plot given in Fig. 2.14. Complexes **2.23**, **2.24** and **2.30** were successfully fitted and afforded the parameters $S = 12$, $g = 2.03$, $D = -0.36$ cm^{-1} (**2.23**), $S = 12$, $g = 2.00$, $D = -0.36$ cm^{-1} (**2.24**) and $S = 12$, $g = 1.98$ and D value of -0.35 cm^{-1} (**2.30**); we were unable to fit the data for the other five complexes, presumably due to the population of low-lying excited states and/or the significant inter-molecular interactions.

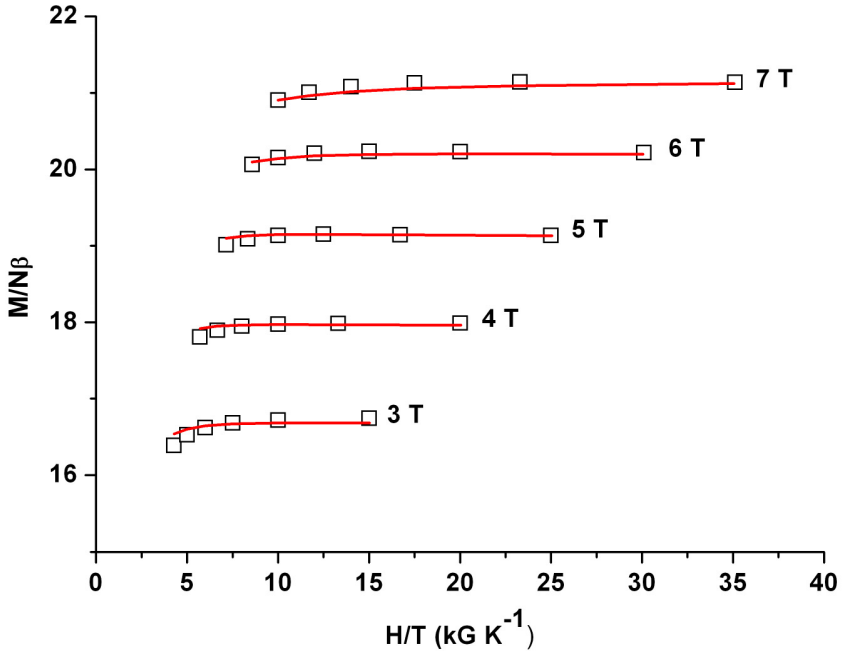

Figure 2.14 Plot of reduced magnetisation ($M/N\mu_B$) versus H/T for **2.30** in the noted field ranges and the 2 – 6 K temperature range. The solid lines correspond to the fit of the data as documented in Table 3.

Ac magnetic susceptibility measurements

Ac magnetic susceptibility measurements were carried out on crystalline samples of **2.22**-**2.30** in the 2-10 K temperature range in a 3.5 G ac field oscillating at frequencies ranging from 50 to 1000 Hz. Complexes **2.25**, **2.26** and **2.28** have in-phase (χ_M') signals (plotted as $\chi_M'T$ vs. T, top of Fig. 2.15) that decrease with decreasing temperature. This indicates the presence of low-lying excited states with larger S values than the ground state. For complexes **2.23**-**2.24**, **2.27**, **2.29** and **2.30**

the in-phase signals increase upon decrasing temperature (middle of Fig. 2.15), indicating low-lying excited states with smaller *S* values than the ground state. Fully visible out-of-phase (χ_M'') signals indicative of SMM behaviour were seen for all complexes (the bottom of Fig. 2.15 shows those for **2**.**27**), except for **2**.**24** where only the tails and not the peaks were observed. The ac data obtained were fitted to the Arrhenius equation (5), to give the effective barrier to magnetisation reorientation (U_{eff}) for each complex. These are summarised in Table 2.4 and range in height from ~31 to 78 K.

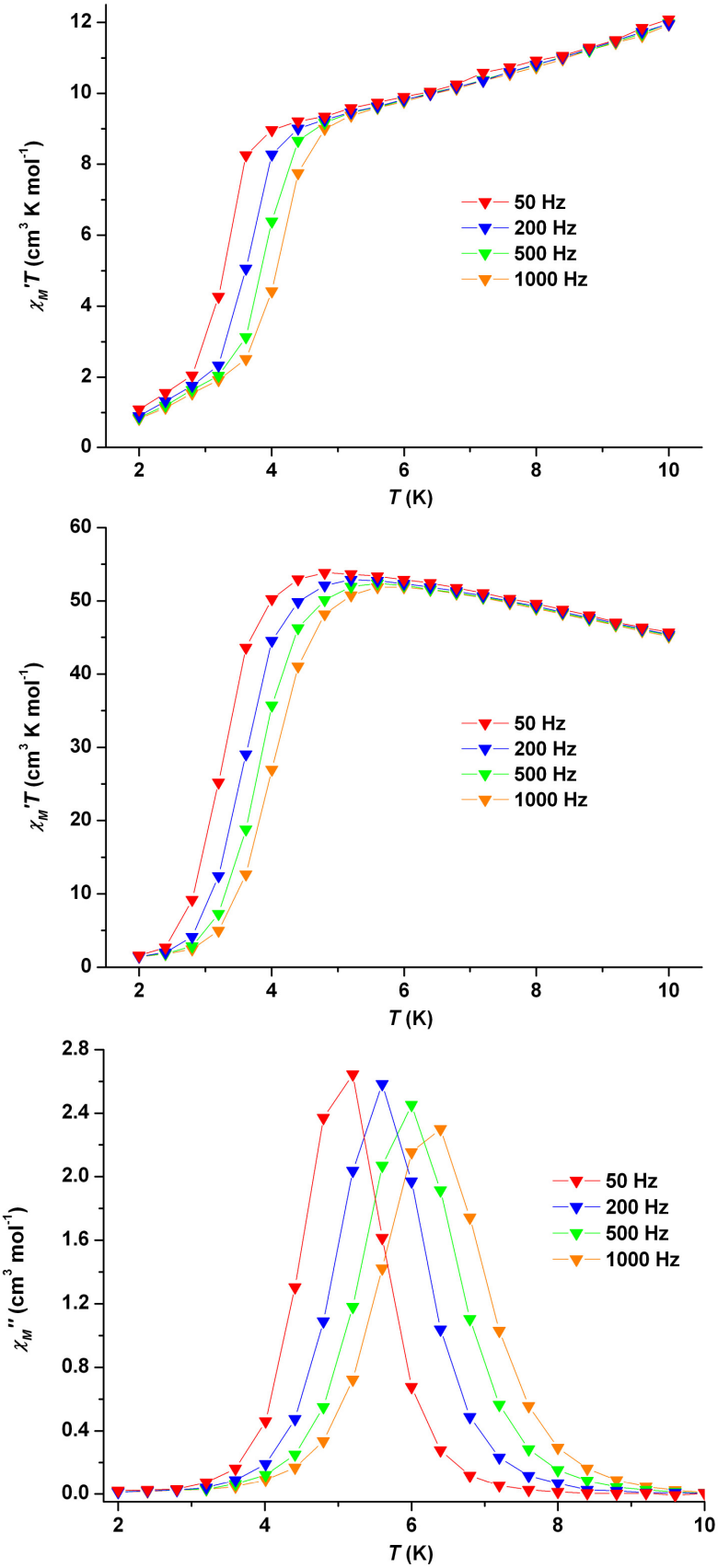

Figure 2.15 AC in-phase $\chi'_M T$ vs. T plots for **2.28** (top) and **2.30** (middle). AC out-of-phase χ''_M vs. T plot obtained for complex **2.27** (bottom) in an oscillating field of 3.5 Oe and frequencies of 50-1000 Hz.

Discussion

This new family of complexes allows for a good comparison between the Mn-N-O-Mn torsion angles (α) and the magnetic exchange as this is the first time the whole series of R-saoH_2 ligands (R = H, Me, Et and Ph) have made complexes with the same terminally bound X ligands, where X = O_2PHPh or $O_2P(Ph)_2$. Studying the results in Tables 2.3 and 2.4 and combining them with our previous studies on similar Mn_6 complexes, allows us to draw some conclusions:

i) In all cases the exchange *between* the [Mn_3] triangles appears to be ferromagnetic.

ii) The exchange between Mn_2 pairs is dominated by the Mn-O-N-Mn torsion angles; the larger the torsion angle, the more ferromagnetic the pairwise interaction; the smaller the Mn-N-O-Mn torsion angle the more antiferromagnetic the pairwise interaction.

iii) Above a torsion angle of approximately 31^o the exchange switches from antiferromagnetic to ferromagnetic, i.e. if $\alpha > 31^o$, then $J > 0$ (F); if $\alpha < 31^o$ then $J < 0$ (AF). When a [Mn_3] triangle contains torsion angles that are both above and below this value the data can only be simulated using both F and AF exchange.

iv) It is the individual torsion angles between neighbouring Mn ions that dictates the behaviour of the complex, and *not* the average torsion angle.

v) The presence and nature of the X ligand appears to have little effect on the sign and magnitude of *J*.

vi) There seems to be no correlation between the out-of-plane shift of the oxide ion and *J*. For example, complexes **2.28** and **2.29** both have the oxide ~0.12 Å above the Mn_3 plane, yet **2.28** displays dominant antiferromagnetic exchange and an $S = 4$ ground state and **2.29** shows dominant ferromagnetic exchange and an $S = 12$ ground state.

Conclusions

We have synthesised and characterised eight new Mn_6 complexes that are new members of the [$Mn^{III}_6O_2$(R-sao)$_6$(X)$_2$(solvent)$_{4-6}$] family of SMMs. For the first time the whole series of R-saoH_2 ligands (R = H, Me, Et and Ph) have made complexes with the same terminally bound X ligands. This allows us, in combination with our previous studies, to conclude that the structural distortion of the Mn-N-O-

Mn unit imposed on the molecule through the use of derivatised R-saoH_2 ligands, is the dominant factor which controls the magnetic exchange.

These complexes also demonstrate that the central Mn_6-oximate core is a stable fragment/building block whose organic periphery can be changed, and this is a very exciting prospect.

Table 2.3 Selected interatomic distances (Å) and angles (°) for complexes **2.23**-**2.30**.

Complex	Mn-(μ_3-O) distance (Å) Mn1-O, Mn2-O, Mn3-O	Mn-(μ_3-O)-Mn angles (°) Mn1-2, Mn2-3, Mn1-3	Mn_{3plane}-(μ_3-O) (Å)	Mn-O_{phen} (Å)	Mn-Hal^- / -O_2PR distance (Å)
$[Mn_6O_2(Et\text{-}sao)_6(Br)_2(EtOH)_6]$ (**2.23**)	1.882(2), 1.888(2), 1.875(2)	118.85(11), 120.75(11), 120.38(11)	0.014	2.429	2.688 (7)
$[Mn_6O_2(Me\text{-}sao)_6(I)_2(EtOH)_6]$ (**2.24**)	1.873(2), 1.883(2), 1.887(2)	120.03(9), 119.08(9), 120.06(9)	0.099	2.513	2.918(5)
$[Mn_6O_2(sao)_6(O_2P(Ph)_2)_2(MeOH)_6]$ (**2.25**)	1.902(4), 1.900(3), 1.889(3)	119.76(8), 119.34(10), 119.68(13)	0.217	2.555	2.075(3)
$[Mn_6O_2(Me\text{-}sao)_6(O_2P(Ph)_2)_2(MeOH)_6]\cdot 3MeOH$ (**2.26**)	1.875(3), 1.873(2), 1.878(3)	121.38(10), 120.78(10), 116.63(12)	0.120	2.478	2.084(3)
$[Mn_6O_2(Et\text{-}sao)_6(O_2P(Ph)_2)_2(MeOH)_6]$ (**2.27**)	1.889(2), 1.889(2), 1.879(2)	116.90(8), 121.64(8), 120.47(8)	0.109	2.498	2.115(2)
$[Mn_6O_2(Ph\text{-}sao)_6(O_2P(Ph)_2)_2(MeOH)_4]$ (**2.28**)	1.899(4), 1.895(4), 1.868(5)	118.99(19), 119.72(14), 120.08(18)	0.120	2.323	2.106(4)
$[Mn_6O_2(Me\text{-}sao)_6(O_2PHPh)_2(MeOH)_6]\cdot MeOH$ (**2.29**)	1.884(3), 1.873(3), 1.892(3)	119.45(19), 121.79(15), 117.52(15)	0.121	2.474	2.080(3)
$[Mn_6O_2(Et\text{-}sao)_6(O_2PHPh)_2(MeOH)_6]\cdot MeOH$ (**2.30**)	1.892(3), 1.892(2), 1.876(2)	117.73(12), 120.58(10), 120.68(9)	0.111	2.501	2.084(3)

Table 2.4 Magnetostructural parameters for complexes **2.23**-**2.30**; Mn-N-O-Mn torsion angles *vs*. *J* and *S*.

Cmpl.	Crystal Sys.	Sp. Grp.	α / ° Mn1-2 / Mn2-3 / Mn1-3	J / cm^{-1} [a] J_1 / J_2 / J_3	S [b]	$1^{st}_{exc.\ st.}$ (cm^{-1}) [b]	g [c]	D /cm^{-1} [d]	τ_0 / s [e]	U_{eff} / K [e]
(**2.23**)	Monoclinic	$P2_1/c$	33.40, 43.89, 33.00	+1.03, +0.83	12	11(3.99)	2.03	-0.36	5.45×10^{-10}	54.1
(**2.24**)	Monoclinic	$P2_1/c$	33.01, 31.28, 37.16	+0.95, +0.40	12	11(2.05)	2.00	-0.36	n.a.	n.a.
(**2.25**)	Monoclinic	*C*2/*c*	17.78, 32.88, 13.53	n.a.	n.a.	n.a.	n.a.	n.a.	1.34×10^{-9}	31.04
(**2.26**)	Monoclinic	*C*2/*c*	41.68, 27.64, 35.82	n.a.	n.a.	n.a.	n.a.	n.a.	3.05×10^{-10}	44.67
(**2.27**)	Monoclinic	*C*2/*c*	30.22, 24.23, 43.51	2.88, -1.25	12	11(2.51)	2.00	n.a.	6.93×10^{-10}	77.92
(**2.28**)	Triclinic	P-1	51.76, 28.04, 14.08	-1.10, 2.85, 1.55	4	5(5.74)	2.01	n.a.	1.50×10^{-09}	47.98
(**2.29**)	Triclinic	P-1	32.31, 38.40, 37.43	1.25, 0.40	12	11(4.15)	1.98	n.a.	5.19×10^{-10}	48.77
(**2.30**)	Triclinic	P-1	40.22, 23.28, 40.39	2.15, -1.00	12	11(2.03)	1.98	-0.35	8.64×10^{-10}	48.99

[a]Calculated from dc susceptibility studies. [b]Calculated from both dc susceptibility and magnetization measurements. [c]Calculated from dc susceptibility measurements. [d]Calculated from magnetization measurements. [e]Calculated from ac susceptibility data; n.a. = not available.

2.4 References

1. G. Rajaraman, M. Murugesu, E. C. Sañudo, M. Soler, W. Wernsdorfer, M. Helliwell, C. Muryn, J. Raftery, S. J. Teat and B. E. K., *J. Am. Chem. Soc.*, 2004, **126**, 15445.
2. E. K. Brechin, *Chem. Commun.*, 2005, 5141.
3. M. Soler, P. Artus, K. Folting, J. C. Huffman, D. N. Hendrickson and G. Christou, *Inorg. Chem.*, 2001, **40**, 4902.
4. M. Soler, S. K. Chandra, D. Ruiz, J. C. Huffman, D. N. Hendrickson and G. Christou, *Polyhedron*, 2001, **20**, 1279.
5. N. E. Chakov, M. Soler, W. Wernsdorfer, K. A. Abboud and G. Christou, *Inorg. Chem.*, 2005, **44**, 5304.
6. S. M. J. Aubin, Z. P. Sun, L., J. Krzystek, K. Folting, L. C. Brunel, A. L. Rheingold, G. Christou and D. N. Hendrickson, *Inorg. Chem.*, 1999, **38**, 5329.
7. P. Artus, C. Boscovic, J. Yoo, W. E. Streib, L. C. Brunel, D. N. Hendrickson and G. Christou, *Inorg. Chem.*, 2001, **40**, 4199.
8. N. E. Chakov, W. Wernsdorfer, K. A. Abboud, D. N. Hendrickson and G. Christou, *Dalton Trans.*, 2003, 2243.
9. C. J. Milios, C. P. Raptopoulou, A. Terzis, F. Lloret, R. Vicente, S. P. Perlepes and A. Escuer, *Angew. Chem., Int. Ed.*, 2004, **43**, 210.
10. T. C. Stamatatos, D. Foguet-Albiol, C. C. Stoumpos, C. P. Raptopoulou, A. Terzis, W. Wernsdorfer, S. P. Perlepes and G. Christou, *J. Am. Chem. Soc.*, 2005, **127**, 15380.
11. J. B. Vincent, H.-R. Chang, K. Folting, J. C. Huffman, G. Christou and D. N. Hendrickson, *J. Am. Chem. Soc.*, 1987, **109**, 5703.
12. C. J. Milios, R. Inglis, R. Bagai, W. Wernsdorfer, A. Collins, S. A. Moggach, S. Parsons, S. P. Perlepes, G. Christou and E. K. Brechin, *Chem. Commun.*, 2007, **33**, 3476.
13. C. J. Milios, A. Vinslava, W. Wernsdorfer, A. Prescimone, P. A. Wood, S. Parsons, S. P. Perlepes, G. Christou and E. K. Brechin, *J. Am. Chem. Soc.*, 2007, **129**, 6547.
14. C. J. Milios, A. Vinslava, W. Wernsdorfer, S. A. Moggach, S. Parsons, S. P. Perlepes, G. Christou and E. K. Brechin, *J. Am. Chem. Soc.*, 2007, **129**, 2754.
15. C. Boskovic, M. Pink, J. C. Huffman, D. N. Hendrickson and G. Christou, *J. Am. Chem. Soc.*, 2001, **123**, 9914.
16. E. K. Brechin, R. A. Coxall, A. Parkin, S. Parsons, P. A. Tasker and R. E. P. Winpenny, *Angew. Chem., Int. Ed.*, 2001, **40**, 2700.
17. C. He and S. J. Lippard, *J. Am. Chem. Soc.*, 2000, **122**, 184.
18. D. J. Watkin, C. K. Prout, J. R. Carruthers, P. W. Betteridge and R. I. Cooper, Chemical Crystallography Laboratory, University of Oxford, Oxford, UK, 2003.
19. W. Wernsdorfer, *Adv. Chem. Phys.*, 2001, **118**, 99.
20. I. D. Brown and D. Altermatt, *Acta Crystallogr.*, 1985, **B41**, 244.
21. W. Liu and H. H. Thorp, *Inorg. Chem.*, 1993, **32**, 4102.

22. J. P. Naskar, S. Hati and D. Datta, *Acta Crystallogr.*, 1997, **B53**, 885.
23. H. H. Thorp, *Inorg. Chem.*, 1992, **31**, 1585.
24. C. J. Milios, S. Piligkos and E. K. Brechin, *Dalton Trans.*, 2008, 1809.
25. J. J. Borras-Alemnar, J. M. Clemente-Juan, E. Coronado and B. S. Tsukerblat, *J. Comp. Chem.*, 2001, **22**, 985.
26. J. Cano, T. Cauchy, E. Ruiz, C. J. Milios, C. C. Stoumpos, T. C. Stamatatos, S. P. Perlepes, G. Christou and E. K. Brechin, *Dalton Trans.*, 2008, 234.
27. C. J. Milios, P. A. Wood, S. Parsons, D. Foguet-Albiol, C. Lampropoulos, G. Christou, S. P. Perlepes and E. K. Brechin, *Inorg. Chim. Acta*, 2007, **360**, 3932.
28. C. J. Milios, R. Inglis, A. Vinslava, R. Baghi, W. Wernsdorfer, S. Parsons, S. P. Perlepes, G. Christou and E. K. Brechin, *J. Am. Chem. Soc.*, 2007, **129**, 12505.
29. C. J. Milios, A. G. Whittaker and E. K. Brechin, *Polyhedron*, 2007, **26**, 1927.
30. P. Chaudhuri, *Coord. Chem. Rev.*, 2003, **243**, 143.
31. S. Bahr, C. J. Milios, E. K. Brechin, V. Mosser and W. Wernsdorfer, *Phys. Rev. B*, 2008, **78**, 132401.
32. S. Carretta, T. Guidi, P. Santini, G. Amoretti, O. Pieper, B. Lake, J. Van Slageren, H. Mutka, M. Russina, C. J. Milios and E. K. Brechin, *Phys. Rev. Lett.*, 2008, **100**, 157203.
33. S. Piligkos, University of Copenhagen, Copenhagen, Denmark.
34. A. Bencini and D. Gatteschi, *EPR of Exchange Coupled Systems*, Springer, Berlin, 1990.
35. S. Piligkos, J. Bendix, H. Weihe, C. J. Milios and E. K. Brechin, *Dalton Trans.*, 2008, 2277.
36. W. Wernsdorfer, M. Murugesu and G. Christou, *Phys. Rev. Lett.*, 2006, **96**, 057208.
37. M. Mola, S. Hill, P. Goy and M. Gross, *Rev. Sci. Instrum.*, 2000, **71**, 186.
38. S. Takahashi and S. Hill, *Rev. Sci. Instrum.*, 2005, **76**, 023114.
39. S. Takahashi, R. S. Edwards, J. M. North, S. Hill and N. S. Dalal, *Phys. Rev. B*, 2004, **70**, 094429.
40. S. Datta, E. Bolin, R. Inglis, C. J. Milios, E. K. Brechin and S. Hill, *Polyhedron*, 2009, **28**, 1788.
41. S. Hill, S. Datta, J. Liu, R. Inglis, C. J. Milios, P. L. Feng, J. J. Henderson, E. d. Barco, E. K. Brechin and D. N. Hendrickson, *Dalton Trans.*, 2010, **39**, 4693.
42. D. Gatteschi, O. Kahn and R. D. Willett, *Magneto Structural Correlation in Exchange Coupled Systems*, D. Reidel, Dordrecht, 1985.
43. M. F. Charlot, O. Kahn and M. Drillon, *Chem. Phys.*, 1982, **70**, 177.
44. V. H. Crawford, H. W. Richardson, J. R. Wasson, D. J. Hodgson and W. E. Hatfield, *Inorg. Chem.*, 1976, **15**, 2107.
45. J. Glerup, D. J. Hodgson and E. Petersen, *Acta Chem. Scand. A*, 1983, **A37**, 161.
46. S. M. Gorun and S. J. Lippard, *Inorg. Chem.*, 1991, **30**, 1625-1630.
47. W. E. Hatfield, *Comments on Inorganic Chemistry*, 1981, **1**, 105.
48. C. P. Landee and R. E. Greeney, *Inorg. Chem.*, 1986, **25**, 3371.
49. W. E. Marsh, K. C. Patel, W. E. Hatfield and D. J. Hodgson, *Inorg. Chem.*, 1983, **22**, 511.

50. S. S. Tandon, L. K. Thompson, M. E. Manuel and J. N. Brisdon, *Inorg. Chem.*, 1994, **33**, 5555.
51. H. Weihe and H. U. Güdel, *J. Am. Chem. Soc.*, 1997, **119**, 6539.
52. T. Cauchy, E. Ruiz and S. Alvarez, *J. Am. Chem. Soc.*, 2006, **128**, 15722.
53. J. M. Clemente-Juan, B. Chansou, B. Donnadieu and J.-P. Tuchagues, *Inorg. Chem.*, 2000, **39**, 5515.
54. M. A. Halcrow, J.-S. Sun, J. C. Huffman and G. Christou, *Inorg. Chem.*, 1995, **34**, 4167.
55. K. Isele, F. Gigon, A. F. Williams, G. Bernardinelli, P. Franz and S. Decurtins, *Dalton Trans.*, 2007, 332.
56. F. Neese, *J. Am. Chem. Soc.*, 2006, **128**, 10213.
57. M. R. Pederson and S. N. Khanna, *Phys. Rev. B*, 1999, **59**, R693.
58. A. V. Postnikov, J. Kortus and M. R. Pederson, *Physica Status Solidi B*, 2006, **243**, 2533.
59. T. C. Stamatatos, D. Foguet-Albiol, S.-C. Lee, C. C. Stoumpos, C. P. Raptopoulou, A. Terzis, W. Wernsdorfer, S. Hill, S. P. Perlepes and G. Christou, *J. Am. Chem. Soc.*, 2007, **129**, 9484.
60. R. D. Cannon and R. P. White, *Prog. Inorg. Chem.*, 1988, **36**, 195.
61. A. L. Spek, *J.Appl.Cryst.*, 2003, **36**, 7.
62. R. Inglis, L. F. Jones, C. J. Milios, S. Datta, A. Collins, S. Parsons, W. Wernsdorfer, S. Hill, S. P. Perlepes, S. Piligkos and E. K. Brechin, *Dalton Trans.*, 2009, **18**, 3403.

Chapter 3
Strategies for Making Ferromagnetic Mn_3 Triangles

3.1 Introduction

The synthesis and study of polymetallic clusters containing paramagnetic transition metal ions has provided scientists with molecules displaying fascinating new physics.[1-19] The emergence of *Molecular Nanomagnets* in proposed applications as diverse as information storage, molecular spintronics, quantum computation and magnetic refrigeration has seen synthetic chemists, physicists, theoreticians and materials scientists working in tandem to create, understand and design molecules with specific properties. For example, combining the organic chemistry of rotaxanes with the inorganic chemistry of heterometallic wheels recently resulted in the assembly a beautiful family of inorganic-organic molecular shuttles comprising inorganic rings assembled around organic threads.[20] The amalgamation of two previously unconnected areas of chemistry is a timely illustration that with some imagination chemists can create molecules with untold potential.

Oxide-centred $[Mn^{III}_3]$ triangles have interested inorganic coordination chemists for many years not only for the study of their intrinsic magnetism but because they represent the basic building block from which a plethora of beautiful polymetallic clusters with fascinating physical properties are constructed.[21] The first ferromagnetic $[Mn^{III}_3O]^{7+}$ triangle, $[Mn_3O(bamen)](ClO_4)$ (where H_2bamen is 1,2-bis(biacetylmonoximeimino)ethane was only reported in 2002,[22] with a second example, $[Mn_3O(mpko)_3(O_2CR)_3](ClO_4)$ (mpkoH = methyl 2-pyridyl ketone oxime) appearing in 2005.[23] Both molecules can be considered simple structural analogues of the well known basic carboxylates of general formula $[Mn^{III}_3O(O_2CR)_6L_3]^+$ (R = Me, Et, Ph; L = H_2O, py, MeCN *etc*) in which the bridging carboxylates (Mn-O-C-O-Mn) have been replaced with bridging oximes (Mn-N-O-Mn) – all six in the former and only the "lower" three in the latter (Fig. 3.1).

The publication of these two molecules was fascinating and prompted us to ask the following questions: why do these oxime-bridged triangles display dominant ferromagnetic exchange between the metal centres and thus S = 6 ground states, while the carboxylate-only $[Mn^{III}_3O]$ triangles display dominant antiferromagnetic exchange? And why did our own (and at the time unpublished) oxime-based

triangles of general formula $[Mn^{III}_3O(sao)_3(O_2CR)L_4]$ (where $saoH_2$ is salicylaldoxime and L = H_2O, py; Fig. 3.1)[24, 25] display dominant antiferromagnetic exchange and $S = 2$ ground states?

An initial inspection of the molecular structures (Fig. 3.1) of the three molecules provided a possible clue to the puzzle and implanted an idea. Both $[Mn_3O(bamen)](ClO_4)$ and $[Mn_3O(mpko)_3(O_2CR)_3](ClO_4)$ (Fig. 3.1) have structures that are essentially analogous to the well known $[Mn^{III}_3O(O_2CR)_6L_3]^+$ family[26] where the bridging oximes simply replace the carboxylates and thus occupy a plane at approximately 60° to the $[Mn_3O]$ plane, while the oxime bridges in the $[Mn^{III}_3O(sao)_3(O_2CR)L_4]$ family are in exactly the same plane as the $[Mn_3O]$ unit (Fig. 3.1). Clearly these three family types, despite being closely related, are different because their formulae and structural architectures are not the same, nevertheless we wondered if forcing or "twisting" the planar equatorial Mn-N-O-Mn unit out of the $[Mn^{III}_3O]$ plane in the latter (R-$saoH_2$) family would have any significant effect and if so whether this would be large enough to switch the pairwise exchange from antiferromagnetic to ferromagnetic.

We speculated that a change from salicylaldoxime to its alkyl/aryl-substituted derivatives (R-$saoH_2$) would provide the steric perturbation required to do this, and indeed this has already proven successful for a family of hexametallic single-molecule magnets (SMMs) of formula $[Mn_6O_2(R\text{-}sao)_6(X)_2(L)_{4\text{-}6}]$ (R = H, Me, Et, Ph; X = O_2CR', halide, phosphinate; L = MeOH, EtOH, H_2O) with spin ground states ranging from $S = 4$ to $S = 12$.[27-33] This chapter returns to the $[Mn^{III}_3O(sao)_3(O_2CR)L_4]$ molecules and reports a family of over twenty $[Mn^{III}_3]$ triangles whose ground state spin values appear to be controlled by the puckering or twisting of their central cores. Initial studies by us,[34-36] and more recently by others on related systems[37] have suggested this to be the case.

The puckering of a planar $[Mn_3O(oxime)_3]$ triangle can be achieved in three ways: (a) through the use of derivatised salicylaldoxime (R-$saoH_2$) ligands that occupy the equatorial ($[Mn_3]$) plane - in the same manner as that already achieved for the $[Mn_6]$ SMMs; (b) by employing small "pincer" type tripodal ligands (ClO_4^-, ReO_4^- *etc*) to sit on the "upper" triangular face; and (c) by employing large sterically bulky ligands to occupy the "lower" triangular face.[34-36]

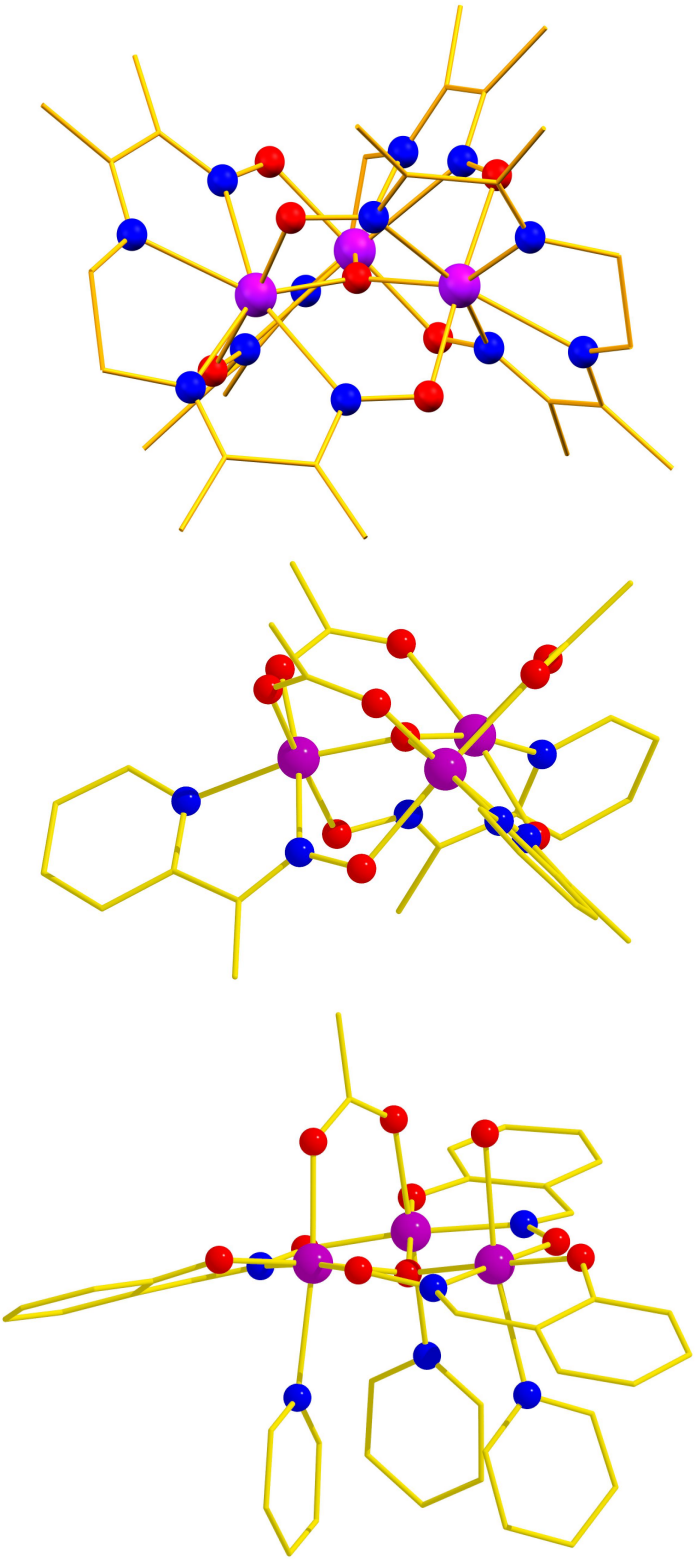

Figure 3.1 Top-bottom: the molecular structures of $[Mn_3O(bamen)]^+$, $[Mn_3O(mpko)_3(O_2CR)_3]^+$ and $[Mn^{III}_3O(sao)_3(O_2CR)L_4]$ (R = Me; L = py, H_2O). Colour code: Mn = purple, O = red, N = blue, C = gold.

3.2 Strategies for Making Ferromagnetic Mn_3 Triangles

3.2.1 Experimental Section

Synthesis

All manipulations were performed under aerobic conditions, using materials as received. CAUTION! Although no problems were encountered in this work, care should be taken when using the potentially explosive perchlorate anion.

General synthetic strategies:

For complexes **3.1**-**3.2**, **3.13**, **3.16**-**3.19** and **3.21**: $Mn^{II}(ClO_4)_2{\cdot}6H_2O$ (1 mmol) and the (derivatised) salicylaldoxime ligand R-saoH_2 (R = H, Naphth, Et, Ph; 1 mmol) were dissolved in a mixture of pyridine (or derivatised pyridine) (5 ml) and MeOH (20ml) with NEt_4OH (1 mmol). Complexes **3.13** and **3.19** were dissolved only in MeOH and for **3.19**, $NaReO_4$ (1 mmol) was also added to the reaction mixture. The solutions were left stirring for ~1 hr and then filtered. Et_2O was diffused into one half of the solution and the remainder was left to slowly evaporate. Suitable crystals grew after 3-5 days from both solutions.

For complexes **3.3**-**3.6**, **3.8**-**3.10**: $Mn^{II}X_2{\cdot}nH_2O$ (X = ClO_4, O_2CCH_3, O_2CPh, O_2C-Naphth) (1 mmol) and the (derivatised) salicylaldoxime ligand R-saoH_2 (R = H, Me, ^{t}Bu; 1 mmol) were dissolved in a mixture of pyridine (5 ml) and EtOH (20ml) with NEt_4OH (CH_3ONa or NBu_4MnO_4) (1 mmol). The solutions were left stirring for ~1 hr and then filtered. The solutions were left to slowly evaporate and suitable crystals grew after 3-5 days.

For complexes **3.7**, **3.11**-**3.12**, **3.14**-**3.15** and **3.20**: $Mn^{II}(ClO_4)_2{\cdot}6H_2O$ (1 mmol) and the derivatised salicylaldoxime ligand R-saoH_2 (R = Me, ^{t}Bu, Et, Ph; 1 mmol) were dissolved in MeOH (or EtOH) with the corresponding carboxylic acid (or sodium carboxylate) and NEt_4OH (CH_3ONa, or triethanolamine) (1 mmol). For **3.7** and **3.14**, $Mn^{II}(ClO_4)_2{\cdot}6H_2O$ was replaced with $Mn^{II}(O_2CCH_3)_2{\cdot}4H_2O$ and $Mn^{II}(O_2CPh)_2{\cdot}4H_2O$ respectively. The solutions were left stirring for ~1 hr and then filtered. Suitable crystals grew after 3-5 days from slow evaporation of the solutions.

X-ray crystallography

Diffraction data were collected at 150 K on a Bruker Smart Apex CCDC diffractometer, equipped with an Oxford Cryosystems LT device, using Mo radiation.[38] See CIF files for full details.

Magnetic measurements

Variable temperature, solid-state direct current (dc) and alternating current (ac) magnetic susceptibility data down to 1.8 K were collected on a Quantum Design MPMS-XL SQUID magnetometer equipped with a 7 T dc magnet. Diamagnetic corrections were applied to the observed paramagnetic susceptibilities using Pascal's constants. Magnetic studies below 1.8 K were carried out on single crystals using a micro-SQUID apparatus operating down to 40 mK.[39]

3.2.2 Results and Discussion

Description of structures

The twenty-one complexes (Table 3.1, page 94) can be divided into three structural types. Complexes **3.3**-**3.6** and **3.8**-**3.10** can be represented by the general formula (*type 1*) $[Mn^{III}_3O(R\text{-}sao)_3(X)(sol)_{3\text{-}4}]$ (where R = H, Me, ^{t}Bu; X = ^-O_2CR (R = H, Me, Ph *etc*); sol = py and/or H_2O). Complexes **3.7**, **3.11**-**3.12**, **3.14**-**3.15** and **3.20** can be described by (*type 2*) $[Mn^{III}_3O(R\text{-}sao)_3(X)(sol)_{3\text{-}5}]$ (where R= Me, Et, Ph, ^{t}Bu; X = ^-O_2CR (R = H, Me, Ph *etc*); sol = MeOH, EtOH and/or H_2O), and complexes **3.1**-**3.2**, **3.13**, **3.16**-**3.19** and **3.21** can be represented by the formula (*type 3*) $[Mn^{III}_3O(R\text{-}sao)_3(sol)_3(XO_4)]$ (where R = H, Et, Ph, Naphth; sol = py, MeOH, β-pic, Et-py, ^{t}Bu-py; X = Cl, Re) (Fig. 3.2). Inter-atomic distances and angles relevant to the discussion herein are shown in Table 3.1. Each complex consists of the same core comprising a $[Mn^{III}_3O]^{7+}$ triangular unit (Fig. 3.2) with three R-sao^{2-} ligands bridging between adjacent Mn^{III} centres in a η^1:η^1:η^1:μ-fashion. For *type 1* complexes the three axial sites at the base of the molecule are occupied by pyridine molecules. The η^1:η^1:μ-bridging carboxylate ligand connects two Mn^{III} centres (Mn1 and Mn2) on the upper face of the molecule. The remaining site on the upper face is occupied by a pyridine or H_2O molecule in **3.3**, **3.6** and **3.9**, but remains unoccupied in **3.4**, **3.5**, **3.8**

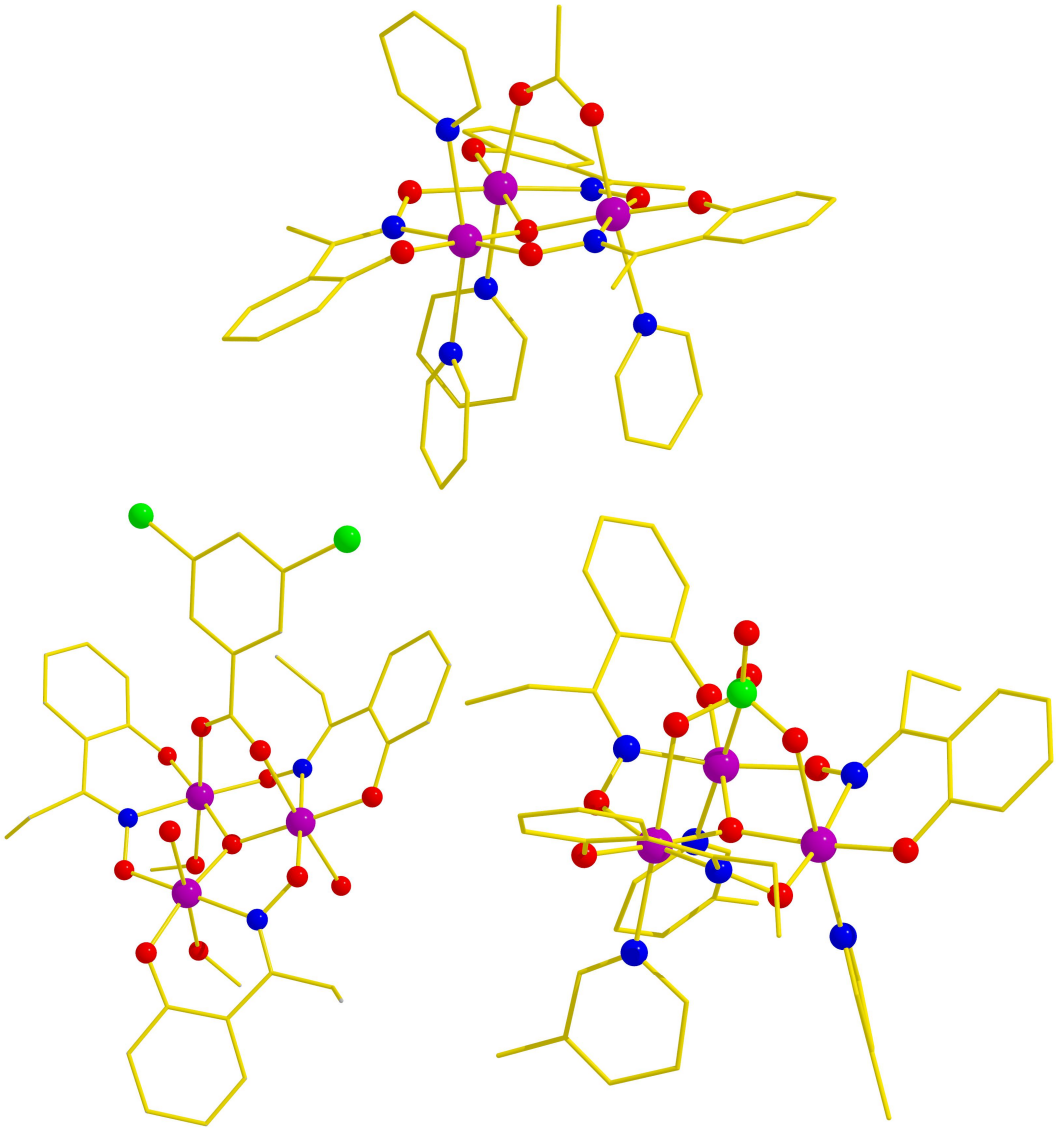

Figure 3.2 The molecular structures of **3.9** (top, *type 1*), **3.12** (bottom left, *type 2*) and **3.16** (bottom right, *type 3*) representing the three different structural types in the [Mn_3] family. Colour code: Mn = purple, O = red, N = blue, C = gold, Cl = green.

and **3.10** (Mn3 is five-coordinate) owing to the presence of a bulkier carboxylate group. Each Mn^{III} centre adopts a distorted octahedral geometry and displays Jahn-Teller elongation, with Mn-O_2CR bond lengths in the range 2.13-2.27 Å and Mn-N bond lengths in the range 2.22-2.58 Å; *i.e.* the JT axes are perpendicular to the [Mn_3] plane. In **3.8**, a six-coordinate Na^+ ion connects two symmetry equivalent $\{Mn^{III}_3O(Me\text{-}sao)_3(O_2C_{15}H_9)(py)_3\}$ moieties together forming a [{Mn_3}-Na-{Mn_3}] dimer, with charge balanced by two symmetry-equivalent ClO_4^- counter ions and one pyridinium cation, which is H-bonded to the pyridine solvent molecule. *Type 2*

molecules have the same core structure as *type 1*, the only difference being the terminally bonded pyridine molecules are replaced by alcohol and/or H_2O molecules. Complexes **3**.**7** and **3**.**11** have the carboxylate bonded terminally with the vacant site on the other Mn centre taken up by another solvent molecule. In **3**.**11** the Mn centre attached to the carboxylate is five-coordinate. Complex **3**.**14** has two carboxylate ligands in its structure, with one bridging Mn1 and Mn2 on the upper face and the other terminally bound to Mn3 on the lower face. The charge is balanced by a protonated triethanolamine ligand which is connected to Mn3.

Type 3 molecules have the upper face of the molecule capped by a η^1:η^1:η^1:μ_3 coordinated XO_4^- (X = Cl, Re) anion with the three axial sites on the lower face occupied by solvent molecules.

Type 2 molecules (and complex **3**.**13**) have extensive inter-molecular interactions propagated by the terminal alcohol/H_2O molecules and carboxylate ligands in all three dimensions that severely affect their magnetic behaviour (*vide infra*). For example, the molecules in **3**.**12** are arranged with their upper faces face-to-face. The water molecule which is attached on the upper face of the Mn3 triangle is hydrogen bonded to a carboxylate O-atom [∠O2-H22···O24 160.0°, O···O 2.913(2) Å and H···O 2.130 Å] that belongs to the same cluster and to a phenolate O-atom of a neighbouring cluster [∠O2-H21···O13 (1-x, -y, -z) 174.0°, O···O 2.791(2) Å and H···O 1.980 Å] creating a hydrogen-bonded dimer (Fig. 3.3). The dimers assemble with the bases of the Mn_3 triangles face-to-face through two complementary hydrogen bonds that involve a methanolic OH group of one cluster and a phenolate O- atom of a neighbouring cluster [∠O25-H251···O11 (1-x, -y, 1-z) 165.0°, O···O 2.783(2) Å and H···O 1.980 Å] to create a zig-zag chain that runs parallel to the *a* axis (Fig. 3.3). All Mn_3 mean planes within a chain are parallel, with the inter-plane distances being 4.011 Å within a dimer and 3.471 Å between dimers, respectively. Clusters of **3**.**15** assemble through the coordinated water molecules of the upper face of the Mn_3 triangle and a phenolate O-atom to form a hydrogen-bonded dimer [∠O47-H472···O26 (1-x, -y, 2-z) 156.0°, O···O 2.812(4) Å and H···O 2.060 Å]. The dimers assemble *via* the coordinated water and ethanol molecules of the Mn_3 triangle base with the lattice ethanol and water molecules to form a two-dimensional hydrogen-bonded layer that runs parallel to the *ab* plane (Fig. 3.4). All Mn_3 mean

planes within a layer are again parallel and form an angle of approximately 42° with respect to the mean plane of the layer and the *ab* plane. The inter-plane $Mn_3\cdots Mn_3$ distance within a dimer is 3.929 Å.

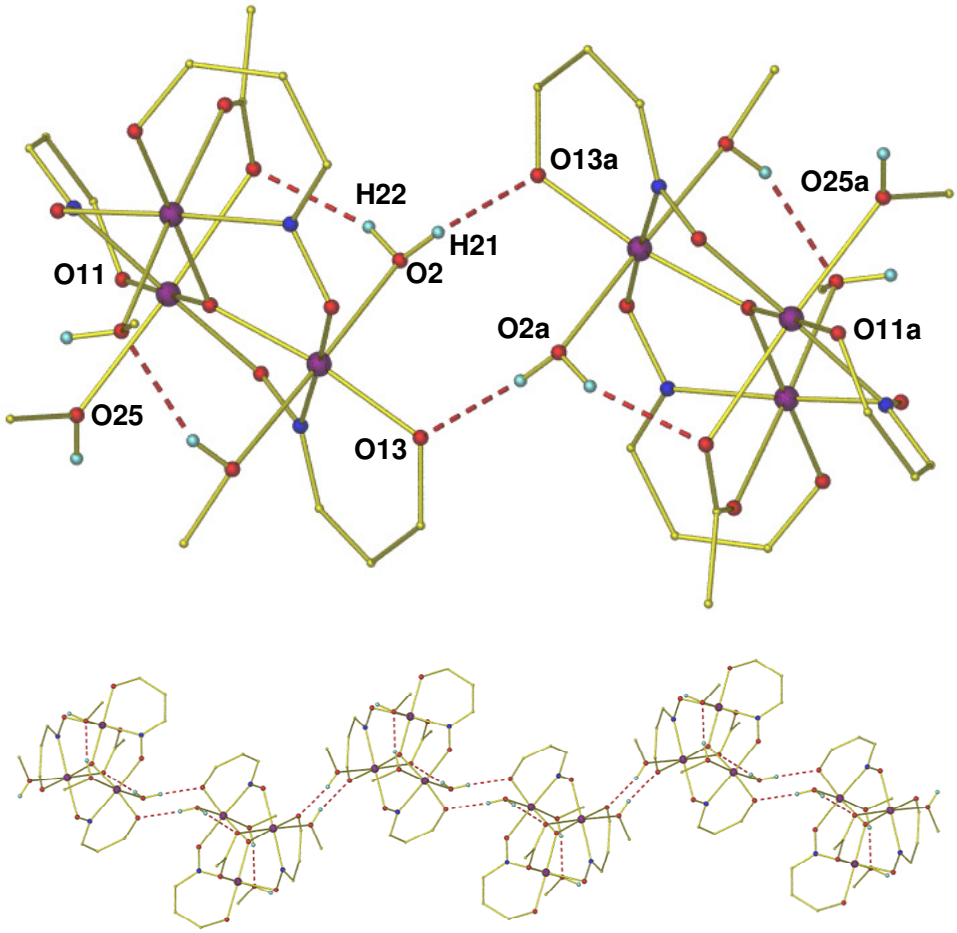

Figure 3.3 The hydrogen bonded dimer (top) and the chain (bottom) of **3.12**. Most hydrogen and carbon atoms have been omitted for clarity. Colour code: Mn = purple, O = red, N = blue, C = gold, H = cyan. Symmetry code: a 1-x, -y, -z.

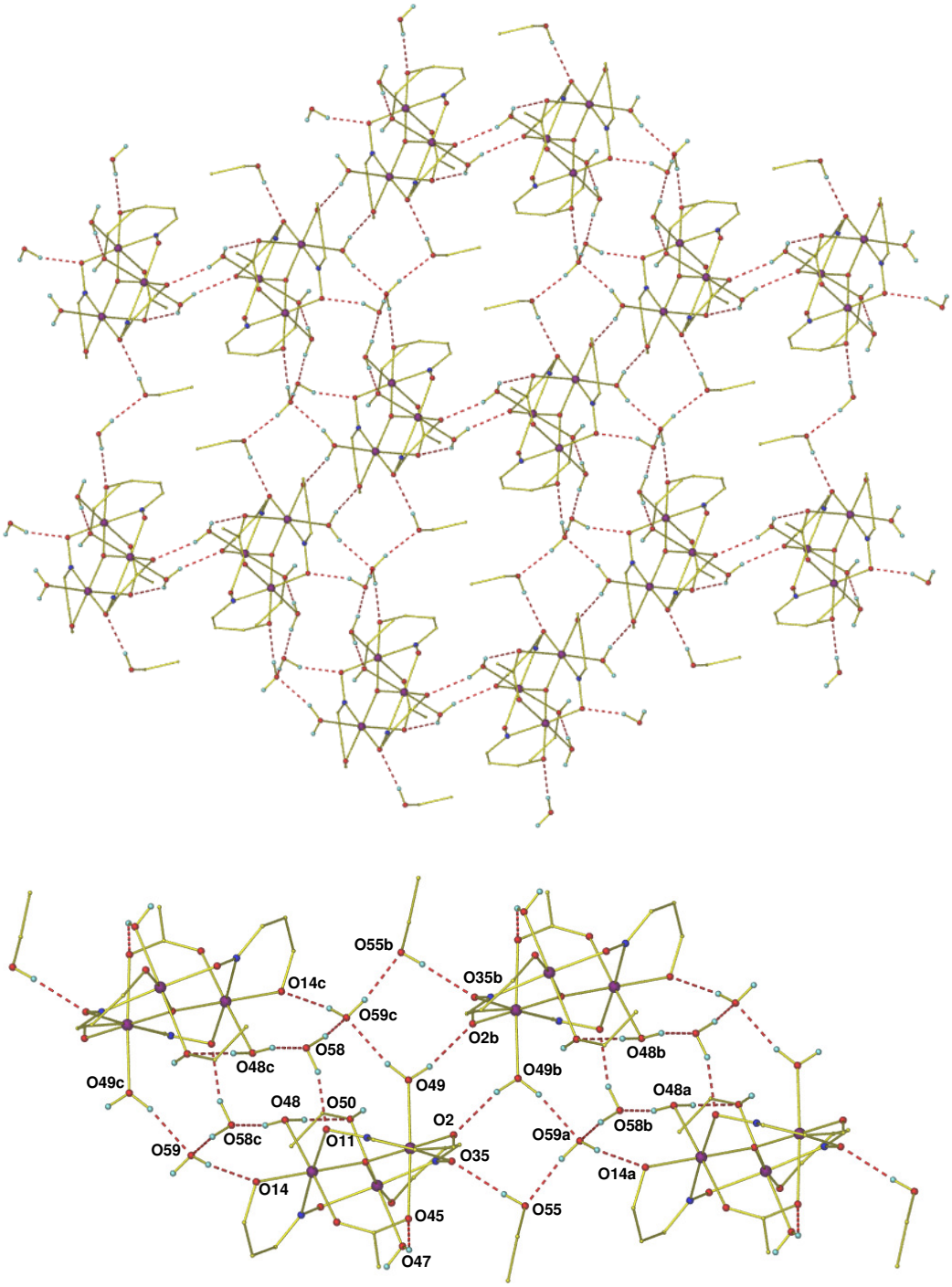

Figure 3.4 The hydrogen bonded layer (left) and the chain (right) in **3.15**. Colour code: Mn, purple; O, red; N, blue; C, gold; H, cyan. Most hydrogen and carbon atoms have been omitted for clarity. Symmetry codes: a x-1, y, z; b -x, 1-y, 2-z; c 1-x, 1-y, 2-z.

The presence of the capping ClO_4^- anion on the upper triangular face of **3.13** and the absence of solvate molecules forces the Mn_3 clusters to self-assemble through the three MeOH molecules which are attached on the base of the triangle. Each Mn_3 is hydrogen-bonded to three neighbours through six complementary hydrogen bonds

(one unique) that involve the terminal MeOH molecules and the phenolate O atoms of the Et-sao^{2-} ligands [∠O15-H1···O8 (1-x, 1-y, 1-z) 168°, O···O 2.734(1) Å and H···O 1.95 Å]. In this arrangement an undulated two-dimensional hydrogen bonded layer forms that conforms to a (6,3) net and lies parallel to the *ab* plane (Fig. 3.5) The Mn_3 triangles are arranged with their upper faces above and below the plane of the hydrogen-bonded framework with their mean planes parallel to each other and to the mean plane of the framework. The layers stack in an off-set fashion with the Mn_3 triangles of one layer lying above and below the hexagonal cavities of the two neighbouring frameworks. The Mn_3 clusters in **3.20** have assembled with a Ph-saoH_2 molecule of crystallisation. The MeOH molecule at the upper face of the Mn_3 triangle forms an intra-molecular hydrogen bond with one carboxylate O-atom [∠O18-H18···O24 162°, O···O 2.876(3) Å and H···O 2.09 Å]. Two of the three MeOH molecules at the base of the triangle are hydrogen-bonded with themselves [∠O17-H17···O15 167°, O···O 2.833(3) Å and H···O 2.02 Å and ∠O15-H15···O16 171°, O···O 2.695(2) Å and H···O 1.90 Å] with the third being attached to the Ph-saoH_2 molecule [∠O16-H16···N99 163°, O···O 2.751(3) Å and H···O 1.95 Å]. The salicyl OH group of the Ph-saoH_2 molecule forms an intra-molecular hydrogen bond with the oximic O-atom [∠O19-H19···O109 168°, O···O 2.577(3) Å and H···O 1.69 Å] while the latter attaches to a phenolate O-atom of the triangle [∠O109-H109···O103 163°, O···O 2.643(2) Å and H···O 1.82 Å]. The Mn_3·Ph-saoH_2 units interact with five neighbouring assemblies through ten (five unique) C-H···π interactions to create a three-dimensional framework with $4^6.6^4$-**bnn** topology (Fig. 3.5).[40]

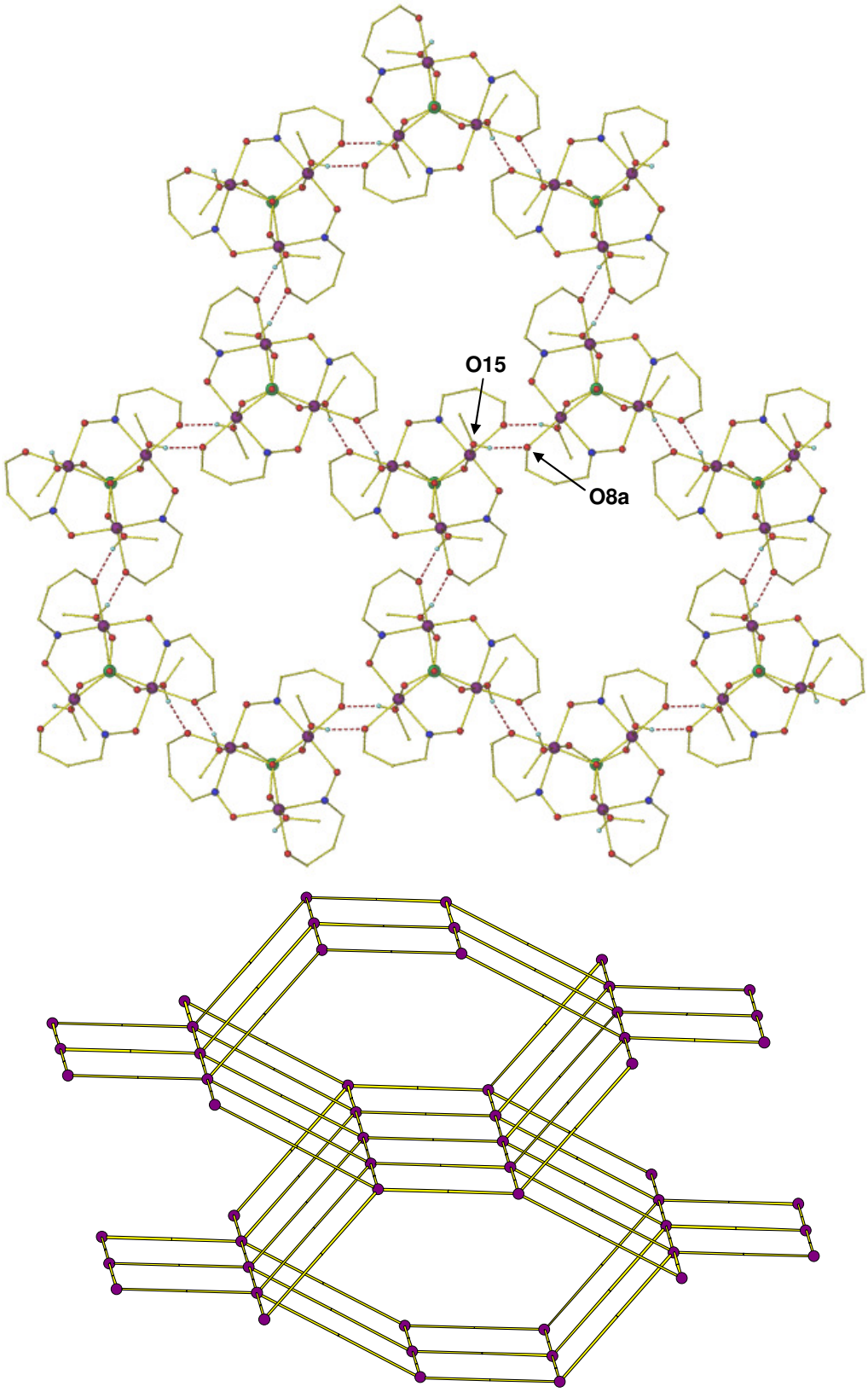

Figure 3.5 (top) The hydrogen bonded (6,3) layer in **3.13**. Most hydrogen and carbon atoms have been omitted for clarity. Symmetry code: a 1-x,1-y,1-z. (bottom) The $4^6.6^4$-**bnn** hydrogen bonded network found in **3.20**. Purple spheres represent the Mn_3·Ph-saoH_2 assemblies while the gold lines represent the C-H···π interactions.

3.2.3 Magnetochemistry

Dc magnetic susceptibility and magnetisation measurements

Dc magnetic susceptibility studies were carried out on powdered crystalline samples of **3**.**1**-**3**.**21** in the 5 - 300 K temperature range in a field of 0.1 T. The magnetic susceptibility data obtained for each were simulated using the program MAGPACK[41] employing the Hamiltonians in equations (1)-(3) (Scheme 3.1) to provide the isotropic parameters summarised in Table 3.2. No attempt was made to simulate the data for **3.5** and **3**.**18** as the crystal structures contain two independent molecules with different geometries (Table 3.1), and for **3.3** and **3**.**6** as the crystal structures are highly disordered. We also stress that what follows should be regarded as qualitative interpretation. It is clear that these molecules (and their [Mn_6] forefathers) are complicated molecules in which excited states (a direct result of the weak magnetic coupling) and inter-molecular interactions - play an important role. The analysis is thus confined within our simplistic model, but allows us to identify and define clear trends in behaviour which is invaluable for future synthetic molecular design.

$$\hat{H} = -2J(\hat{S}_1 \cdot \hat{S}_2 + \hat{S}_2 \cdot \hat{S}_3 + \hat{S}_1 \cdot \hat{S}_3) \qquad (1)$$

$$\hat{H} = -2J_1(\hat{S}_1 \cdot \hat{S}_2 + \hat{S}_2 \cdot \hat{S}_3) - 2J_2(\hat{S}_1 \cdot \hat{S}_3) \qquad (2)$$

$$\hat{H} = -2J_1(\hat{S}_1 \cdot \hat{S}_2) - 2J_2(\hat{S}_2 \cdot \hat{S}_3) - 2J_3(\hat{S}_1 \cdot \hat{S}_3) \qquad (3)$$

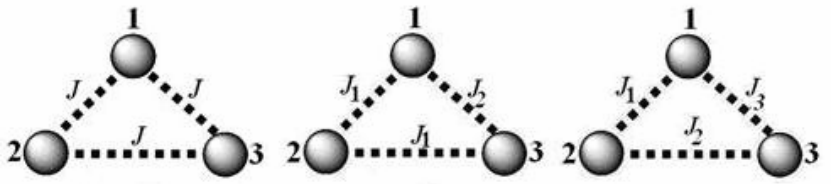

Scheme 3.1 Schematic detailing the 1, 2 and 3-*J* models employed to simulate the experimental data for **3**.**1**-**3**.**21**.

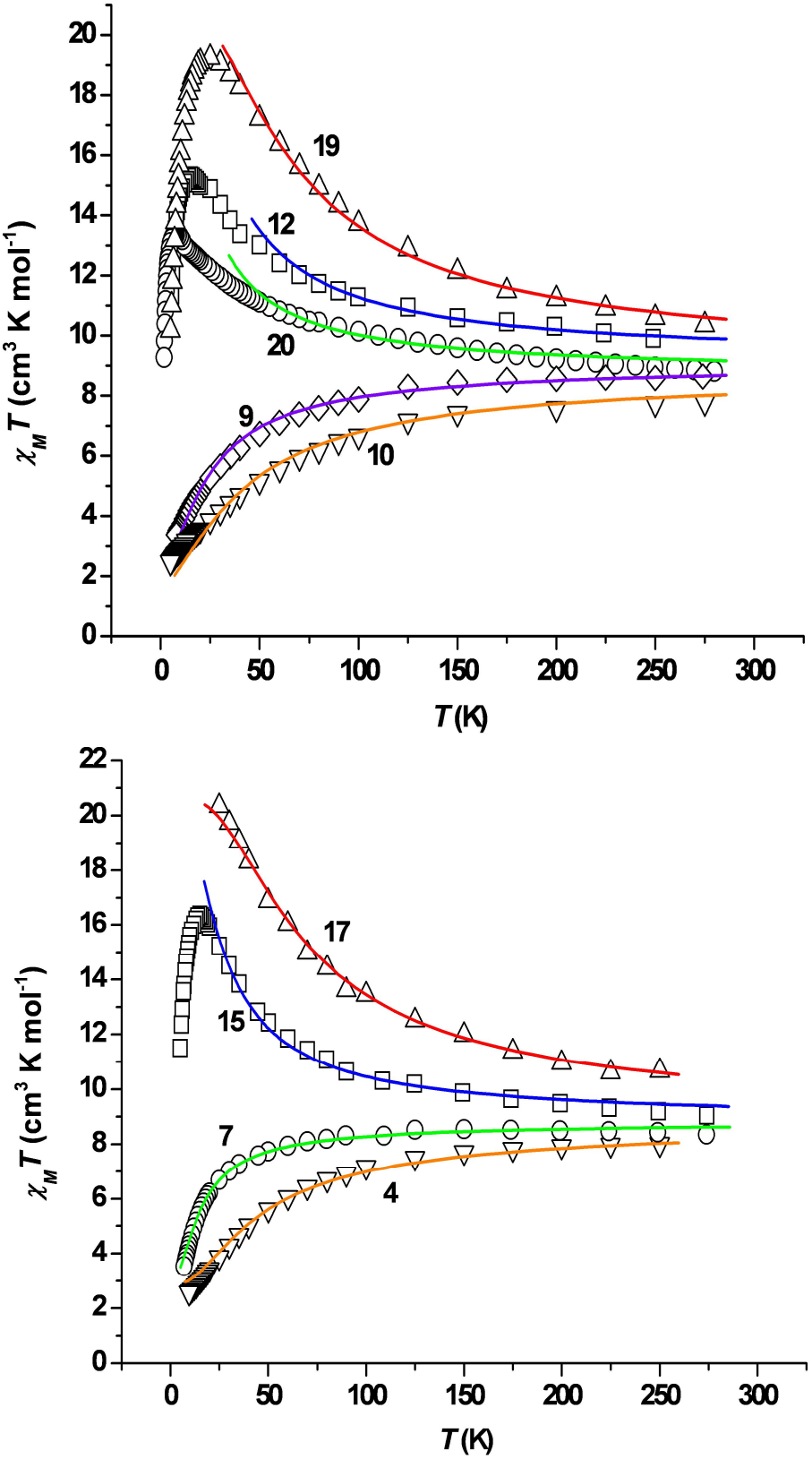

Figure 3.6 Plots of $\chi_M T$ vs. T for complexes **3.1**-**3.21**. The solid lines represent simulations of the experimental data. For parameters see Table 3.2.

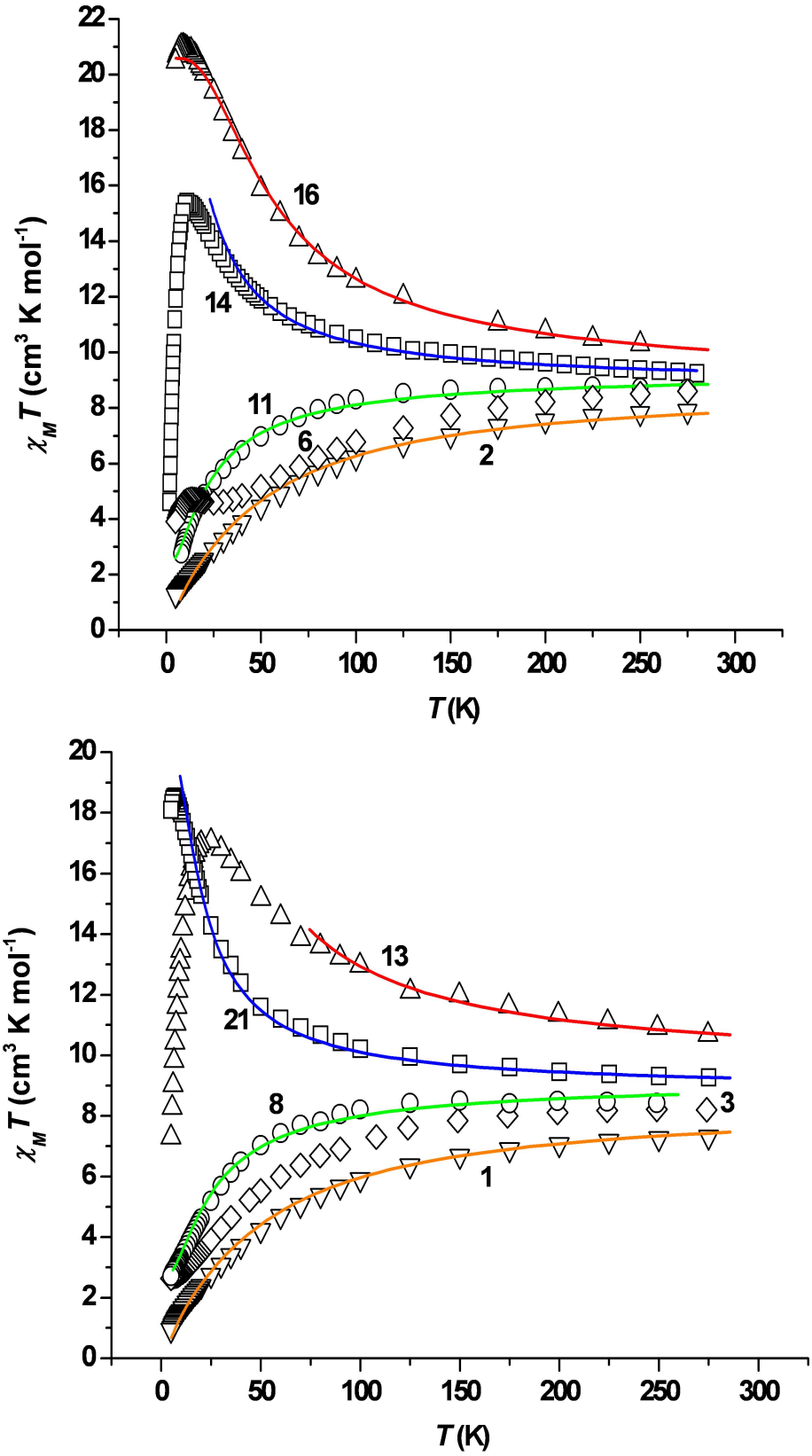

Figure 3.7 Plots of $\chi_M T$ vs. T for complexes **3.1**-**3.21**. The solid lines represent simulations of the experimental data. For parameters see Table 3.2.

The $\chi_M T$ vs. T data are plotted in Figs. 3.6 and 3.7 along with their associated simulations (solid lines). Room-temperature $\chi_M T$ values for **3.1**-**3.11** range from 7.25 to 8.69 cm^3 K mol^{-1}. This is lower than the expected spin-only (g = 2) value for three non-interacting Mn^{III} centres of 9 cm^3 K mol^{-1}, suggesting the presence of dominant antiferromagnetic exchange between the Mn^{III} centres. The $\chi_M T$ values then decrease gradually until approximately 100 K where they decrease more rapidly to values between 0.93 and 3.92 cm^3 K mol^{-1} at 5 K. For all complexes the data was simulated using the simplest model possible. Thus, the data for complexes **3.1**-**3.2** was simulated using the *1*-*J* model of Eqn. (1) and Scheme 3.1, giving the parameters S = 0, g = 1.94, J = –3.10 cm^{-1} and S = 0, g = 1.98, J = –3.02 cm^{-1}, with the first excited state (S = 1) 6.20 cm^{-1} and 6.04 cm^{-1} above the ground state, respectively. The data obtained for complexes **3.4**, **3.9** and **3.11** were simulated using the 2-*J* model of Eqn. (2), with J_1 mediated through oxide, oxime and carboxylate, and with $J_2 = J_3$ mediated through oxide and oxime only. Despite many attempts using the 2-*J* model, the data for complexes **3.7**, **3.8** and **3.10** could only be simulated using the 3-*J* model of Eqn. (3) and Scheme 3.1 in which $J_1 \neq J_2 \neq J_3$. These results are all summarised in Table 3.2.

For **3.12**-**3.15**, **3.19** and **3.20** the room temperature $\chi_M T$ values range from 9.06 to 10.67 cm^3 K mol^{-1}, indicating the presence of ferromagnetic exchange between the Mn^{III} centres. In each case the $\chi_M T$ values increase gradually as temperature is decreased before increasing more rapidly at lower temperatures, reaching maximum values of between ~13 and ~19 cm^3 K mol^{-1}. A sharp drop in $\chi_M T$ then occurs for each at ~20 K with the low temperature maxima being significantly smaller than the expected value of 21 cm^3 K mol^{-1} expected for S = 6. The drop in $\chi_M T$ is attributed to the strong inter-molecular interactions discussed above (and/or zero-field splitting effects). The ("high temperature") data for **3.12**-**3.15** and **3.19** was simulated using the 1-*J* model of Eqn. (1) and afforded the parameters S = 6, with J values ranging from 1.40 to 4.02 cm^{-1} (Table 3.2). This model was unsuccessful for **3.20** and required the 2-*J* model of equation (2), giving S = 6, g = 1.98, J_1 = 0.85 and J_2 = 1.44 cm^{-1}. The room temperature $\chi_M T$ values for **3.16**, **3.17** and **3.21** range from 9.27 to 10.66 cm^3 K mol^{-1} and increase gradually as temperature is decreased, reaching maximum values of between ~18 and ~21 cm^3 K mol^{-1} at the lowest temperature

measured. In each case the data could be simulated with the simple 1-*J* model affording $S = 6$, $g = 1.98$, $J = 3.40$ cm^{-1}; $S = 6$, $g = 1.98$, $J = 4.10$ cm^{-1} and $S = 6$, $g = 1.98$, $J = 1.20$ cm^{-1}, respectively. It is clear from Figs. 3.6 and 3.7 that inter-molecular interactions are playing a very important role in the observed behaviour for all the ferromagnetically coupled complexes. Thus we add a note of caution to the absolute validity/accuracy of the simulation parameters, though they are well within the range observed for *all* previously reported (and analogous) salicylaldoxime-bridged [Mn(III)$_3$] and [Mn(III)$_6$] clusters.[27-36]

Variable field and temperature dc magnetisation data were collected in the 0.5 – 7 T and 2-7 K field and temperature ranges. In each case we attempted to fit the data with an axial ZFS plus Zeeman Hamiltonian (4) in the whole field and temperature range,[42]

$$\hat{\mathcal{H}} = D(\hat{S}_z^2 - S(S+1)/3) + \mu_B g H \hat{S} \qquad (4)$$

where D is the axial anisotropy, μ_B is the Bohr magneton, $\hat{S}_z$ is the easy-axis spin operator, and H is the applied field. The results are summarised in Table 3.2 with representative plots given in Fig. 3.8. Complexes **3.3**-**3.11** possess a spin ground state $S = 2$ with D values ranging from –2.33 to –3.77 cm^{-1}, while complexes **3.12**-**3.20** have the maximum ground state $S = 6$ with smaller D values ranging from –0.37 to –0.92 cm^{-1}. Despite the ferromagnetically coupled complexes being rather similar in structure, the calculated D values span a wide range, and therefore must be treated with caution. Though one would expect some variation due to the varying Jahn Teller tilts, it is clear that the strong inter-molecular interactions, disorder (in **3.15**, **3.16**, **3.17**) which causes a distribution in molecular environments, the presence of weak exchange and thus the likely population of excited states in the temperature range studied, and the simplistic model employed, do not allow for an accurate determination of D. Indeed, magnetisation and HF-EPR studies of analogous molecules in which there are no inter-molecular interactions suggest $|D|$ values ≥ 0.8 cm^{-1} which would be consistent only with **3.14** and **3.15**.[37] Further proof for this assumption emerges in the analysis of the ac data and single crystal hysteresis loop measurements discussed below.

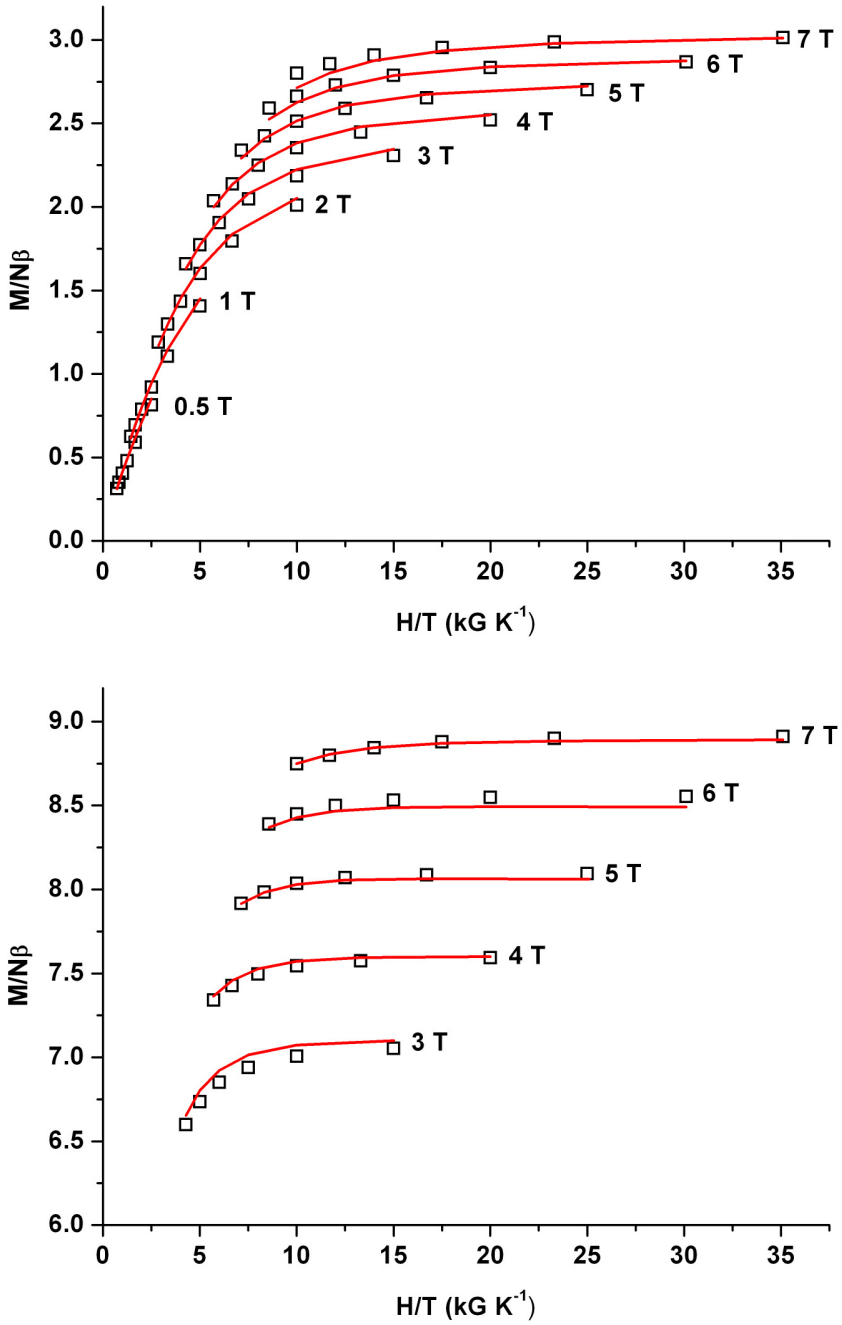

Figure 3.8 Plots of reduced magnetisation ($M/N\mu_B$) versus H/T for **3.10** (top) and **3.15** (bottom) in the noted field ranges and the 2 – 7 K temperature range. The solid lines correspond to the fit of the data as documented in Table 2.

Ac magnetic susceptibility and hysteresis loop measurements

Ac magnetic susceptibility measurements were carried out on crystalline samples of **3.3**-**3.21** in the 2-10 K temperature range in a 3.5 G ac field oscillating at frequencies ranging from 50 to 1000 Hz. Fully visible out-of-phase (χ_M'') signals indicative of

SMM behaviour (Fig. 3.6 shows those obtained for complex **3.17**) were observed for *all* $S = 6$ family members except for $[Mn_3O(Ph\text{-}sao)_3(O_2C\text{-}anthra)(MeOH)_4](Ph\text{-}saoH_2)$ (**3.20**) and $[Mn_3O(Ph\text{-}sao)_3(\beta\text{-}pic)_3](ClO_4)$ (**3.21**), in which only the tails of the signals were observed. The ac data obtained were combined with single-crystal dc relaxation measurements performed on a μ-SQUID[39, 43] (vide infra) and fitted to the Arrhenius equation (5),

$$\tau = \tau_o \exp(U_{eff}/(kT)) \qquad (5)$$

where τ_o is the pre-exponential factor, τ is the relaxation time, U_{eff} is the barrier to the relaxation of the magnetisation and k is the Boltzmann constant, to give the effective barrier to magnetisation reorientation (U_{eff}) for each $[Mn_3]$ complex. These data are summarised in Fig. 3.9 and Table 3.2 and span barrier heights of between ~25-57 K. These are amongst the largest effective barriers observed for any low nuclearity SMMs, but they are also *larger* than the theoretical upper limit [$U = S^2|D|$] calculated using the D values obtained from the powder dc magnetisation measurements (~30 K (**3.12**); ~40 K (**3.13**); ~48 K (**3.14**); ~42 K (**3.15**); ~27 K (**3.16**); ~25 K (**3.17**); ~39 K (**3.19**)). Indeed, only **3.14** has an effective barrier lower than the theoretical upper limit, with **3.15** having an experimental value close to its theoretical value. This is to be expected for exchange-coupled SMMs since the spin reversal is hindered by the relatively weak inter-molecular coupling. For stronger inter-molecular exchange coupling one would move away from the biased-SMM regime into a 3D system where the collective modes (domain wall propagation *etc*) would reduce the effective barriers. It also points to a possible underestimation in the ZFS parameters obtained from the powder dc measurements, which is confirmed in the single crystal low temperature magnetisation studies (below).

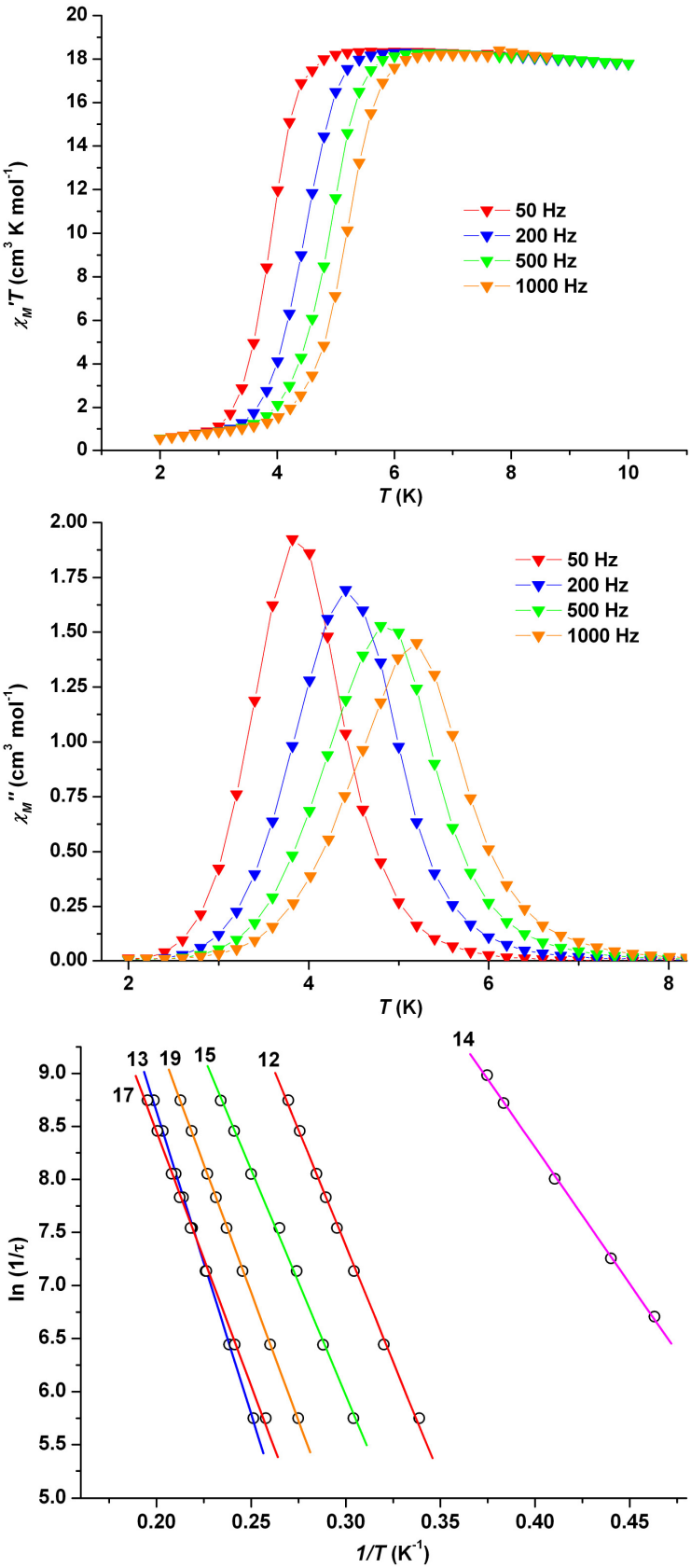

Figure 3.9 AC in-phase $\chi'_M T$ vs. T (top) and out-of-phase χ''_M vs. T (middle) plots obtained for complex **3.17** in an oscillating field of 3.5 Oe and frequencies of 50-1000 Hz. Plots of ln(1/ τ) vs. 1/T obtained from the ac magnetic susceptibility data for a cross section of family members (bottom).

Hysteresis loop and relaxation measurements were carried out on single crystals of all the ferromagnetically coupled complexes using a μ-SQUID assembly, with the field applied along the easy axis of magnetisation.[39, 43] In each case temperature and sweep rate dependent hysteresis loops were observed, confirming SMM behaviour for all complexes. Representative examples are shown for complexes **3.13** and **3.16** in Fig. 3.10. For all *type 2* molecules, in which significant inter-molecular interactions are observed in the crystal lattice, the loops display step-like features separated by plateaus. After saturating the magnetisation, the first resonance is seen in negative fields, indicative of the presence of small and antiferromagnetic inter-molecular interactions as was first observed in the complex $[Mn_4O_3Cl_4(O_2CEt)_3(py)_3]$ which crystallises as a supramolecular H-bonded dimer of cubanes ($[Mn_4]_2$).[44] The hysteresis loops show that the collective spins of each $[Mn_3]$ molecule are coupled antiferromagnetically to its neighbouring molecules, acting as a bias that shifts the quantum tunnelling resonances with respect to the isolated SMM. The majority of the small steps observed in all the loops are therefore due to molecules having one (or several) "reversed" ("spin up - spin down") neighbouring molecules - though some may be attributed to multi-body quantum effects.[45, 46] The complexity of the three dimensional H-bonding networks seen in the crystal structures makes it essentially impossible (or at least extremely difficult) to determine all of the active exchange paths and to identify all of the steps.

Type 3 molecules, however, in which the lower face of the $[Mn_3]$ triangle is occupied by derivatised pyridine analogues show no significant H-bonding in the crystal and this is reflected in the appearance of much simpler looking hysteresis loops - particularly at the lowest temperatures measured (below 1.5 K). Those for **3.16** are shown in the middle and lower panels of Fig. 3.10. Above ~1.5 K the loops appear more complicated with the emergence of fine structure which can be attributed to the contribution of excited states, crystal defects, nuclear spins, dipolar interactions or most likely the disorder associated with one of the β-picoline ligands (see CIF file for full details). Data obtained at very low temperatures however are remarkably simple showing only resonances originating from the ground state. The data obtained at 40 mK are shown in the lower panel of Fig. 3.10 and show hysteresis loops with a step at zero field. A step indicates a surge in the magnetisation relaxation rate due to

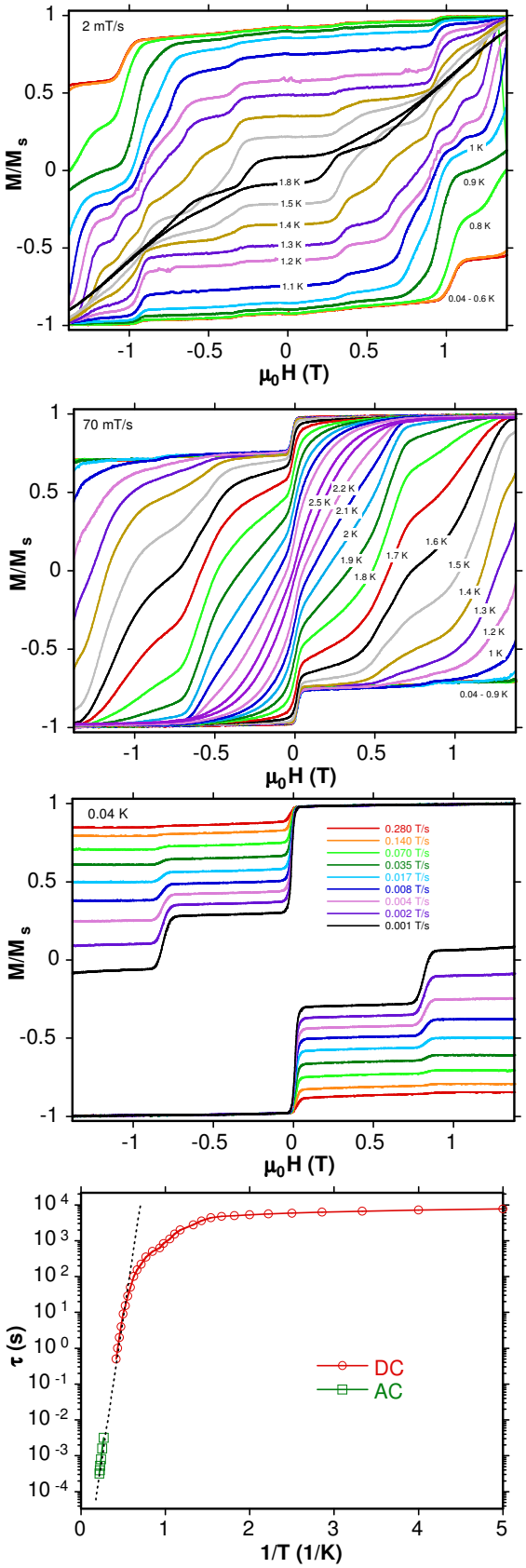

Figure 3.10 Magnetisation versus field hysteresis loops for single crystals of **3.13** (top) and **3.16** (middle) at the indicated temperatures and field sweep rate. *M* is normalised to its saturation value. Arrhenius plot (bottom) using ac and dc data for **3.16**. The dashed line is the fit of the thermally activated region.

quantum tunnelling of the magnetisation through the barrier, occurring at a field position where there is an avoided level crossing. At H = –1 T all the molecules are in the M_S = +6 state. When the field is swept in a positive direction there is resonance between the +6 and –6 M_S levels at H = 0, and some of the molecules tunnel. As the field sweep rate is decreased a second step emerges at *ca.* 0.80 T. The separation between the steps is related to D by the equation $\Delta H = |D|/g\mu_B$. Measurement of the step positions for complex **3.16** thus afford an average field separation of ~0.8 T and thus a $|D|/g$ value of ~0.38 cm^{-1}. Assuming g = 2.00, this corresponds to a $|D|$ value of approximately 0.76 cm^{-1}, somewhat larger than that obtained from the dc magnetisation measurements (–0.52 cm^{-1}), and consistent with earlier comments regarding the validity of the D values obtained from the fit of the magnetisation *versus* field data, and with previous reports of analogous "uncoupled" $[Mn^{III}_3]$ triangles; *i.e.* the magnitude of D for all four complexes appears to be somewhat underestimated. New clusters with these intermolecular interactions (and disorder) removed will be required to get an accurate representation of the spin Hamiltonian parameters and of the relaxation dynamics. **3.16** represents a rare example of a rather simple SMM in which the influence of inter-molecular interactions and excited states are negligible at low temperatures. This is potentially an exciting discovery since it gives us access to a molecule containing only three metal ions that displays beautiful low temperature SMM behaviour and tunnel effects, and thus a model system with which to go beyond the giant spin approximation to potentially yield much fruitful physical information.

High Frequency Electron Paramagnetic Resonance Studies

High-frequency EPR measurements were performed at various discrete frequencies in the range from 52 to 344 GHz on single crystals of complex **3.3** (S = 2), **3.12** ($S \approx$ 5 6, *vide infra*) and **3.13** (S = 6) to verify their ground state spin values and zero field splitting (ZFS) parameters. Prior to measurement, crystals were quickly transferred from their mother liquor and coated in silicone grease in order to avoid solvent loss. The samples were also initially cooled under atmospheric helium gas, with a total transfer time from the mother liquor to the cryostat of ~5 minutes. An oversized cylindrical resonator was employed in order to provide enhanced

sensitivity, and a Millimeter-wave Vector Network Analyzer (MVNA) served as a superheterodyne spectrometer. Both single- (complexes **3.3** and **3.13**) and double-axis (complexes **3.12** and **3.13**) field-orientation dependent studies were performed in order to ensure magnetic field alignment either perpendicular or approximately parallel to the magnetic easy axes of the crystals. Details of the experimental technique can be found elsewhere.[47, 48] The most comprehensive study involved the high-symmetry (*R-3*) complex **3.13**, for which measurements were performed on separate crystals in two different spectrometers with single- (15 T) and double-axis (7 T) rotation capabilities. The quality of the hard-plane spectra obtained in the former were superior, but we first present high-frequency data obtained in the 7 T system. Angle-dependent studies were performed to obtain approximate alignment of the field with the sample's easy-axis. Once aligned, measurements were performed as a function of frequency and temperature so as to provide data sets which maximally constrain the axial ZFS parameters. Fig. 3.11 displays representative temperature dependent spectra obtained at 273 GHz (inset), together with plots of EPR peak positions deduced from measurements at four additional high frequencies (main panel, open symbols).

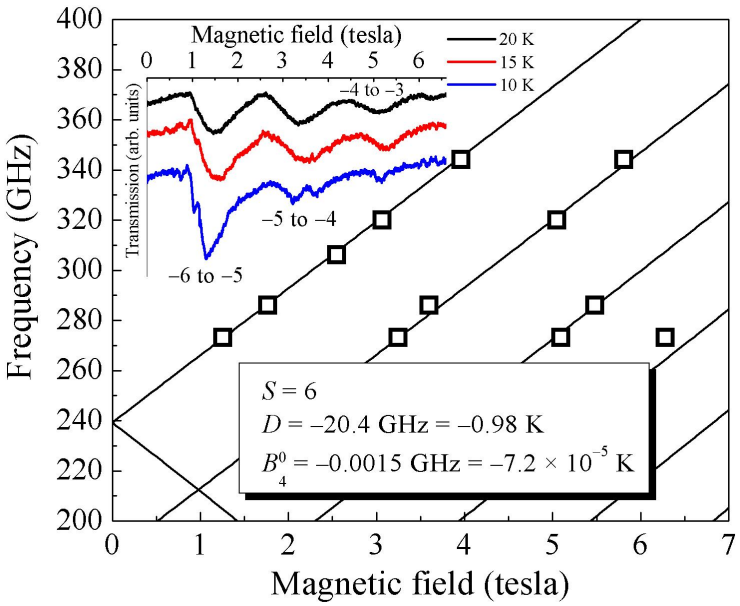

Figure 3.11 Frequency dependence of EPR peak positions (black squares) obtained with the field applied approximately parallel to the easy-axis of **3.13** at 20 K. Superimposed on the data is the best simulation based on Eq. (6); the obtained ZFS parameters are given in figure. The inset displays representative spectra obtained at 273 GHz and at three different temperatures. The various fine structures have been labelled according to the spin projection along the easy axis.

Before discussing the simulations in Fig. 3.11 (solid lines in main panel), we comment on the spectra. The peaks are rather broad, indicating disorder in the crystals. It is also apparent that additional fine-structure splittings appear at the lowest temperature, which is a sign of intermolecular exchange interactions.[49] The data points in the main panel of Fig. 3.11 were extracted from the 20 K spectra so as to avoid complications due to such intermolecular interactions. The solid curves were simulated using the following spin Hamiltonian, containing only axial ZFS parameters.

$$\hat{H} = D\hat{S}_z^2 + B_4^0 [35S_z^4 - \{30S(S+1)\}S_z^2] + \mu_B \boldsymbol{B}\cdot g\cdot\hat{S} \qquad (6)$$

The operators and fundamental constants in equation (6) are defined elsewhere,[49] and the obtained ZFS parameters are given in the Fig. 3.11. The most important observation is the robust agreement with a spin $S = 6$ Hamiltonian. Attempts to fit to a spin state with $S < 6$ were unsuccessful. Thus, these EPR studies confirm the findings of the preceding magnetic studies. Nevertheless, evidence for considerable mixing between the ground and excited spin states is given by the significant 4th order ZFS parameter.[50] Interestingly, the values of D and B_4^0 are quite comparable to those reported recently for a family of very similar Mn_3 complexes.[37] In particular, there is a good correlation between B_4^0 and the exchange constant, J, among these complexes, e.g. $B_4^0 = -7.2 \times 10^{-5}$ K and $J = +4.0$ K for complex **3.13**, while B_4^0 ranges from 3.8×10^{-5} K to 11×10^{-5} K and J from +2.3 to 4.7 K for the ferromagnetic complexes in ref. [28]. This correlation is significant, because it provides further proof that the fourth order terms are a direct consequence of spin mixing between low-lying multiplets, *i.e.* J and B_4^0 are directly related.[50]

91 GHz temperature dependent spectra obtained for **3.13** with the field in the hard plane are displayed in Fig. 3.12. The fine structure peaks have been labelled according to a scheme described elsewhere.[51] The spectra are superior to those presented in Fig. 3.11, likely due to a higher quality sample. The signal-to-noise is also vastly improved by virtue of the lower frequency employed. Nevertheless, the appearance of multiple peaks associated with each cluster of fine-structure transitions suggests the presence of multiple species in the crystal, very similar to recently

reported results for a family of Ni_4 complexes.[52] These spectra and their temperature dependence are fully consistent with a spin $S = 6$ state possessing significant axial anisotropy. Indeed, simulations assuming $S = 6$ confirm the axial ZFS parameters obtained from the easy-axis measurements. However, the best simulation necessitates inclusion of transverse ZFS terms (see Fig. 3.13). The nature of these terms is not well determined, but this nevertheless suggests the presence of transverse anisotropy. Attempts to fit to an $S < 6$ model were unsuccessful.

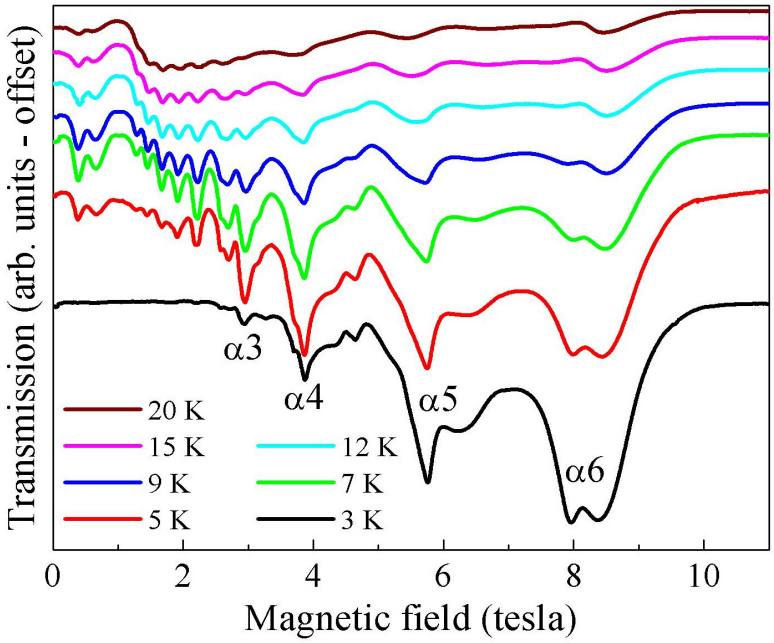

Figure 3.12 Hard plane temperature dependence spectra obtained at 91 GHz for complex **3.13**.

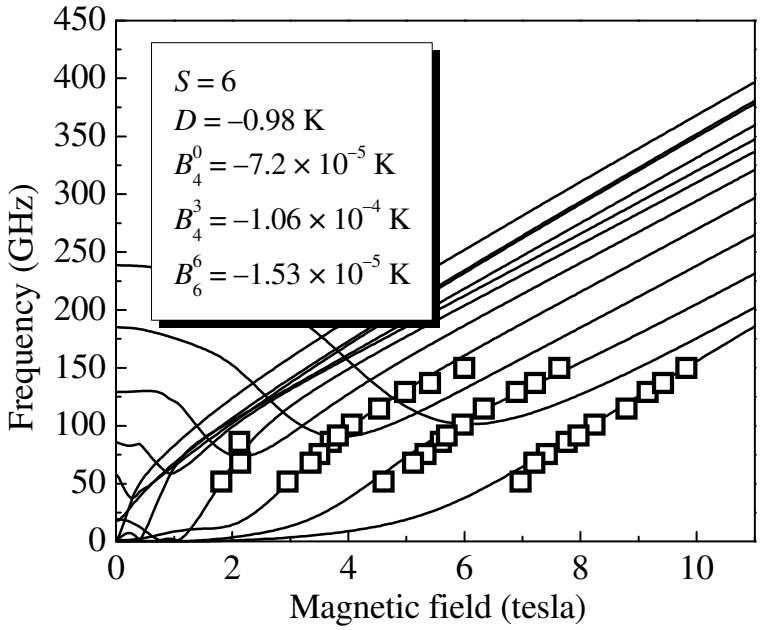

Figure 3.13 Energy difference diagram constructed from frequency-dependent measurements for the hard plane orientation for complex **3.13** at a temperature of 5 K. The solid lines are simulations using the parameters shown in the figure.

Plots of the 10 K EPR peak positions obtained from multi-frequency measurements on complex **3.12** with the field approximately aligned with its easy axis are displayed in Fig. 3.14. Simulations of these data are far less satisfactory than those for **3.13**. Indeed, simulations assuming $S = 5$ (Fig. 3.14(a)) are marginally better than those for $S = 6$ (Fig. 3.14 (b)); the corresponding ZFS parameters are given in the figure. It is notable from Table 3.2 that complex **3.12** sits right at the borderline between the F and AF cases. It is thus very likely that the $S = 6$ state for **3.12** is not well developed, *i.e.* it is strongly mixed with low-lying $S < 6$ states. In this situation, one would not expect good fits to equation (6), as confirmed in Fig. 3.14. Furthermore, the anisotropy is significantly depressed relative to complex **3.12**: the simulations in Fig. 3.14 suggest a barrier of only ~15 K (both for $S = 5$ and 6), in contrast to a value of 35 K for **3.13**. Note that both of these values are significantly lower than those deduced on the basis of magnetic studies (Table 3.2). This is not surprising given the marginal applicability of the models used to estimate these numbers (*e.g.* equation (4)).What is more, it has recently been shown that ac susceptibility measurements often overestimate the barrier, particularly for SMMs with low-lying excited spin multiplets.[53]

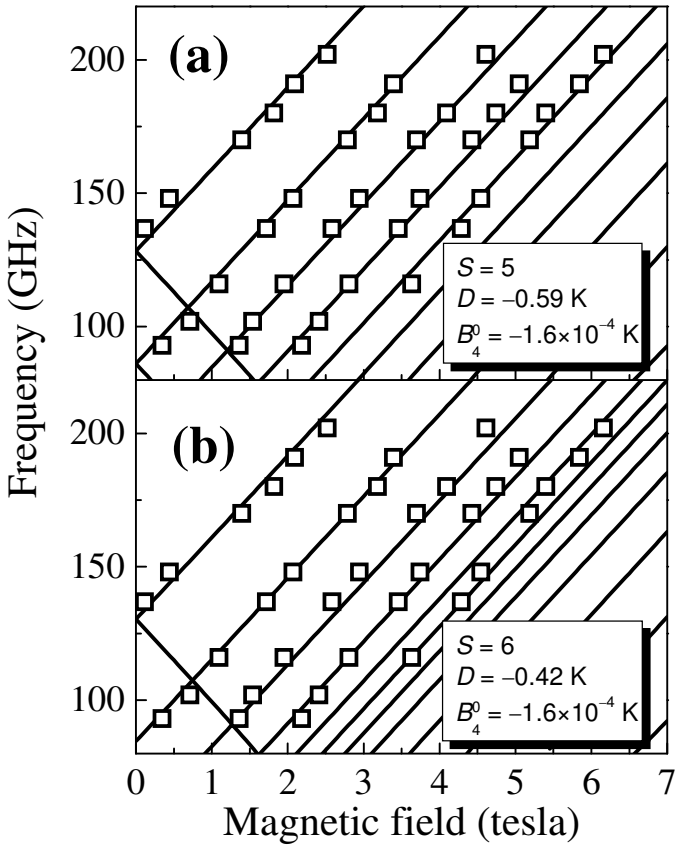

Figure 3.14 Frequency dependence of EPR peak positions (black squares) obtained with the field applied approximately parallel to the easy-axis of **3.12**; the temperature was 10 K for these measurements. Superimposed on the data are simulations based on Eq. (5) with (a) $S = 5$ and (b) $S = 6$; the obtained ZFS parameters are given in figure.

Finally, Fig. 3.15 shows hard-plane temperature dependent data obtained at 52 GHz for complex **3.3**. The overall appearance of the spectrum is consistent with that of a molecule with a relatively low spin quantum number (there are far fewer peaks as compared to Fig. 3.12) and a very significant axial anisotropy. However, it is not possible to make meaningful peak assignments or to fit data to equation (6). Nevertheless, one can make a crude estimate of the anisotropy on the basis of the position of the highest field (ground state) transition relative to the expected isotropic position (1.9 T for $g = 2$); this deviation ΔB provides a rough measure of the product of D and S or, rather, $|^1/_2 D(2S-1)| \approx \Delta B \times 28$ GHz/T ≈ 336 GHz or 16 K.[49] If one assumes a spin $S = 2$ state, then this implies an extraordinarily large molecular D value of nearly –11 K (–7.5 cm^{-1}). From this, one can estimate an equally large single-ion D_1 value of approximately –5 cm^{-1} for the Mn^{III} ions (this assumes identical values for all three ions and parallel Jahn-Teller axes).[54] Note that a similar

estimate for **3.13** gives a value for D_1 of approximately –2.6 cm^{-1}. While large, these values are not unprecedented.[55] Nevertheless, the value for **3.3** should not be taken too seriously given the many assumptions that went into estimating both the molecular and single-ion *D* values.

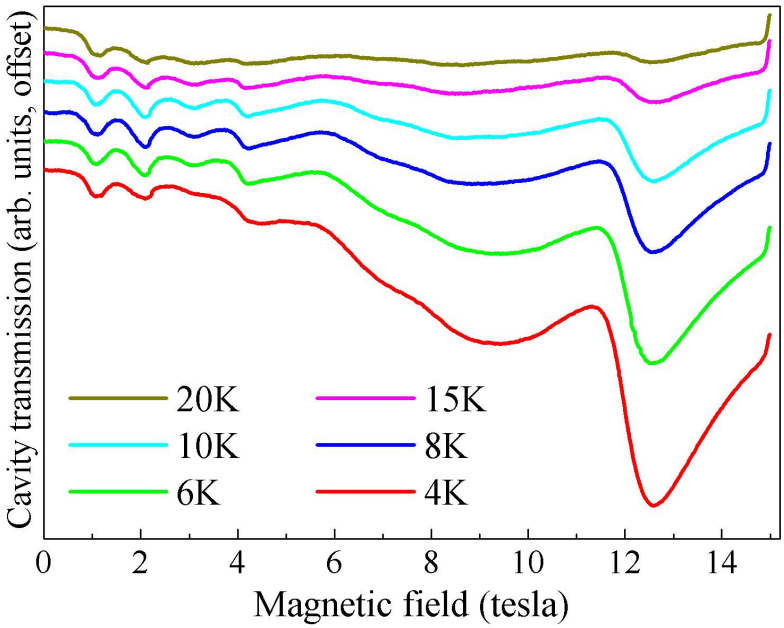

Figure 3.15 Hard plane temperature dependence spectra of complex **3.3** obtained at 52 GHz.

Discussion and Conclusions

We have demonstrated three simple strategies for making ferromagnetic salicylaldoxime-based [Mn^{III}_3] triangles, all of which are based on the deliberate puckering of the magnetic core of the molecule: a) when the parent oxime ligand ($saoH_2$) occupies the same plane as the [Mn_3O] moiety, the Mn-N-O-Mn unit is easily made non-planar by derivatising the oximic carbon, *i.e.* by making R-$saoH_2$ ligands. When R = Et or Ph the puckering appears to be at its greatest. This effect is then re-inforced by (b) employing small "pincer" type tripodal ligands (ClO_4^-, ReO_4^- *etc*) to sit on the "upper" triangular face and (c) employing large sterically bulky ligands to occupy the "lower" triangular face. The combined effect is the production of highly distorted or "bowl-shaped" molecules. When alcohol solvent molecules occupy the lower face, the molecules are involved in extensive H-bonding in the crystal lattice and the effect is clearly manifested in the magnetic behaviour and the

triangles behave as exchange-biased SMMs. These inter-molecular interactions are removed and the molecules isolated from each other by replacing the alcohols with derivatised pyridine molecules such as β-picoline or ethyl-pyridine *etc*. The result is much cleaner and simpler magnetic data as reflected in both the bulk powder dc (and ac) data and the single-crystal hysteresis loop measurements. The emergence of families of such [Mn_3] SMMs in which the influence of inter-molecular interactions and/or excited states can be nullified is an exciting discovery since it gives access to very simple molecules (3 spins) that display beautiful SMM behaviour and tunnelling effects, and model systems with which to go beyond the giant spin approximation to yield much fruitful physical information.

Understanding the relationship between the structure and magnetic behaviour in these [Mn_3] triangles, however, is a difficult task (even with twenty members) since one must consider all contributions to the exchange. This means we must consider the combination of different bridging and non-bridging ligand types (oxime, oxide, carboxylate or perchlorate, alcohol or pyridine); their relative positions and the bond lengths and angles associated with each. In earlier work on analogous [Mn_6] complexes we discovered that the *dominant* factor governing the exchange between nearest neighbours appeared to be the twisting of the Mn-O-N-Mn moiety with respect to the [Mn_3] plane as induced by the distortion imposed on the molecule by bulkier oximes (R-sao^{2-}). An examination of the data of Tables 3.1 and 3.2 suggests that this also appears to be true here, with the more puckered triangles displaying larger (more positive) exchange constants and the more planar triangles displaying more negative exchange constants. There does not appear to be any obvious correlation between J and the out-of-plane shift of the central oxide, the Mn-(μ_3-O)-Mn angle, the Mn^{III}-O^{2-} distances, or the Mn-N-O-Mn distances. For example, the presence of the carboxylate *versus* perchlorate/perrhenate seems to have little influence and there are antiferromagnetic triangles in which the central oxide is displaced more from the [Mn_3] plane than that seen in the ferromagnetic triangles. For the [Mn_6] family a Mn-N-O-Mn torsion angle of around 31° proved to be the "switching point", consistent with that observed here. Of course this analysis is purely *qualitative* in nature, since in each case we simulated the experimental susceptibility data using the most simple model possible. Indeed even with 21

members to dissect, definitive answers are difficult to come by. It is clear that the majority of family members are rather complicated molecules and we will need to synthesise and analyse more of the "isolated" siblings to gain more understanding.

Table 3.1 Selected interatomic distances (Å) and angles (°) for complexes **3.1**-**3.21**.

Complex	Mn-(μ_3-O) distance (Å) Mn1-O, Mn2-O, Mn3-O	Mn-(μ_3-O)-Mn angles (°) Mn1-2, Mn2-3, Mn1-3	Mn_3 plane-μ_3O dist(sd) (Å)	Mn-O_2CR / Mn-O_4X distance (Å)
$[Mn_3O(Naphth\text{-}sao)_3(py)_3](ClO_4)$ (**3.1**)	1.8898(25)	118.327(132)	0.2464(0.0025)	2.4901(33)
$[Mn_3O(sao)_3(Et\text{-}py)_3].(ClO_4)$ (**3.2**)	1.8981(9)	117.64(6)	0.2944(0.0042)	2.463(3)
$[Mn_3O(sao)_3(O_2CPh)(H_2O)(py)_3]$ (**3.3**)	1.9021(5), 1.9021(6), 1.9014(7)	116.97(5)	0.3350(0.0023)	n.a.
$[Mn_3O(sao)_3(O_2C\text{-}Naphth)(py)_3].(py)$ (**3.4**)	1.9126(56), 1.9343(49), 1.8843(53)	112.271(291), 113.197(271), 117.666(272)	0.4602(0.0055)	2.1967(72), 2.2031(72)
$[Mn_3O(sao)_3(O_2CC_{10}H_{13})(py)_3].EtOH$ (**3.5**)[a]	1.9112(32), 1.9081(33), 1.8740(42)	112.80(2), 116.30(2), 119.00(2)	0.3834(0.0043)	2.1656(38), 2.1870(43)
	1.9177(41), 1.8700(33), 1.9080(32)	112.70(2), 118.20(2), 117.10(2)		2.1674(37), 2.1870(45)
$[Mn_3O(sao)_3(O_2CCH_3)(H_2O)(py)_3].(py)$ (**3.6**)	1.8972(10), 1.8979(8), 1.8980(9)	116.59(7), 116.55(7), 116.63(7)	0.3548(0.0035)	2.241(11)
$[Mn_3O(Me\text{-}sao)_3(O_2CCH_3)(MeOH)_5].(Me\text{-}saoH_2)$ (**3.7**)	1.855(3), 1.881(3), 1.893(3)	119.88(15), 119.01(15), 120.57(15),	0.0800(0.0034)	2.457(4)
$(Na)(PyH)[Mn_3O(Me\text{-}sao)_3(O_2C\text{-}Anthra)(py)_3]_2[ClO_4]_2.py$ (**3.8**)	1.9195(23), 1.9032(18), 1.8789(21)	110.80(1), 114.86(1), 116.99(1)	0.4654(0.0029)	2.1924(24), 2.2655(27)
$[Mn_3O(Me\text{-}sao)_3(O_2CCH_3)(py)_4].2(py)$ (**3.9**)	1.8799(10), 1.8988(10), 1.9005(10)	113.57(5), 117.89(5), 118.00(5)	0.3590(0.0010)	2.1519(11), 2.1616(11)
$[Mn_3O(^tBu\text{-}sao)_3(O_2CC_9O_3H_{11})(py)_3]$ (**3.10**)	1.8670(27), 1.9013(24), 1.8968(30)	114.696(14), 118.778(14), 119.925(16)	0.2825(0.0027)	2.1262(34), 2.2078(36)
$[Mn_3O(^tBu\text{-}sao)_3(O_2CPh(CH_3)_2)(MeOH)_4]$ (**3.11**)	1.8967(31), 1.8910(23), 1.8862(30)	119.232(15), 120.618(14), 120.15(14)	0.0022(0.0027)	2.0777(28)
$[Mn_3O(Et\text{-}sao)_3(O_2CPh(Cl)_2)(H_2O)(MeOH)_3]$(**3.12**)	1.8792(14), 1.8884(13), 1.8738(14)	115.33(7), 120.10(7), 118.71(7)	0.2648(0.0015)	2.2036(15), 2.2082(15)
$[Mn_3O(Et\text{-}sao)_3(MeOH)_3](ClO_4)$ (**3.13**)	1.8770(2), 1.8791(2), 1.8794(3)	119.150(1), 119.022(7), 119.130(8)	0.1792(0.0017)	2.5496(11)
$[Mn_3O(Et\text{-}sao)_3(O_2CPh)(C_6H_{16}NO_3)(O_2CPh)(H_2O)_2]$ (**3.14**)	1.8794(19), 1.871(2), 1.8762(19),	115.18(10), 120.59(10), 119.72(11),	0.2314(0.0022)	2.180(2), 2.288(2), 2.189(2)
$[Mn_3O(Et\text{-}sao)_3(O_2CPh(CF_3)_2)(EtOH)(H_2O)_3].EtOH$ (**3.15**)	1.8803(26), 1.8674(28), 1.8740(26)	115.83(13), 119.96(14), 119.84(14)	0.2274(0.0026)	2.1779(36), 2.3222(28)
$[Mn_3O(Et\text{-}sao)_3(\beta\text{-}pic)_3](ClO_4)$ (**3.16**)	1.9007(4), 1.8995(4), 1.9005(4)	117.917(1), 117.865(1), 117.927(1)	0.2776(0.0026)	2.5667(18)
$[Mn_3O(Et\text{-}sao)_3(Et\text{-}py)_3](ClO_4)$ (**3.17**)	1.8936(4), 1.8934(4), 1.8947(4)	117.909(1), 117.961(1), 117.900(1)	0.2754(0.0025)	2.5416(15)
$[Mn_3O(Et\text{-}sao)_3(^tBu\text{-}py)_3](ClO_4)$ (**3.18**)[a]	1.8866(11), 1.8883(9), 1.8883(10)	118.070(31), 117.986(30), 118.07(3)	0.2664(0.0045)	2.4871(34), 2.4871(33)
	1.9008(8), 1.9008(9), 1.9008(10)	117.690(22), 117.690(24), 117.690(28)	0.2916(0.0040)	2.4703(29), 2.4703(30)
$[Mn_3O(Et\text{-}sao)_3(EtOH)(H_2O)_2](ReO_4).3EtOH$ (**3.19**)	1.892(3), 1.888(3), 1.881(3)	121.33(17), 119.69(17), 118.86(16)	0.0371(0.0027)	2.382(4), 2.377(3), 2.443(4)
$[Mn_3O(Ph\text{-}sao)_3(O_2C\text{-}Anthra)(MeOH)_4].(Ph\text{-}saoH_2)$ (**3.20**)	1.8744(14), 1.8710(17), 1.8696(16)	115.80(8), 121.54(8), 119.98(8)	0.1778(0.0015)	2.1665(22), 2.2059(19)
$[Mn_3O(Ph\text{-}sao)_3(\beta\text{-}pic)_3](ClO_4)$ (**3.21**)	1.8820(18), 1.9044(18), 1.8963(17)	117.428(92), 118.214(92), 118.946(93)	0.2565(0.0019)	2.6553(25), 2.5378(22), 2.4829(22)

[a] Two Mn_3 complexes in the asymmetric unit, therefore two sets of data documented. $teaH_3$ = triethanolamine.

Table 3.2 Magnetostructural parameters for complexes **3.1**-**3.21**; Mn-N-O-Mn torsion angles *vs.* *J* and *S*.

Complex	Crystal System	Space Group	α / ° Mn1-2 / Mn2-3 / Mn1-3	J / cm^{-1}[a] J_1 / J_2 / J_3	S[b]	1$^{st}_{exc.\ st.}$(cm^{-1})[b]	g[c]	D / cm^{-1}[d]	τ_0 / s[e]	U_{eff} / K[e]	θ / K[f]
(**3.1**)	Cubic	Pa-3	4.11	-3.10	0	1(6.2)	1.94	n.a.	n.a.	n.a.	-36.00
(**3.2**)	Trigonal	P-3	13.11	-3.02	0	1(6.04)	1.98	n.a.	n.a.	n.a.	-43.73
(**3.3**)	Trigonal	P-3	8.96	n.a.	2	n.a.	1.96	-2.39	n.a.	n.a.	-28.75
(**3.4**)	Triclinic	P-1	27.88, 35.82, 6.64	-2.95, +0.16	2	1(13.08)	1.98	-2.33	n.a.	n.a.	-21.44
(**3.5**)	Triclinic	P-1	31.99, 11.06, 3.04 24.38, 5.33, 11.06	n.a.	n.a.	n.a.	n.a.	n.a.	n.a.	n.a.	n.a.
(**3.6**)	Trigonal	P-3	7.32	n.a.	2	n.a.	n.a.	n.a.	n.a.	n.a.	-44.52
(**3.7**)	Monoclinic	$P2_1$	26.78, 30.70, 38.11	-1.20, -0.96, +0.56	2	3(6.46)	1.98	n.a.	n.a.	n.a.	0.545
(**3.8**)	Triclinic	P-1	16.35, 11.74, 26.58	-1.20, -1.94, -0.40	2	1(2.89)	2.02	-3.61	n.a.	n.a.	-2.96
(**3.9**)	Monoclinic	$P2_1/n$	4.15, 4.45, 23.44	-1.56, -0.36	2	1(3.36)	2.01	n.a.	n.a.	n.a.	-12.46
(**3.10**)	Monoclinic	C 2/c	14.38, 35.36, 1.31	-3.85, -3.05, +0.4	2	1(16.93)	1.98	-3.77	n.a.	n.a.	-20.51
(**3.11**)	Triclinic	P-1	13.07, 20.23, 32.09	-1.65, +0.10	2	1(7.40)	2.02	n.a.	n.a.	n.a.	-1.32
(**3.12**)	Triclinic	P-1	44.60, 38.17, 39.07	+1.84	6	5(22.08)	2.02	-0.59	1.27×10^{-9}	43.69	27.82
(**3.13**)	Trigonal	R-3	42.12	+2.80	6	5(33.60)	2.06	-0.77	1.98×10^{-9}	57.02	30.77
(**3.14**)	Triclinic	P-1	44.60, 35.76, 37.18,	+1.40	6	5(16.80)	1.98	-0.92	8.40×10^{-9}	25.73	19.82
(**3.15**)	Triclinic	P-1	46.66, 38.56, 40.35	+1.52	6	5(18.24)	1.98	-0.82	7.40×10^{-9}	42.53	16.98
(**3.16**)	Trigonal	P-3 c1	44.96	+3.40	6	5(40.80)	1.99	-0.52	2.97×10^{-8}	42.74	37.47
(**3.17**)	Trigonal	R-3	46.78	+4.10	6	5(49.20)	1.98	-0.48	1.46×10^{-8}	47.97	38.19
(**3.18**)	Trigonal	R 3 c	45.40 40.42	n.a.	n.a.	n.a.	n.a.	n.a.	n.a.	n.a.	n.a.
(**3.19**)	Triclinic	P-1	41.65, 40.25, 43.53	+4.02	6	5(48.24)	2.00	-0.75	5.55×10^{-9}	48.31	40.78
(**3.20**)	Triclinic	P-1	32.98, 34.41, 41.44	+0.85, +1.44	6	5(13.80)	1.98	-0.51	n.a.	n.a.	20.44
(**3.21**)	Monoclinic	$P2_1/n$	46.22, 39.31, 40.78	+1.20	6	5 (14.40)	1.98	-0.37	n.a.	n.a.	15.51

[a]Calculated from dc susceptibility studies. [b]Calculated from both dc susceptibility and magnetization measurements. [c]Calculated from dc susceptibility measurements. [d]Calculated from magnetization measurements. [e]Calculated from ac susceptibility data and / or single-crystal relaxation measurements performed on a micro-SQUID. [f]Calculated from dc susceptibility measurements; n.a. = not available.

3.3 References

1. D. Gatteschi and R. Sessoli, *Angew. Chem., Int. Ed.*, 2003, **42**, 268.
2. R. Sessoli, D. Gatteschi, A. Caneschi and M. A. Novak, *Nature*, 1993, **365**, 141.
3. W. Wernsdorfer and R. Sessoli, *Science*, 1999, **284**, 133.
4. W. Wernsdorfer, N. Aliaga-Alcalde, D. N. Hendrickson and G. Christou, *Nature*, 2002, **416**, 406.
5. S. Hill, R. S. Edwards, N. Aliaga-Alcalde and G. Christou, *Science*, 2003, **302**, 1015.
6. M. N. Leuenberger and D. Loss, *Nature*, 2001, **410**, 789.
7. A. Caneschi, D. Gatteschi, N. Lalioti, C. Sangregorio, R. Sessoli, G. Venturi, A. Vindigni, A. Rettori, M. G. Pini and M. A. Novak, *Angew. Chem., Int. Ed.*, 2001, **40**, 1760.
8. S. Carretta, P. Santini, G. Amoretti, M. Affronte, A. Candini, A. Ghirri, I. S. Tidmarsh, R. H. Laye, R. Shaw and E. J. L. McInnes, *Phys. Rev. Lett.*, 2006, **97**, 207201.
9. F. Troiani, A. Ghirri, M. Affronte, S. Carretta, P. Santini, G. Amoretti, S. Piligkos, G. A. Timco and R. E. P. Winpenny, *Phys. Rev. Lett.*, 2005, **94**, 207208.
10. J. Lehmann, A. Gaita-Arino, E. Coronado and D. Loss, *Nat. Nanotechnol.*, 2007, **2**, 312.
11. E. Coronado, J. R. Galán-Mascarós, C. J. Gómez-García and V. Laukhin, *Nature*, 2000, **408**, 447.
12. M. Evangelisti, A. Candini, A. Ghirri, M. Affronte, E. K. Brechin and E. J. L. McInnes, *Appl. Phys. Lett.*, 2005, **87**, 072504.
13. L. Bogani and W. Wernsdorfer, *Nat. Mater.*, 2008, **7**, 179.
14. D. Gatteschi, R. Sessoli and J. Villain, *Molecular Nanomagnets*, Oxford University Press, Oxford, 2006.
15. G. Aromí and E. K. Brechin, in *Structure and Bonding*, Springer, 2006, vol. 122, ch. 1.
16. R. Bircher, G. Chaboussant, C. Dobe, H. U. Güdel, S. T. Ochsenbein, A. Sieber and O. Waldmann, *Adv. Funct. Mater.*, 2006, **16**, 209.
17. M. Evangelisti, F. Luis, L. J. de Jongh and M. Affronte, *J. Mater. Chem.*, 2006, **16**, 2534.
18. M. Affronte, S. Carretta, G. A. Timco and R. E. P. Winpenny, *Chem. Commun.*, 2007, 1789.
19. G. A. Timco, S. Carretta, F. Troiani, F. Tuna, R. J. Pritchard, C. A. Muryn, E. J. L. McInnes, A. Ghirri, A. Candini, P. Santini, G. Amoretti, M. Affronte and R. E. P. Winpenny, *Nat. Nanotechnol.*, 2009, **4**, 173.
20. C.-F. Lee, D. A. Leigh, R. G. Pritchard, D. Schultz, S. J. Teat, G. A. Timco and R. E. P. Winpenny, *Nature*, 2009, **458**, 314.
21. G. Christou, *Polyhedron*, 2005, **24**, 2065.
22. S. G. Sreerama and S. Pal, *Inorg. Chem.*, 2002, **41**, 4843.

23. T. C. Stamatatos, D. Foguet-Albiol, C. C. Stoumpos, C. P. Raptopoulou, A. Terzis, W. Wernsdorfer, S. P. Perlepes and G. Christou, *J. Am. Chem. Soc.*, 2005, **127**, 15380.
24. C. J. Milios, PhD Thesis, University of Patras, Greece, 2004.
25. C. J. Milios, A. G. Whittaker and E. K. Brechin, *Polyhedron*, 2007, **26**, 1927.
26. R. D. Cannon and R. P. White, *Prog. Inorg. Chem.*, 1988, **36**, 195.
27. R. Inglis, L. F. Jones, C. J. Milios, S. Datta, A. Collins, S. Parsons, W. Wernsdorfer, S. Hill, S. P. Perlepes, S. Piligkos and E. K. Brechin, *Dalton Trans.*, 2009, **18**, 3403.
28. C. J. Milios, S. Piligkos and E. K. Brechin, *Dalton Trans.*, 2008, 1809.
29. C. J. Milios, R. Inglis, A. Vinslava, R. Baghi, W. Wernsdorfer, S. Parsons, S. P. Perlepes, G. Christou and E. K. Brechin, *J. Am. Chem. Soc.*, 2007, **129**, 12505.
30. C. J. Milios, R. Inglis, R. Bagai, W. Wernsdorfer, A. Collins, S. A. Moggach, S. Parsons, S. P. Perlepes, G. Christou and E. K. Brechin, *Chem. Commun.*, 2007, **33**, 3476.
31. C. J. Milios, A. Vinslava, W. Wernsdorfer, A. Prescimone, P. A. Wood, S. Parsons, S. P. Perlepes, G. Christou and E. K. Brechin, *J. Am. Chem. Soc.*, 2007, **129**, 6547.
32. C. J. Milios, A. Vinslava, W. Wernsdorfer, S. A. Moggach, S. Parsons, S. P. Perlepes, G. Christou and E. K. Brechin, *J. Am. Chem. Soc.*, 2007, **129**, 2754.
33. C. J. Milios, A. Vinslava, P. A. Wood, S. Parsons, W. Wernsdorfer, G. Christou, S. P. Perlepes and E. K. Brechin, *J. Am. Chem. Soc.*, 2007, **129**, 8.
34. R. Inglis, L. F. Jones, G. Karotsis, A. Collins, S. Parsons, S. P. Perlepes, W. Wernsdorfer and E. K. Brechin, *Chem. Commun.*, 2008, 5924.
35. R. Inglis, L. F. Jones, K. Mason, A. Collins, S. A. Moggach, S. Parsons, S. P. Perlepes, W. Wernsdorfer and E. K. Brechin, *Chem. Eur. J*, 2008, **14**, 9117.
36. C. J. Milios, R. Inglis, L. F. Jones, A. Prescimone, S. Parsons, W. Wernsdorfer and E. K. Brechin, *Dalton Trans.*, 2009, **15**, 2812.
37. P. L. Feng, C. Koo, J. J. Henderson, P. Manning, M. Nakano, E. del Barco, S. Hill and D. N. Hendrickson, *Inorg. Chem.*, 2009, **48**, 3480.
38. D. J. Watkin, C. K. Prout, J. R. Carruthers, P. W. Betteridge and R. I. Cooper, Chemical Crystallography Laboratory, University of Oxford, Oxford, UK, 2003.
39. W. Wernsdorfer, *Adv. Chem. Phys.*, 2001, **118**, 99.
40. M. O'Keeffe, M. A. Peskov, S. J. Ramsden and O. M. Yaghi, *Acc. Chem. Res*, 2008, **41**, 1782.
41. J. J. Borras-Alemnar, J. M. Clemente-Juan, E. Coronado and B. S. Tsukerblat, *J. Comp. Chem.*, 2001, **22**, 985.
42. S. Piligkos, University of Copenhagen, Copenhagen, Denmark.
43. W. Wernsdorfer, *Supercond. Sci. Technol.*, 2009, **22**, 064013.
44. R. Tiron, W. Wernsdorfer, N. Aliaga-Alcalde and G. Christou, *Phys. Rev. B*, 2003, **68**, 140407.
45. W. Wernsdorfer, S. Bhaduri, R. Tiron, D. N. Hendrickson and G. Christou, *Phys. Rev. Lett.*, 2002, **89**, 197201.
46. W. Wernsdorfer, S. Bhaduri, A. Vinslava and G. Christou, *Phys. Rev. B*, 2005, **72**, 214429.
47. M. Mola, S. Hill, P. Goy and M. Gross, *Rev. Sci. Instrum.*, 2000, **71**, 186.

48. S. Takahashi and S. Hill, *Rev. Sci. Instrum.*, 2005, **76**, 023114.
49. E. del Barco, A. D. Kent, S. Hill, J. M. North, N. S. Dalal, E. M. Rumberger, D. N. Hendrickson, N. E. Chakov and G. Christou, *J. Low Temp. Phys.*, 2005, **140**, 119.
50. A. Wilson, J. Lawrence, E.-C. Yang, M. Nakano, D. N. Hendrickson and S. Hill, *Phys. Rev. B*, 2006, **74**, 140403.
51. S. Takahashi, R. S. Edwards, J. M. North, S. Hill and N. S. Dalal, *Phys. Rev. B*, 2004, **70**, 094429.
52. J. Lawrence, E.-C. Yang, R. S. Edwards, M. M. Olmstead, C. Ramsey, N. S. Dalal, P. K. Gantzel, S. Hill and D. N. Hendrickson, *Inorg. Chem.*, 2008, **47**, 1965.
53. C. Lampropoulos, S. Hill and G. Christou, *ChemPhysChem*, 2009, **10**, 2397.
54. S. Datta, E. Bolin, R. Inglis, C. J. Milios, E. K. Brechin and S. Hill, *Polyhedron*, 2009, **28**, 1788.
55. J. Krzystek, A. Ozarowski and J. Telser, *Coord. Chem. Rev.*, 2006, **250**, 2308.

Chapter 4
Assembling Molecular Triangles into Discrete and Infinite Architectures

4.1 Introduction

With the realisation that crystal packing effects may play an important role in influencing the properties of molecular materials, the field of crystal engineering has enabled scientists to develop an understanding of how intermolecular interactions synergistically work and how to deploy them to evolve new areas of chemical research.[1-3] For this purpose, two special issues were recently devoted to the crystal engineering of molecular magnetic materials, highlighting the recent developments at the interface of supramolecular chemistry and molecular magnetism.[4-6]

Although Single-Molecule Magnets (SMMs) are indeed molecules and their properties are of molecular origin, crystal packing effects, which include weak interactions (*e.g.* hydrogen bonding, π···π interactions *etc*), often influence their magnetic response especially at low temperatures.[7-15] To this end, we have recently initiated a project to both study crystal packing effects upon SMM behaviour and to attempt to utilise SMMs as building blocks for the construction of supramolecular architectures (*i.e.* polygons, polyhedra) and extended networks (*i.e.* coordination polymers).[16-20]

We recently demonstrated that certain members of a family of hexanuclear and trinuclear Mn^{III} complexes of general formulae $[Mn^{III}_6O_2(R\text{-sao})_6(O_2CR)_2(L)_{4\text{-}6}]$ {hereafter denoted as $[Mn_6]$} and $[Mn^{III}_3O(R\text{-sao})_3(X)(L)_3]$ {hereafter denoted as $[Mn_3]$} ($saoH_2$ = salicylaldoxime; R = H, Me, Et *etc*; X = RCO_2^-, ClO_4^-; L = solvent);[21-27] with the latter being the analogous "half" molecules of the former, exhibit the phenomenon of single-molecule magnetism. We showed in each case that it was possible to significantly increase the ground spin state from $S = 4$ to $S = 12$ in the former and from $S = 2$ to $S = 6$ in the latter, enhancing the effective energy barrier for magnetisation reversal to record levels.[21-27] The origin of the AF→F switch arises from an intra-cluster structural distortion of the molecule induced by the 'twisting' of the (-Mn-N-O-) ring, as evidenced by the significant increases in the Mn-N-O-Mn torsion angles observed when derivatised salicylaldoximes were employed.[21, 27] The replacement of the axial ligands (*e.g.* ClO_4^- or RCO_2^-) provides an additional/alternative route to influence the magnetic response and that, in

combination with the high yields and solution stability of the molecular triangles, enables them to serve as building blocks. Since this system was found to be susceptible to subtle changes around the metal core, we reasoned that it would be possible to further influence their magnetic response by incorporating them into supramolecular architectures by means of host-guest interactions and coordination driven self-assembly.[28-31]

Taking advantage of the potentially "vacant" coordination axes on each Mn^{III} ion of [Mn_3] this chapter describes the isolation of a series of discrete and infinite assemblies by attaching terminal (4-chlorostilbazole, 4Cl-sbz and 4-methylstilbazole, 4Me-sbz) or bridging (4,4'-bipyridine, 4,4'-bpy and *trans*-1,2-bis(4-pyridyl)ethylene, 4,4'-bpe) pyridyl-type ligands to them (Scheme 4.1).

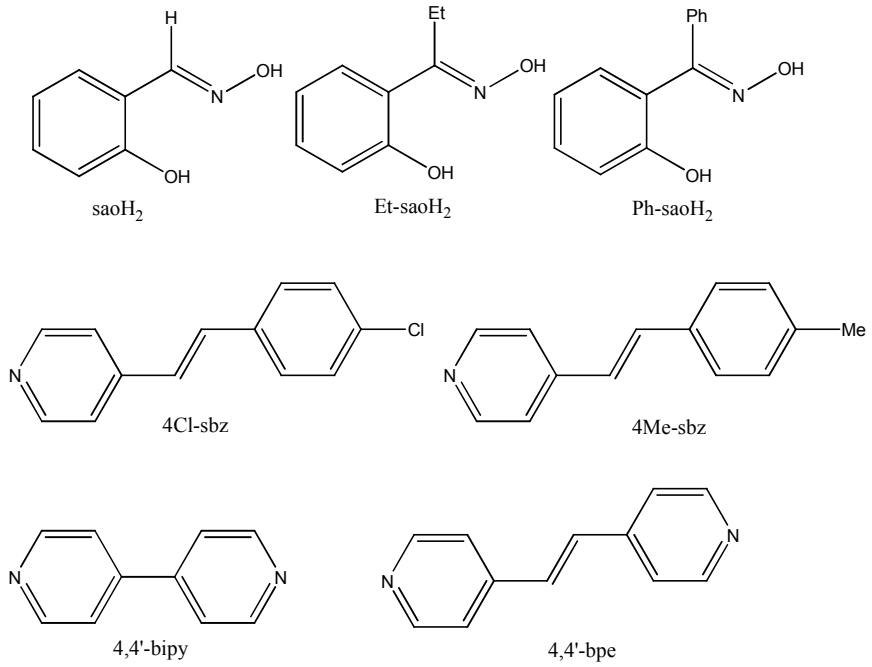

Scheme 4.1 The structural formulae of the ligands discussed in the text.

4.2 Assembling Molecular Triangles into Discrete and Infinite Architectures

4.2.1 Experimental section

Synthesis

All manipulations were performed under aerobic conditions, using materials as received. CAUTION! Although no problems were encountered in this work, care should be taken when using the potentially explosive perchlorate anion. Substituted salicylaldoximes[32] and stilbazoles[33] were synthesised following known procedures. The syntheses, structures and magnetic properties of the $[Mn_3]$ and $[Mn_6]$ precursors have already been reported.[21-27]

General synthetic strategies:

The supramolecular architectures reported here may be obtained using two synthetic procedures. The first involves the reaction of an appropriate Mn^{II} salt with a (substituted) salicylaldoxime and a base (Et_3N, Et_4NOH, MeONa or $LiOH{\cdot}H_2O$) in alcohol (MeOH or EtOH) to afford a dark green solution into which either solid or a CH_2Cl_2 solution of the pyridyl ligand was added resulting in the desired assemblies. The second procedure involves the synthesis and isolation of a precursor $[Mn_3]$ triangle (or $[Mn_6]$ in the case of **4.5**) followed by dissolution in alcohol (MeOH or EtOH) or in a mixture of alcohol/CH_2Cl_2 and addition of solid or a CH_2Cl_2 solution of the pyridyl ligand.

X-ray crystallography

Diffraction data were collected at 150 K on a Bruker Smart Apex CCDC diffractometer, equipped with an Oxford Cryosystems LT device, using Mo radiation.[34] See CIF files for full details.

Magnetic measurements

Variable temperature, solid-state direct current (dc) and alternating current (ac) magnetic susceptibility data down to 1.8 K were collected on a Quantum Design MPMS-XL SQUID magnetometer equipped with a 7 T dc magnet. Diamagnetic

corrections were applied to the observed paramagnetic susceptibilities using Pascal's constants.

4.2.2 Results and Discussion

Description of structures

For the sake of comparison, the structures of representative [Mn_3] precursors are briefly discussed in terms of describing the structural features that we took under consideration to design the supramolecular assemblies. The representative SMM [Mn^{III}_3O(Et-sao)$_3$(MeOH)$_3$](ClO_4)[27] (Fig. 4.1) consists of a [$Mn^{III}_3(\mu_3$-O)]$^{7+}$ triangular unit with the three η^1:η^1:η^1:μ-Et-sao^{2-} ligands bridging along the edges of the [Mn_3] core. A threefold axis which is perpendicular to the [Mn_3] mean plane passes through the central μ_3-O^{2-}, the perchlorate chlorine atom and one of the ClO_4^- oxygen atoms. A MeOH molecule is attached to each Mn^{III} ion, with all three being oriented on the same (bottom) side of the triangular unit which is further capped by a η^1:η^1:η^1:μ_3 weakly coordinated ClO_4^- anion on the opposite (upper) side. In this arrangement, each Mn^{III} ion adopts a distorted octahedral geometry and displays Jahn–Teller (JT) elongation, as expected for high-spin $3d^4$ ions in near octahedral geometry. The central μ_3-O^{2-} ion deviates by approximately 0.18 Å from the [Mn_3] plane towards the terminally bonded MeOH molecules, while the phenyl groups of the Et-sao^{2-} ligands lean toward the perchlorate. The three Mn-N-O-Mn torsion angles are 42.12°. Due to the presence of the capping ClO_4^- anion, the JT axes of the Mn^{III} ions are not parallel and form an angle of ~22.4° to each other and an angle of ~12.96° to the [Mn_3] plane converging towards the ClO_4^- anion. Substitution of the terminally bound MeOH molecules at the bottom face of the [Mn_3] triangle by substituted pyridine molecules such as β-picoline (β-pic) or 4-ethyl pyridine (4Etpy) does not disturb the metal core or the connectivity of the rest of the ligands resulting in the SMMs [Mn^{III}_3O(Et-sao)$_3$(β-pic)$_3$](ClO_4)[27] and [Mn^{III}_3O(Et-sao)$_3$(4Etpy)$_3$](ClO_4) (Fig. 4.1).[27]

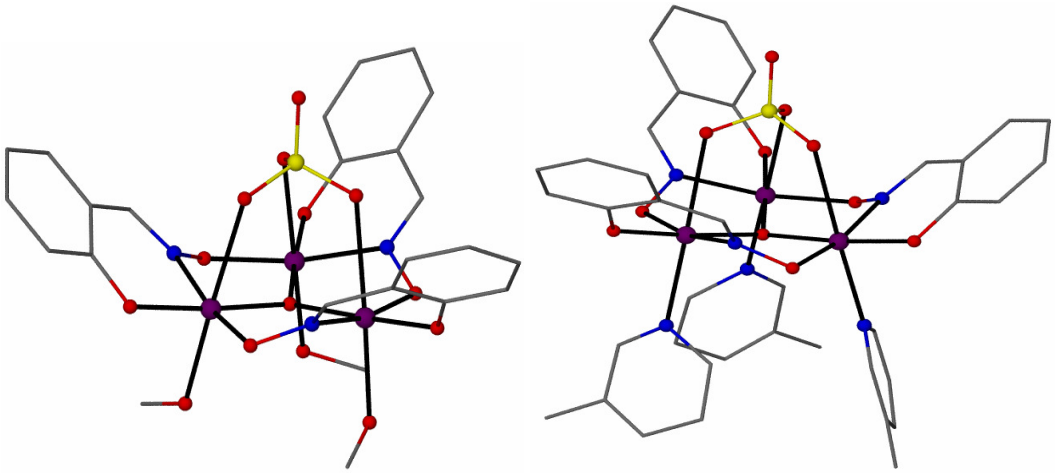

Figure 4.1 The molecular structures of $[Mn^{III}_3O(Et\text{-}sao)_3(MeOH)_3](ClO_4)$ and $[Mn^{III}_3O(Et\text{-}sao)_3(\beta\text{-}pic)_3](ClO_4)$. All hydrogen atoms and ethyl groups of the Et-sao^{2-} ligands have been omitted for clarity. Colour code: Mn: purple, O: red, N: blue, Cl: yellow, C: grey.

Having in mind the shape of the $[Mn_3]$ triangles, we reasoned that substitution of the terminally bonded MeOH or pyridine ligands with longer pyridyl-type ligands such as the stilbazoles would create some sort of cavity at the bottom face of the $[Mn_3]$ plane. That came to fruition when 4Cl-sbz was introduced to the methanolic reaction mixture of $Mn(ClO_4)\cdot 6H_2O$/Ph-saoH$_2$/Et$_3$N from which $[Mn^{III}_3O(Ph\text{-}sao)_3(4Cl\text{-}sbz)_3(MeOH)_3]_2(OH)(ClO_4)\cdot 2MeOH$ (**4.1**·2MeOH) was obtained.

Complex **4.1** (Table 4.1, Fig. 4.2) crystallises in the rhombohedral space group $R\bar{3}$ and consists of a $[Mn^{III}_3(\mu_3\text{-}O)]^{7+}$ triangular unit with the three Ph-sao^{2-} ligands bridging in a $\eta^1{:}\eta^1{:}\eta^1{:}\mu$ fashion along the edges of the $[Mn_3]$ core. A threefold rotation axis which is perpendicular to the $[Mn_3]$ mean plane passes through the central μ_3-O^{2-} (O111). A 4Cl-sbz molecule is attached to each Mn^{III} ion, with all three being oriented on the same (bottom) side of the $[Mn_3]$ plane which is further capped by three terminal MeOH molecules on the opposite (upper) side instead of the capping ClO_4^- anion found in the precursors, resulting in a cationic $[Mn_3]^+$ complex where all Mn^{III} atoms are in an axially elongated octahedral environment (Fig. 4.2). The three stilbazole molecules diverge from the bottom of the $[Mn_3]$ triangle toward the outside, creating an open bowl-shaped cavity. Two such $[Mn_3]^+$ complexes have assembled with their bottom faces being parallel and face-to-face having turned by 60° along the three fold axis with respect to each other such that the 4Cl-sbz of one $[Mn_3]^+$ is sitting between two 4Cl-sbz molecules of the other $[Mn_3]^+$.

In this [inter-digitated] arrangement, a closed cavity is formed where a disordered ClO_4^- (over two positions with 50 % occupancy) is situated, being hydrogen bonded (with 12 H-bonds, 4 unique) to the pyridyl and ethylene hydrogen atoms of the 4Cl-sbz ligands (Fig. 4.3). The $[Mn_3]$ planes within the $\{[Mn_3]\text{-}(ClO_4^-)\text{-}[Mn_3]\}^+$ assembly are separated by 16.151 Å. The $\{[Mn_3]\text{-}(ClO_4^-)\text{-}[Mn_3]\}^+$ units assemble in columns running along *c* with the upper faces of the $[Mn_3]$ units being face-to-face having a disordered OH^- in between them. The coordination of 4Cl-sbz has disturbed the metal core. The central μ_3-O^{2-} ion deviates by ~0.272 Å from the $[Mn_3]$ plane towards the terminally bound 4Cl-sbz ligands, the phenyl groups of the Ph-sao^{2-} now lean toward the 4-chlorostilbazoles (*i.e.* toward the bottom face of the triangle) while the Mn-N-O-Mn torsion angles are reduced to 16.2°.

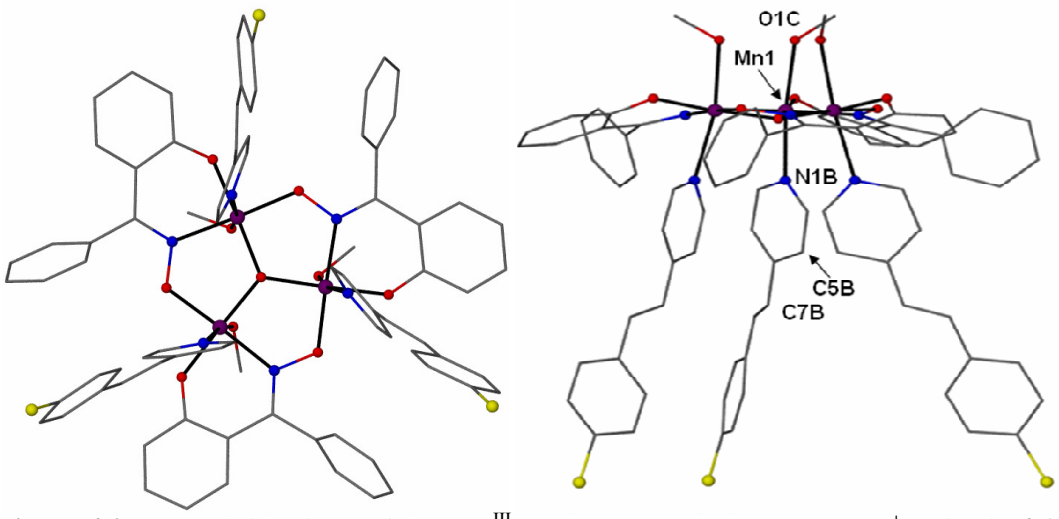

Figure 4.2 Top and side views of the $[Mn^{III}_3O(Ph\text{-}sao)_3(4Cl\text{-}sbz)_3(MeOH)_3]^+$ cation in **4.1**.

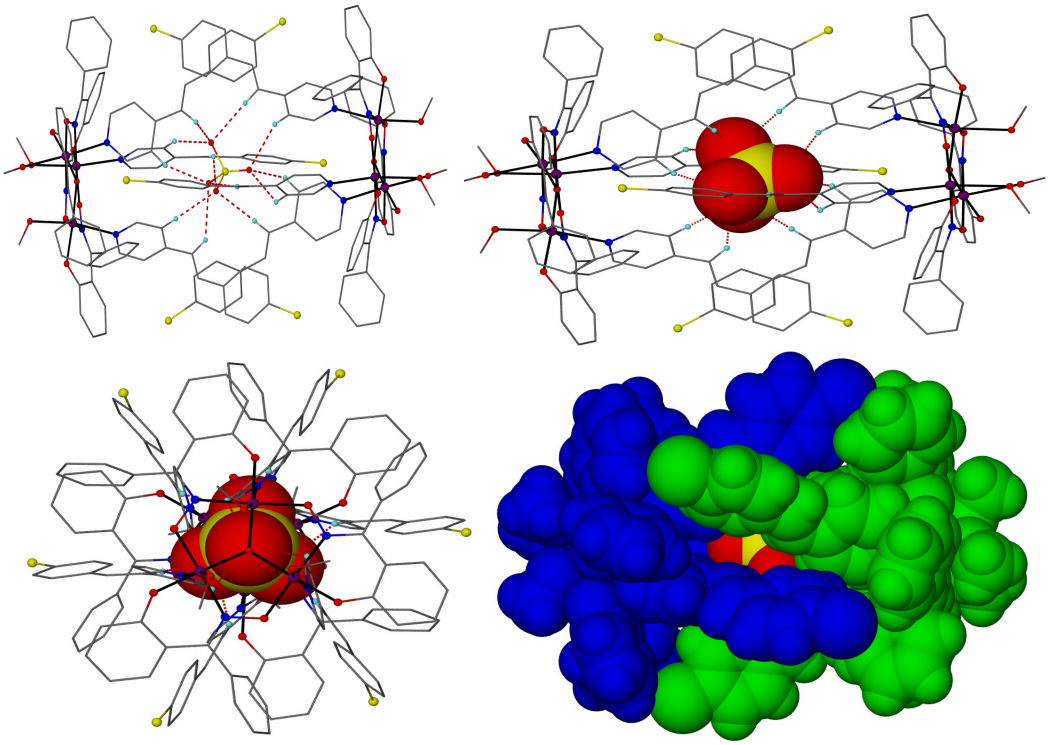

Figure 4.3 Perspective views of the $\{[Mn_3]\text{-}(ClO_4^-)\text{-}[Mn_3]\}^+$ assembly found in the crystals of **4.1**. Most hydrogen atoms have been omitted for clarity. Colour code as in Fig. 4.1, H: cyan. Bottom right: space filling model of the assembly with the $[Mn_3]^+$ triangles in blue and green.

Complex $[Mn^{III}_3O(Ph\text{-}sao)_3(4Me\text{-}sbz)_3(EtOH)_3]_2(OH)(NO_3)$ (**4.2**) (Table 4.1, Fig. 4.4) also crystallises in the rhombohedral space group $R\bar{3}$ and consists of a $[Mn^{III}_3(\mu_3\text{-}O)]^{7+}$ triangular unit with the three Ph-sao^{2-} ligands bridging in a $\eta^1{:}\eta^1{:}\eta^1{:}\mu$ fashion along the edges of the $[Mn_3]$ core. It is the nitrate version of complex **4.1** with three EtOH molecules at the upper side and three 4Me-sbz molecules at the bottom side of the $[Mn_3]$ triangle. The threefold rotation axis passes perpendicular to the $[Mn_3]$ mean plane through the central μ_3-O^{2-} (O111). Two $[Mn_3]^+$ units assemble in the same fashion as in **4.1** to form a cavity which hosts a disordered NO_3^- (over two positions with 50 % occupancy), held by 9 hydrogen bonds (3 unique) to the pyridyl and ethylene hydrogen atoms of the 4Me-sbz ligands (Fig. 4.4).

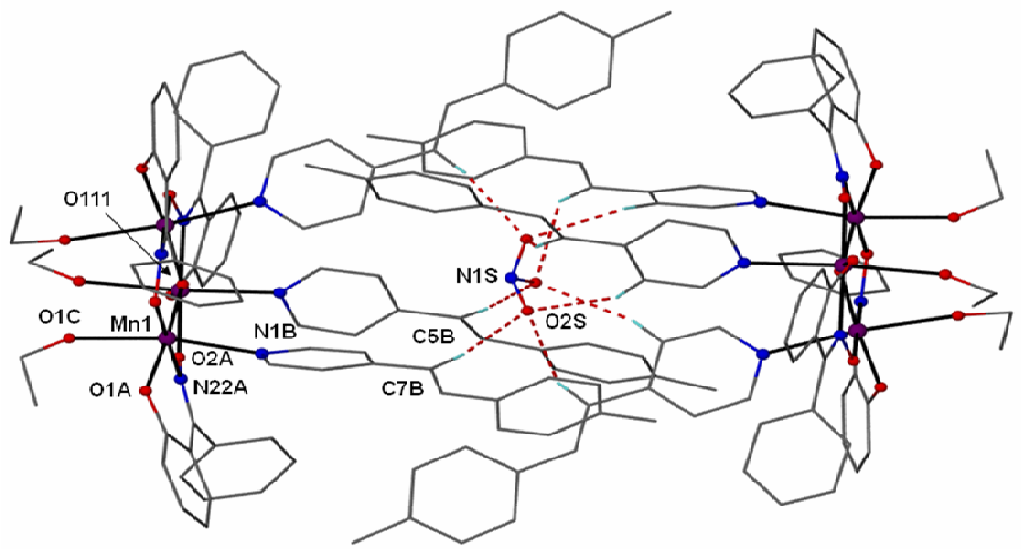

Figure 4.4 Perspective view of the $\{[Mn_3]\text{-}(NO_3^-)\text{-}[Mn_3]\}^+$ assembly found in the crystals of **4.2**. Most hydrogen atoms have been omitted for clarity. Colour code as in Fig. 4.1, H: cyan.

The $[Mn_3]$ planes within the $\{[Mn_3]\text{-}(NO_3^-)\text{-}[Mn_3]\}^+$ assembly are again parallel but the distance between them is reduced to 15.83 Å due to the presence of the smaller nitrate ion in the cavity. A disordered OH^- is situated between the $\{[Mn_3]\text{-}(NO_3^-)\text{-}[Mn_3]\}^+$ units which also assemble in columns along *c* (Fig. 4.5). The central $\mu_3\text{-}O^{2-}$ ion deviates by ~0.275 Å from the $[Mn_3]$ plane towards the 4Me-sbz ligands, the phenyl groups of the Ph-sao^{2-} lean toward the 4Me-sbz, while the Mn-N-O-Mn torsion angles are further reduced to 13.4°. Complexes **4.1** and **4.2** are rare examples of polynuclear metal complexes that have assembled not by coordination bonds[35-37] but by weak host-guest interactions to create a cavity that clathrates a counter anion by C-H···O interactions.[38, 39]

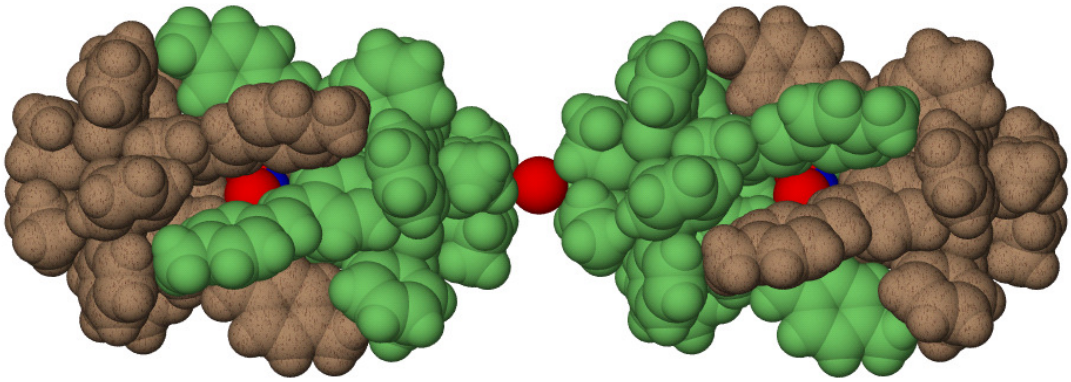

Figure 4.5 The $\{[Mn_3]\text{-}(NO_3^-)\text{-}[Mn_3]\}(OH)$ columns in **4.2** along *c*. Similar packing is observed in $\{[Mn_3]\text{-}(ClO_4^-)\text{-}[Mn_3]\}(OH)$ of **4.1**.

Aiming to create an extended network by assembling the molecular triangles, we employed 4,4'-bipyridine (4,4'-bpy) in the methanolic reaction mixture of $Mn(ClO_4)\cdot 6H_2O$/Et-saoH_2/MeONa from which $\{[Mn^{III}_3O(Et\text{-}sao)_3(4,4'\text{-}bpy)_2(MeOH)]ClO_4\cdot 1.5MeOH\cdot Et_2O\}_n$ (**4.3**·1.5MeOH·Et_2O) was obtained after Et_2O diffusion. Complex **4.3** (Table 4.1, Fig. 4.6) crystallises in the monoclinic space group *C*2/*c* and consists of a $[Mn^{III}_3(\mu_3\text{-}O)]^{7+}$ triangular unit with the three $\eta^1{:}\eta^1{:}\eta^1{:}\mu$-Et-sao^{2-} ligands bridging along the edges of the $[Mn_3]$ core and the central μ_3-O^{2-} ion (O123) deviating only ~0.015 Å from the $[Mn_3]$ plane. The Mn-N-O-Mn torsion angles are 28.41° for Mn1-N-O-Mn3, 12.79° for Mn3-N-O-Mn2 and 14.92° for Mn2-N-O-Mn1. The $[Mn_3]$ triangles and the 4,4'-bpy ligands have assembled to create a ladder-like one dimensional polymer with two 4,4'-bpy molecules bridging between the $[Mn_3]$ units (Fig. 4.6). In this arrangement, Mn1 is in an axially elongated octahedral environment with two pyridyl$_{4,4'\text{-bpy}}$ nitrogen atoms at the axial positions, Mn2 is in a square pyramidal environment with a pyridyl$_{4,4'\text{-bpy}}$ nitrogen atom at the axial position and Mn3 is in an axially elongated octahedral environment with a methanol oxygen atom and a pyridyl$_{4,4'\text{-bpy}}$ nitrogen atom at the axial positions.

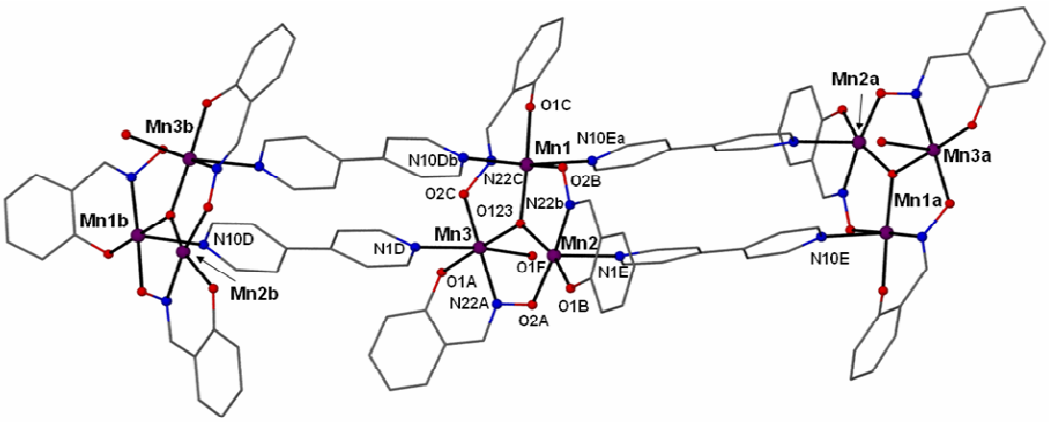

Figure 4.6 View of the polymeric chain of **4.3**. Colour code as in Fig. 4.1. Symmetry codes: a: ½-x, 3/2-y, b: -z; -x, y, ½-z.

A careful inspection of the $\{\text{-}[Mn_3]\text{-}(4,4'\text{-bpy})_2\text{-}[Mn_3]\text{-}\}_n$ chain reveals that Mn1 is connected (through a 4,4'-bpy) to a Mn2 on its right and to a Mn3 on its left (Fig. 4.6). This arrangement dictates that the $[Mn_3]$ core turns around along the polymer axis and this in turn creates a four component repeating unit $([Mn_3]_4)_n$ as shown in Fig. 4.7. Every two $[Mn_3]$ planes within the four component repeating unit are parallel (*i.e.* plane 1 ‖ plane 2 and plane 3 ‖ plane 4 in Fig. 4.7) and separated by

11.228 Å, while the distance between the central μ_3-O^{2-} of planes 2 and 3 is 12.145 Å. The two sets of parallel planes form an angle of 19.03°.

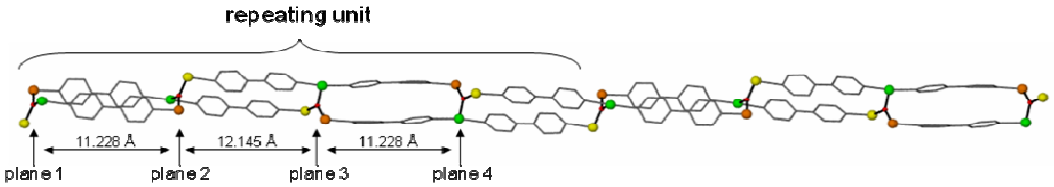

Figure 4.7 The four component repeating unit found in **4.3**. Colour code: Mn1: green, Mn2: orange, Mn3: yellow, O: red.

In order to further exploit the ability of the [Mn_3] triangles to form polymeric structures we employed the longer bis-pyridyl ligand *trans*-1,2-bis(4-pyridyl)ethylene (4,4'-bpe) into a methanolic reaction mixture of $Mn(ClO_4)_2{\cdot}6H_2O$ and $saoH_2$. Dark green crystals of $\{[Mn^{III}_3O(sao)_3(4,4'\text{-bpe})_{1.5}]ClO_4{\cdot}3MeOH\}_n$ (**4.4**·3MeOH) were obtained after slow evaporation of the solution. Complex **4.4** (Table 4.1, Fig. 4.8) crystallises in the trigonal space group *P3̄ /c* and consists of μ_3-O^{2-} centered $[Mn^{III}_3O(sao)_3]ClO_4$ units and 4,4'-bpe molecules.

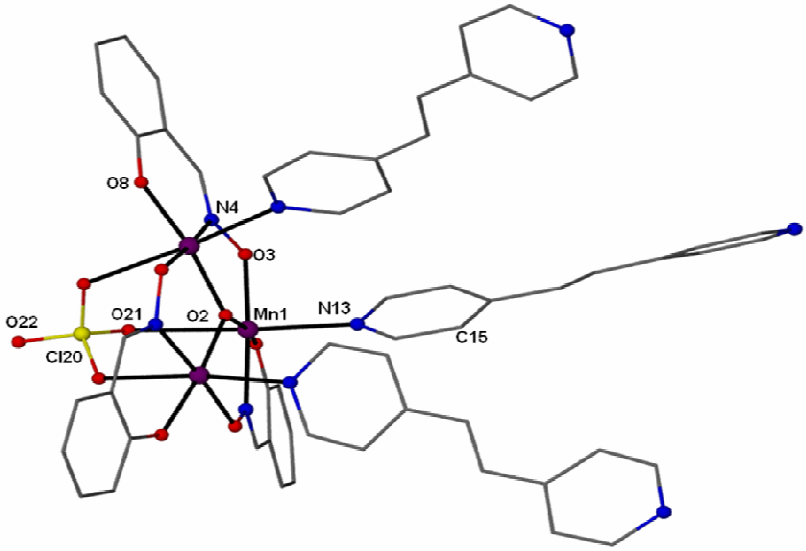

Figure 4.8 The molecular structure of the triangle in **4.4**. All hydrogen atoms have been omitted for clarity. Colour code as in Fig. 4.1.

The components have assembled to form a 2D coordination polymer (Fig. 4.9) where the 4,4'-bpe molecules bridge the [Mn_3] units. Three $\eta^1{:}\eta^1{:}\eta^1{:}\mu$-$sao^{2-}$ ligands and a capping ClO_4^- anion surround the [Mn_3] unit in **4.4**. A threefold axis passes through the central μ_3-O^{2-} (O2), the ClO_4^- chlorine atom (Cl20) and one of the perchlorate oxygen atoms (O22) and is perpendicular to the [Mn_3] plane. The Mn^{III} ions are in

axially elongated octahedral environments with the JT axes [O21-Mn1-N13] converging towards the ClO_4^- side as seen in the precursor triangles $[Mn^{III}_3O(Et\text{-}sao)_3(MeOH)_3](ClO_4)$ and $[Mn^{III}_3O(Et\text{-}sao)_3(\beta\text{-}pic)_3](ClO_4)$. A 4,4'-bpe molecule is attached to each Mn^{III} ion, with all three being oriented on the same (bottom) side of the $[Mn_3]$ plane. The central μ_3-O^{2-} ion deviates by 0.303 Å from the $[Mn_3]$ plane toward the 4,4'-bpe molecules while the Mn-N-O-Mn torsion angles have increased to 17.27° in comparison to those in **4.1** and **4.2,** but are still much smaller than those found in the precursor $[Mn^{III}_3O(Et\text{-}sao)_3(MeOH)_3](ClO_4)$.

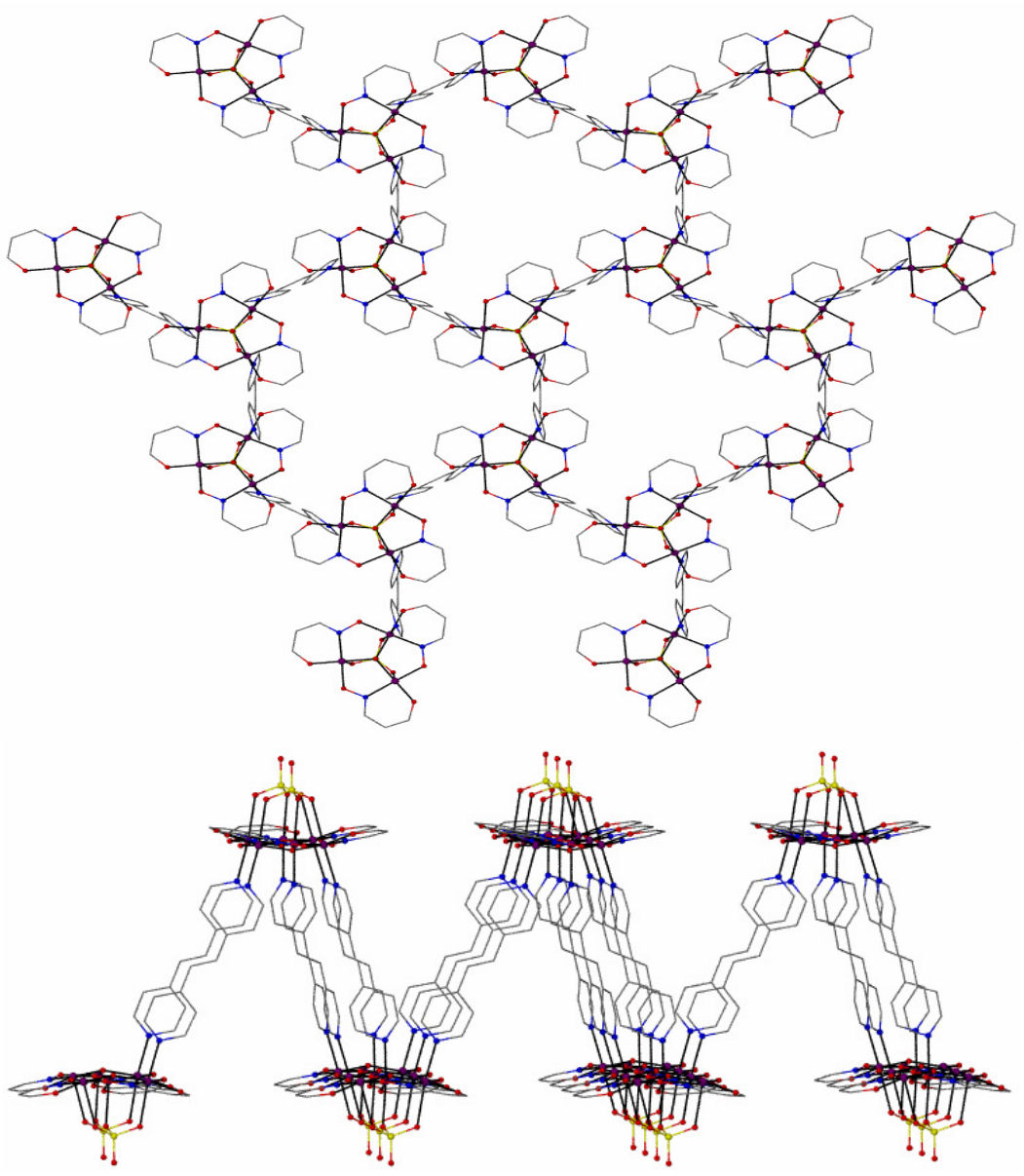

Figure 4.9 Top and side views of the 2D (6,3)-net of **4.4**. All hydrogen atoms and most of the carbon atoms of the sao^{2-} ligands have been omitted for clarity. Colour code as in Fig. 4.1.

The 2D network adopted by **4.4** conforms to a (6,3) regular net with the $[Mn_3]$ units acting as three-connected nodes (Fig. 4.9). Due to the peculiar shape of the $[Mn_3]$ unit which is non-planar and the orientation of the connection sites on the $[Mn_3]$ cluster which are all pointing toward the same side of the $[Mn_3]$ plane and converging towards the ClO_4^- side, the 2D network is highly distorted such that the $[Mn_3]$ units are placed alternately above and below the mean plane of the 2D net. This arrangement gives rise to the formation of conical cavities within the body of the 2D framework which are approximately 12.6 Å thick (Fig. 4.9). The upper rims of the conical cavities are pointing alternately above and below the plane of the net such that half of the rims of the cavities point above and half below the layer. Each cavity is composed of a $[Mn_3]$ unit, which serves as the bottom of the cavity and three 4,4'-bpe molecules, while three other $[Mn_3]$ units from the same net are attached to each of the three 4,4'-bpe molecules narrowing the "gates" of the cavities' rims.

A salient feature of the structure of **4.4** is that the size of each $\{[Mn_3](4,4'\text{-bpe})_3[Mn_3]_3\}$ cavity is large enough to host a $[Mn_3]$ unit of an adjacent net (Figs. 4.10 and 4.11). This host-guest interaction is further supported by three hydrogen-bonding interactions that involve one of the pyridyl C-H groups of the three cavity-forming 4,4'-bpe molecules and the uncoordinated oxygen atom of the ClO_4^- that caps the $[Mn_3]$ guest [one unique: C15-H151···O22 = 3.363 Å]. The $[Mn_3]$ guest is in an eclipse orientation with respect to the $[Mn_3]$ at the bottom of the host cavity while the three $[Mn_3]$ units at the rim's gate of the conical cavity prohibit the $[Mn_3]$ guest from exiting (Fig. 4.10). Therefore, each $[Mn_3]$ serves as (i) the bottom for the conical cavity, (ii) one of the gate-keepers of a neighbouring cavity while (iii) acting as the guest for a cavity belonging to a neighbouring net.

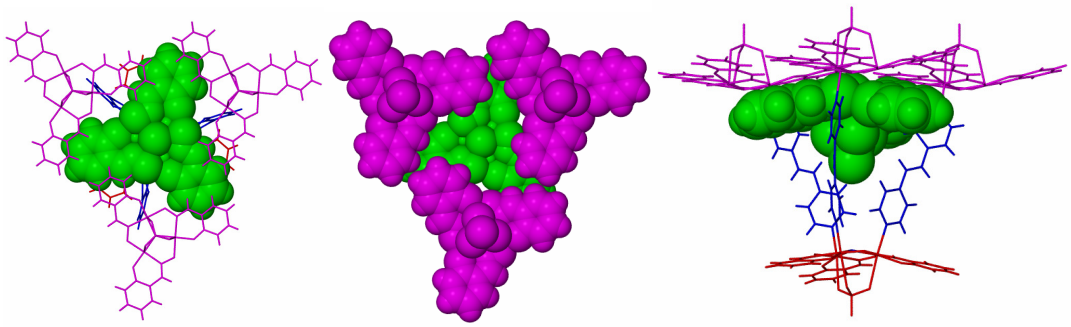

Figure 4.10 Side (left) and top (right) views of the $[Mn_3]\subset\{Mn_3](4,4'\text{-bpe})_3[Mn_3]_3\}$ in **4.4**.

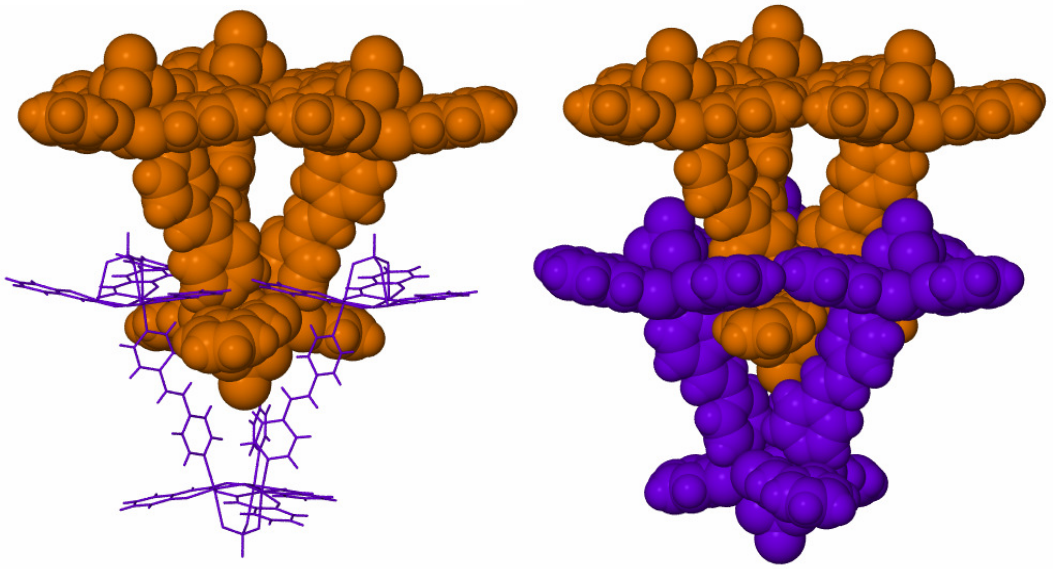

Figure 4.11 Views of conical "ice-cream cone" within an "ice-cream cone" units in **4.4**.

Each layer is interlocked with two other layers, one above and one below the middle layer's plane, resulting in an entangled array with an increased dimensionality (*i.e.* from 2D to 3D) (Fig. 4.12). This interlocking is purely supramolecular in nature since it is based on host-guest and hydrogen bonding interactions as described above. Each layer acts as a host and at the same time as a guest to both neighbouring layers. In principle the layers of **4.4** could be disentangled by stretching out, but that is prohibited since it is impossible to have the 4,4'-bpe molecules and the $[Mn_3]$ units in the same plane due to the orientation of the connection sites on the $[Mn_3]$ units. From the topological point of view, the interlocking of the 2D layers of **4.4** does not belong to any known type of entanglement.[40-49] Topological entanglement (*i.e.* interpenetration and polycatenation) is easily excluded since (i) the dimensionality in

4.4 increases due to the entanglement, (ii) no bond-breaking is required to disentangle the layers, thus excluding interpenetration[42-45] and (ii) the closed circuits [*i.e.* the hexagonal rings of the (6,3) net of **4.4**] are not catenated (*i.e.* do not form Hopf or Borromean links), thus excluding polycatenation.[46-49] Euclidean entanglement (*i.e.* polythreading)[40, 41] can also be excluded since none of the closed loops [*i.e.* the hexagonal circuits of the (6,3) net of **4.4**] are threaded.

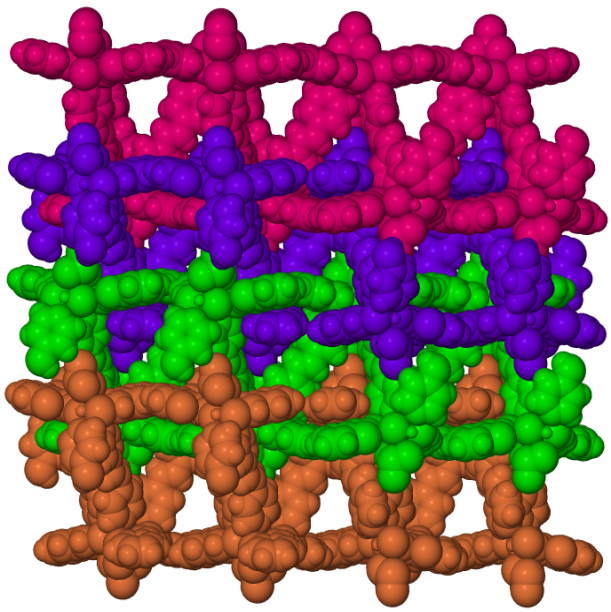

Figure 4.12 View of four entangled layers in the crystal of **4.4**.

That the layers of **4.4** form cavities to host the [Mn_3] units of neighbouring layers resulting in an architecture of increased dimensionality means that that this is a new type of supramolecular entanglement where real host-guest interactions are responsible for the interlocking.

The next step was to employ a [Mn_6] SMM instead of a [Mn_3] as a precursor. For this purpose, [$Mn^{III}_6O_2$(Et-sao)$_6$(O_2CPh)$_2$(EtOH)$_4$(H_2O)$_2$] was treated with 4,4-bpe in EtOH to produce dark green crystals of [{Mn^{III}_3O(Et-sao)$_3$(O_2CPh)(EtOH)}$_2${4,4'-bpe}$_2$] (**4.5**). Complex **4.5** (Table 4.1, Fig. 4.13) crystallises in the monoclinic space group $P2_1/n$ and consists of two [$Mn^{III}_3(\mu_3$-O)]$^{7+}$ triangular units with the three η^1:η^1:η^1:μ-Et-sao^{2-} ligands bridging along the edges of the [Mn_3] core and two 4,4'-bpe molecules bridging the [Mn_3] triangles. An inversion centre in the middle of the molecule correlates the two [Mn_3] units. The two 4,4'-bpe molecules are organised between the two [Mn_3] clusters in a face-to-face stacked arrangement and separated

by 3.5 Å. Two phenyl groups of two Et-sao^{2-} ligands are twisted towards the 4,4'-bpe side with the third pointing in the opposite direction. Two of the three Mn^{III} ions are in distorted octahedral environments with the third adopting a square pyramidal geometry. The capping μ_3-ClO_4^- in **4.4** and in the [Mn_3] precursors has been replaced by a *syn, syn* μ-$PhCO_2^-$ and a terminal EtOH molecule.

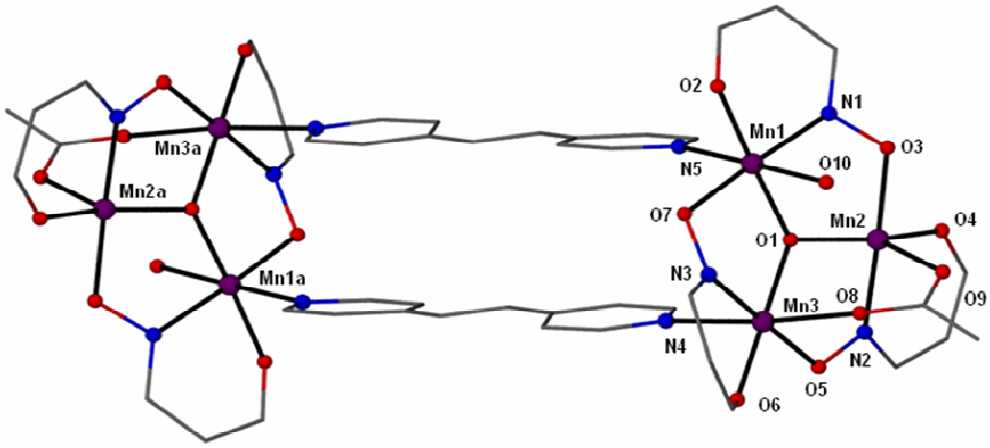

Figure 4.13 The rectangular hexanuclear assembly of **5**. All hydrogen and some carbon atoms have been removed for clarity. Colour code as in Fig. 4.1. Symmetry code: a: -x, 1-y, -z.

The ligation of the $PhCO_2^-$ and the EtOH molecules has destroyed the three fold rotation axis present in **4.1**, **4.2** and the three fold axis in **4.4**, thus releasing the JT axes on the Mn^{III} ions from converging towards the same side of the [Mn_3] plane. The Mn^{III} ions that coordinate to the 4,4'-bpe molecules are those in the octahedral environment, with the oxygen atoms from a $PhCO_2^-$ and an EtOH molecule on the apical positions opposite the nitrogen atoms (N4 and N5) of the 4,4'-bpe molecules. The JT axes on those Mn^{III} ions are inclined to each other at an angle of 19.13° [O10-Mn1N5∠O8-Mn3-N4], and are thus more twisted than the analogous axes in their [Mn_3] precursors, **4.1**, **4.2** and **4.4**, although they do not converge towards the $PhCO_2^-$ and the EtOH ligands. The central μ_3-O^{2-} ion deviates by 0.274 Å from the [Mn_3] plane toward the 4,4'-bpe molecules. The Mn-N-O-Mn torsion angles are 24.17° for Mn1-N-O-Mn2, 10.62° for Mn2-N-O-Mn3 and 42.73° for Mn32-N-O-Mn1. The replacement of the ClO_4^- ligands by a $PhCO_2^-$ and the EtOH molecule in **4.5** has lowered the local symmetry around the [Mn_3] cluster giving rise to a polygon (*i.e.* a rectangle) instead of a coordination polymer as in **4.3** and **4.4**. Alternatively, **4.5** might be described as a "dimer of clusters" or a "pair of clusters"[20, 50, 51] which is

a rather new perspective of looking at how magnetic clusters can be arranged in the crystal lattice with respect to each other.[52]

4.2.3 Magnetochemistry

Dc magnetic susceptibility measurements

Dc magnetic susceptibility studies were carried out on powdered crystalline samples of **4.1**-**4.5** in the temperature range 5 - 300 K in a field of 0.1 T. The $\chi_M T$ vs. T data for **4.2**, **4.3** and **4.5** are plotted in Fig. 4.14 with their simulations (solid lines). The data for complexes **4.1** and **4.4** have been omitted as they are essentially identical to **4.2** and **4.5**, respectively. Room-temperature $\chi_M T$ values for all complexes range from 7.99 to 8.22 cm^3 K mol^{-1}, lower than the expected spin-only (g = 2) value for three non-interacting Mn^{III} centres of 9 cm^3 K mol^{-1}, suggesting the presence of dominant antiferromagnetic exchange. In all cases the $\chi_M T$ values decrease gradually as temperature is decreased until approximately 150 K where they drop more rapidly to values between 2.09 and 3.28 cm^3 K mol^{-1} at 5 K.

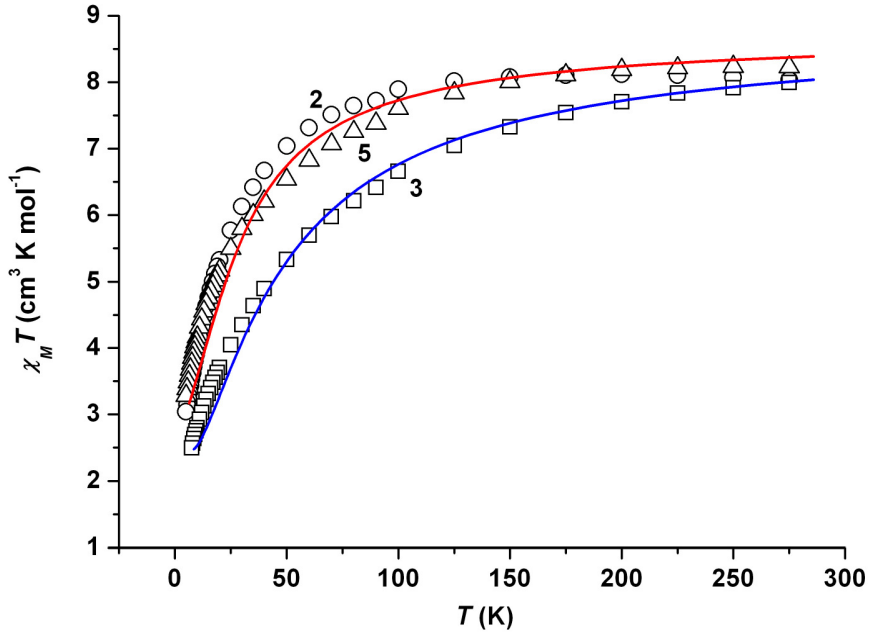

Figure 4.14 $\chi_M T$ vs. T plots for complexes **4.2** (○), **4.3** (□) and **4.5** (Δ). The solid lines represent simulations of the experimental data.

Complex **4.3** was successfully simulated[53] employing the Hamiltonian of equation (1) describing the *2-J* model (isosceles triangle) shown in Scheme 4.2, giving a

ground state $S = 2$ and the parameters $g = 1.98$, $J_1 = -2.80$ and $J_2 = -0.80$ cm^{-1}, with the first excited state ($S = 1$) 4.80 cm^{-1} above the ground state.

Complex **4.5** was successfully simulated using the 3-*J* model (scalene triangle) of equation (2) [Scheme 4.2], affording a ground state $S = 2$ and the parameters $g = 1.97$, $J_1 = -1.30$, $J_2 = -2.80$ and $J_3 = 1.20$ cm^{-1}, with the first excited state ($S = 3$) 11.81 cm^{-1} above the ground state. The isosceles *versus* scalene triangle models were employed based on the symmetry of the [Mn_3] unit and the number of significantly different Mn-N-O-Mn torsion angles.

$$\hat{H} = -2J_1(\hat{S}_1 \cdot \hat{S}_2 + \hat{S}_2 \cdot \hat{S}_3) - 2J_2(\hat{S}_1 \cdot \hat{S}_3) \qquad (1)$$

$$\hat{H} = -2J_1(\hat{S}_1 \cdot \hat{S}_2) - 2J_2(\hat{S}_2 \cdot \hat{S}_3) - 2J_3(\hat{S}_1 \cdot \hat{S}_3) \qquad (2)$$

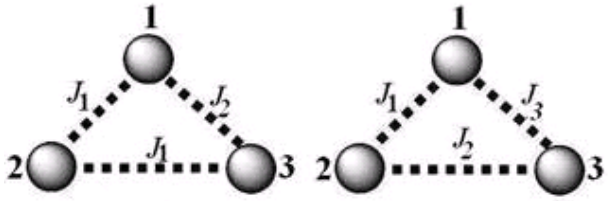

Scheme 4.2 Schematic detailing the 2-*J* (isosceles triangle) and 3-*J* (scalene triangle) models employed to simulate the experimental data for **4.3** and **4.5**, respectively. The different coupling constants (J_1-J_3) represent exchange between metal ions *via* significantly different Mn-N-O-Mn torsion angles.

Complex **4.2** has crystallographically imposed three-fold symmetry and its susceptibility data could not be reproduced satisfactorily. $S = 2$ is not the anticipated ground state for an antiferromagnetic triangle that possesses idealised three-fold symmetry [an equilateral triangle with the same *J* across all three exchange pathways). In fact, one expects a singlet, $S = 0$, ground state due to the frustration inherent in the topology. Our previous studies of isolated (molecular) [Mn_3] triangles have only been successful for those molecules in which the frustration has been relieved, *i.e.* the most distorted complexes.[27] Indeed only two examples of low-spin [Mn_3] complexes from a very large family of molecules, have yielded any useful information - even from single crystal EPR.[27] The presence of weak exchange comparable in magnitude to d_{ion} results in considerable spin-state mixing, making *S* ill-defined.

Conclusions

Our adventures in assembling molecular triangles, $[Mn^{III}_3O(R\text{-}sao)_3]^+$, have resulted in a series of discrete and infinite supramolecular architectures featuring self-assembled dimers of triangles that have assembled not by coordination bonds but by weak host-guest interactions to create a cavity that clathrates a counter anion (*i.e.* ClO_4^- and NO_3^-) by C-H···O interactions, a 1D coordination polymer in which the repeating unit is different than the asymmetric unit,[54] a 2D coordination polymer that exhibits a novel type of a supramolecular entanglement which is based on host-guest interactions and increases the dimensionality of the bulk material to 3D and a polygon. The construction of the polygon was rationalised in terms of changing the capping ClO_4^-, that forces the connection coordination axes on each Mn^{III} ion of the $[Mn_3]$ precursor to converge towards its side, to a $PhCO_2^-$ and an EtOH molecule that lower the local symmetry around the $[Mn_3]$, releasing the JT connection axes and therefore directing the self-assembly process. The $[Mn_3]$ core has proved itself stable enough to maintain its integrity upon reaction with various pyridyl ligands and at the same time adaptable to changes and does that by altering its local symmetry. Although these characteristics proved fruitful/compelling for the construction of the supramolecular architectures, they also proved disadvantageous for the construction of magnetic materials since the changes in the magnetic core dramatically reduced the Mn-N-O-Mn torsion angles resulting in materials with small spin ground states. In other words, the use of long pyridyl-type ligands has the effect of flattening the triangular building blocks and thus promoting AF exchange through the oximate bridges affording $[Mn_3]$ units with $S = 2$ ground states. We further exploit the possibility of utilising the $[Mn_3]$ and $[Mn_6]$ as building blocks for the construction of discrete or infinite architectures by employing polycarboxylate ligands and/or mixed pyridyl/carboxylate ligands.

Table 4.1 Crystallographic data for complexes **4.1**-**4.5**.

	4.1	**4.2**	**4.3**	**4.4**	**4.5**
Chemical formula	$C_{82}H_{73.5}N_6O_{13.5}Cl_{3.5}Mn_3$	$C_{87}H_{84.5}N_{6.5}O_{12}Mn_3$	$C_{53.5}H_{63}N_7O_{14.5}ClMn_3$	$C_{42}H_{42}N_6O_{14}ClMn_3$	$C_{96}H_{96}N_{10}O_{20}Mn_6$
Formula Mass	1647.91	1577.97	1236.39	1055.09	2039.49
Crystal system	Hexagonal	Hexagonal	Monoclinic	Trigonal	Monoclinic
Space group	*R*3	*R*3	*C*2/*c*	*P*3 /*c*	$P2_1/n$
a/Å	21.4412(13)	21.4257(4)	27.8361(10)	15.6887(3)	13.4841(4)
b/Å	21.4412(13)	21.4257(4)	15.6707(6)	15.6887(3)	18.4592(5)
c/Å	28.5829(17)	28.5757(6)	30.6046(12)	22.2702(8)	19.6489(6)
α/°	90.00	90.00	90.00	90	90
β/°	90.00	90.00	112.593(2)	90	104.358(2)
γ/°	120.00	120.00	90.00	120	90
V/Å^3	11379.8(12)	11360.5(4)	12325.5(8)	4747.1(2)	4738.0(2)
Z	3	3	2	4	2
Reflections measured	22940	41157	44430	21939	70341
Independent reflections	7686	5184	8852	4188	12809
R_{int}	0.0459	0.0470	0.0543	0.075	0.059
$wR(F^2)$ (all data)[a]	0.1929	0.1385	0.2261	0.1807	0.1737
R_1 ($I > 2\sigma(I)$)[b,c]	0.0656	0.0511	0.0877	0.0666	0.0717
GOF on F^2	1.037	1.131	1.099	0.7718	0.9928

[a] $wR2 = [\Sigma w(|F_o^2| - |F_c^2|)^2 / \Sigma w|F_o^2|^2]^{1/2}$. [b] For observed data. [c] $R1 = \Sigma||F_o| - |F_c|| / \Sigma|F_o|$.

4.3 References

1. C. B. Aakeroy, N. R. Champness and C. Janiak, *CrystEngComm*, 2010, **12**, 22.
2. E. K. Brechin and L. Cronin, *Angew. Chem., Int. Ed.*, 2009, **48**, 6948.
3. L. R. MacGillivray, G. S. Papaefstathiou, T. Friscic, T. D. Hamilton, D.-K. Bucar, Q. Chu, D. B. Varshney and I. G. Georgiev, *Acc. Chem. Res*, 2008, **41**, 280.
4. C. Rovira and J. Veciana, *CrystEngComm*, 2009, **11**, 2031.
5. C. J. Kepert, *Aust. J. Chem.*, 2009, **62**, 1079.
6. K. S. Murray, *Aust. J. Chem.*, 2009, **62**, 1081.
7. W. Wernsdorfer, N. Aliaga-Alcalde, D. N. Hendrickson and G. Christou, *Nature*, 2002, **416**, 406.
8. S. Hill, R. S. Edwards, N. Aliaga-Alcalde and G. Christou, *Science*, 2003, **302**, 1015.
9. H. Miyasaka, K. Nakata, L. Lecren, C. Coulon, Y. Nakazawa, T. Fujisaki, K. Sugiura, M. Yamashita and R. Clérac, *J. Am. Chem. Soc.*, 2006, **128**, 3770.
10. J. Yoo, W. Wernsdorfer, E.-C. Yang, M. Nakano, A. L. Rheingold and D. N. Hendrickson, *Inorg. Chem.*, 2005, **44**, 3377.
11. C. Boskovic, R. Bircher, P. L. W. Tregenna-Piggott, H. U. Güdel, C. Paulsen, W. Wernsdorfer, A.-L. Barra, E. Khatsko, A. Neels and H. Stoeckli-Evans, *J. Am. Chem. Soc.*, 2003, **125**, 14046.
12. L. Lecren, W. Wernsdorfer, Y.-G. Li, A. Vindigni, H. Miyasaka and R. Clérac, *J. Am. Chem. Soc.*, 2007, **129**, 5045.
13. G. Novitchi, W. Wernsdorfer, L. F. Chibotaru, J.-P. Costes, C. E. Anson and A. K. Powell, *Angew. Chem., Int. Ed.*, 2009, **48**, 1614.
14. L. F. Jones, A. Prescimone, M. Evangelisti and E. K. Brechin, *Chem. Commun.*, 2009, 2023.
15. R. Inglis, L. F. Jones, K. Mason, A. Collins, S. A. Moggach, S. Parsons, S. P. Perlepes, W. Wernsdorfer and E. K. Brechin, *Chem. Eur. J*, 2008, **14**, 9117.
16. C. C. Stoumpos, R. Inglis, G. Karotsis, L. F. Jones, A. Collins, S. Parsons, C. J. Milios, G. S. Papaefstathiou and E. K. Brechin, *Cryst. Growth Des.*, 2009, **9**, 24.
17. G. Karotsis, L. F. Jones, G. S. Papaefstathiou, A. Collins, S. Parsons, T. D. Nguyen, M. Evangelisti and E. K. Brechin, *Dalton Trans.*, 2008, 4917.
18. G. Karotsis, C. C. Stoumpos, A. Collins, F. White, S. Parsons, A. M. Z. Slawin, G. S. Papaefstathiou and E. K. Brechin, *Dalton Trans.*, 2009, 3388.
19. R. Inglis, G. S. Papaefstathiou, W. Wernsdorfer and E. K. Brechin, *Aust. J. Chem.*, 2009, **62**, 1108.
20. A. D. Katsenis, R. Inglis, A. M. Z. Slawin, V. G. Kessler, E. K. Brechin and G. S. Papaefstathiou, *CrystEngComm*, 2009, **11**, 2117.
21. C. J. Milios, R. Inglis, A. Vinslava, R. Baghi, W. Wernsdorfer, S. Parsons, S. P. Perlepes, G. Christou and E. K. Brechin, *J. Am. Chem. Soc.*, 2007, **129**, 12505.

22. C. J. Milios, A. Vinslava, W. Wernsdorfer, S. A. Moggach, S. Parsons, S. P. Perlepes, G. Christou and E. K. Brechin, *J. Am. Chem. Soc.*, 2007, **129**, 2754.
23. C. J. Milios, A. Vinslava, W. Wernsdorfer, A. Prescimone, P. A. Wood, S. Parsons, S. P. Perlepes, G. Christou and E. K. Brechin, *J. Am. Chem. Soc.*, 2007, **129**, 6547.
24. R. Inglis, L. F. Jones, C. J. Milios, S. Datta, A. Collins, S. Parsons, W. Wernsdorfer, S. Hill, S. P. Perlepes, S. Piligkos and E. K. Brechin, *Dalton Trans.*, 2009, **18**, 3403.
25. R. Inglis, L. F. Jones, G. Karotsis, A. Collins, S. Parsons, S. P. Perlepes, W. Wernsdorfer and E. K. Brechin, *Chem. Commun.*, 2008, 5924.
26. C. J. Milios, R. Inglis, L. F. Jones, A. Prescimone, S. Parsons, W. Wernsdorfer and E. K. Brechin, *Dalton Trans.*, 2009, **15**, 2812.
27. R. Inglis, S. M. Taylor, L. F. Jones, G. S. Papaefstathiou, S. P. Perlepes, S. Datta, S. Hill, W. Wernsdorfer and E. K. Brechin, *Dalton Trans.*, 2009, 9157.
28. P. J. Stang, *Chem. Eur. J*, 1998, **4**, 19.
29. S. R. Seidel and P. J. Stang, *Acc. Chem. Res*, 2002, **35**, 972.
30. L. Zhao, B. H. Northrop and P. J. Stang, *J. Am. Chem. Soc.*, 2008, **130**, 11886.
31. B. H. Northrop, H.-B. Yang and P. J. Stang, *Chem. Commun.*, 2008, 5896.
32. C. Birnara, V. G. Kessler and G. S. Papaefstathiou, *Polyhedron*, 2009, **28**, 3291.
33. L. R. MacGillivray, J. L. Reid, J. A. Ripmeester and G. S. Papaefstathiou, *Ind. Eng. Chem. Res.*, 2002, **41**, 4494.
34. D. J. Watkin, C. K. Prout, J. R. Carruthers, P. W. Betteridge and R. I. Cooper, Chemical Crystallography Laboratory, University of Oxford, Oxford, UK, 2003.
35. S. J. Dalgarno, N. P. Power and J. L. Atwood, *Coord. Chem. Rev.*, 2008, **252**, 825.
36. M. Yoshizawa, J. K. Klosterman and M. Fujita, *Angew. Chem., Int. Ed.*, 2009, **48**, 3418.
37. T. D. Hamilton, G. S. Papaefstathiou, T. Friscic, D.-K. Bucar and L. R. MacGillivray, *J. Am. Chem. Soc.*, 2008, **130**, 14366.
38. S. T. Meally, G. Karotsis, E. K. Brechin, G. S. Papaefstathiou, P. W. Dunne, P. McArdlea and L. F. Jones, *CrystEngComm*, 2010, **12**, 59.
39. S. T. Meally, C. McDonald, G. Karotsis, G. S. Papaefstathiou, E. K. Brechin, P. W. Dunne, P. McArdle, N. P. Power and L. F. Jones, *Dalton Trans.*, 2010, **39**, 4809.
40. L. Carlucci, G. Ciani and D. M. Proserpio, *Coord. Chem. Rev.*, 2003, **246**, 247.
41. S. T. Hyde, A.-K. Larsson, T. D. Matteo, S. Ramsden and V. Robins, *Aust. J. Chem.*, 2003, **56**, 981.
42. S. R. Batten, *CrystEngComm*, 2001, **18**, 1.
43. S. R. Batten and R. Robson, *Angew. Chem., Int. Ed.*, 1998, **37**, 1460.
44. I. A. Baburin, V. A. Blatov, L. Carlucci, G. Ciani and D. M. Proserpio, *J. Solid State Chem.*, 2005.
45. V. A. Blatov, L. Carlucci, G. Ciani and D. M. Proserpio, *CrystEngComm*, 2004, **6**, 378.
46. L. Carlucci, G. Ciani and D. M. Proserpio, *CrystEngComm*, 2003, **5**, 269.

47. J.-P. Sauvage, *Acc. Chem. Res*, 1998, **31**, 611.
48. F. M. Raymo and J. F. Stoddart, *Chem. Rev.*, 1999, **99**, 1643.
49. S. A. Nepogodiev and J. F. Stoddart, *Chem. Rev.*, 1998, **98**, 1959.
50. E. C. Sañudo, T. Cauchy, E. Ruiz, R. H. Laye, O. Roubeau, S. J. Teat and G. Aromí, *Inorg. Chem.*, 2007, **46**, 9045.
51. M. J. Knapp, D. N. Hendrickson, V. A. Grillo, J. C. Bollinger and G. Christou, *Angew. Chem., Int. Ed. Engl.*, 1996, **35**, 1818.
52. O. Roubeau and R. Clérac, *Eur. J. Inorg. Chem*, 2008, 4325.
53. J. J. Borras-Alemnar, J. M. Clemente-Juan, E. Coronado and B. S. Tsukerblat, *J. Comp. Chem.*, 2001, **22**, 985.
54. G. S. Papaefstathiou, T. Friscic and L. R. MacGillivray, *ACA Trans.*, 2004, **39**, 110.